University of Liège

Awareness Lost

A neuroimaging-based comparison between pathological and pharmacological loss of consciousness

Pieter Guldenmund

COMA Science Group

Cyclotron research centre

“One does not become enlightened by imagining figures of light,
but by making the darkness conscious.”

C.G. Jung

Awareness Lost

A neuroimaging-based comparison between pathological and pharmacological loss of consciousness.

Ph.D. thesis

for obtaining the degree of Doctor at the University of Liège.

To be defended in public in the summer of 2014

by
Pieter Guldenmund,
born on the 29th of May, 1985,
in Middelburg.

To my family, friends, and Kata.

Doctoral advisors:
Professor **Steven Laureys** and Professor **Andrea Soddu**.

The studies described in this thesis were performed at the Coma Science Group, Cyclotron Research Center, University and University Hospital of Liège, Belgium.

SUMMARY

Consciousness is a phenomenon that has so far evaded detailed description. However, with the help of modern brain imaging techniques, we can examine some of the mechanisms underlying changes in its prominence. In the experiments described in this thesis, we used structural and functional magnetic resonance imaging to discover new brain alterations occurring during two types of loss of consciousness: pharmacological (propofol anesthesia) and pathological (disorders of consciousness: vegetative state/unresponsive wakefulness syndrome, in which no awareness is assumed, and minimally conscious state, with fluctuating low-level consciousness).

In both cases, we found loss of consciousness to be associated with a breakdown of three brain networks involved in higher-order processing: the default mode network, external control network, and salience network. These networks have been associated with internal awareness, external awareness, and saliency detection, respectively. Furthermore, their connectivity with the thalamus was severely disrupted. Our findings suggest that these changes could be a general hallmark of loss of consciousness. Additionally, we developed several novel techniques to examine changing brain dynamics, which could be used to search for other mechanisms underlying loss of consciousness.

In contrast to anesthesia, loss of consciousness in patients with disorders of consciousness is the result of structural brain damage. We performed an analysis of white and gray matter damage occurring in these patients and found it to be widespread, with damage in midline default mode network regions potentially discriminating between unconscious and conscious patients.

Our results indicate that structural and resting state functional magnetic resonance imaging might have the potential to improve differential diagnosis in disorders of consciousness.

LIST OF CONTENTS

Chapter 1

GENERAL INTRODUCTION

Corresponding articles:

Mindsight: Diagnostics in Disorders of Consciousness

P. Guldenmund[1], J. Stender[1,2], L. Heine[1], S. Laureys[1].

(1) Coma Science Group, Cyclotron Research Center and Department of Neurology, University of Liège and University Hospital of Liège, Belgium. (2) BRAINlab, Department of Neuroscience and Pharmacology, Panum Institute, University of Copenhagen, Denmark.

Critical care research and practice 2012

A Default Mode of Brain Function in Altered States of Consciousness

P. Guldenmund, A. Vanhaudenhuyse, M. Boly, S. Laureys, A. Soddu.

Coma Science Group, Cyclotron Research Center and Department of Neurology, University of Liège and University Hospital of Liège, Belgium.

Archives Italiennes de Biologie 2012

1.1. A history of consciousness research

"Legs with joints, veins in its legs, blood in the veins, humors in the blood, drops in the humors, vapors in the drops."[1]

These were constituents of a 17th century mite on the table of French philosopher Blaise Pascal (1623-1662), who then looked up into the starry night sky and went on to write: "The eternal silence of these infinite spaces fills me with dread." The infinitely small and the incredibly big. The former produced his biggest feeling of despair, as it consisted of atoms that made up his very thoughts and fears and moved the fingers around his pen.[1] Pascal did not elaborate on what atoms of thought might look like, and how they could be observed.

Science depends on measurement as a way to learn more about an object or phenomenon. Length, width, height, time, frequency, etcetera. This has proven to be extremely difficult in the case of consciousness. One famous example of an early attempt to measure consciousness, or the soul, is the experiment performed by Duncan MacDougall (1866-1920). The doctor tried to determine the weight of the soul by putting six tuberculosis patients on an industrial sized scale just before the moment of dying. An average of 21 grams discriminated between living and dead tuberculosis patients, and this was attributed to the escape of the soul upon dying. Although the findings are more likely to be related to body fluid loss or related effects, other branches of the animal kingdom were also included in MacDougall's experiments, including sheep, mice and dogs, often leading to incongruent results.[2]

In 19th century Leipzig, Gustav Fechner (1801-1887) and Wilhelm Wundt (1832-1920) were using reaction time experiments to get a glimpse of how 'conscious' and 'unconscious' brain mechanisms work. This approach was inspired by work of Franciscus Donders (1818-1889) and Hermann von Helmholtz (1821-1894). They saw reaction times as a measure of the speed of conscious processing. Reaction times were seen as being dependent on three parts: simple reaction time, perception time, and will time. Where simple reaction time was a reflex, perception time was the time necessary for a stimulus to make it into consciousness. Will time was the time required to make a specific response to one type of stimulus, and another response to another kind of stimulus. Will time could be calculated by subtracting simple reaction time and perception time.[3, 4]

In the 1920s, Hans Berger (1873-1941) measured brain electricity with the help of electrodes placed on the human scalp. Some electrical properties of the brain of animals had already been described by Richard Caton (1842-1926) in 1875, giving rise to the development of electroencephalography. With this technique, Berger discovered that the measured brain electricity comes in sinusoid waves with certain frequencies. One of the waves he observed most is now known as an alpha wave and has a frequency of 8-13 Hertz. He saw patterns in the appearance of these alpha waves, depending on the state of wakefulness of a person. Moreover, the brain produced brain waves even in the absence of a specific task.[5] Later electroencephalography studies further examined the changing array of brain waves within different sleep stages, confirming that the technique is useful for studying aspects of consciousness.[6]

Around the time that Berger published his initial findings, Frédéric Bremer (1892-1982) found that transsection through the midbrain induced a state resembling deep sleep.[7] Giuseppe Moruzzi (1910-1986) and Horace Magoun (1907-1991) published in 1949 that the critical brain activating areas were found in the reticular core of the upper brainstem. Electrical activation of this area produced an active electroencephalogram in a before drowsy animal, supporting this idea.[8, 9] These discoveries led to the conception of the ascending reticular activating system, which later proved to be a rather rough sketch of the brain's arousal (wakefulness) system. Other regions are now also associated with the maintenance of wakefulness.[10]

The advent of the brain scanning machines in the 1980s and '90s is often seen as the birth of consciousness research as a respectable field of science. Indeed, in addition to the possibility to study brain structure *in vivo* in great detail, neuroimaging has provided us with unprecedented insight into the workings of the brain during cognitive processes and different states of consciousness. It has the power to roughly visualize the footprints of our thoughts; the material and examinable dynamics of the brain underlying normal, altered or lost consciousness. Neuroimaging is used to search for patterns in the way neurons become active and inactive. Activity of neurons in specific brain regions can be attributed to a type of mental activity, such as language processing or memory processing. Of further importance is how all brain regions communicate with each other. Such communication enables highly efficient integration of brain information, coming from all regions of the brain, into one percept of consciousness. Examining the patterns underlying such integration is one of the main areas of neuroimaging-based consciousness research and constitutes the topic of this thesis.

Increased success in recognizing neural patterns of consciousness using neuroimaging has many practical uses in the clinical setting, including estimation of consciousness levels in patients with disorders of consciousness.[11] In this thesis, we used magnetic resonance-based neuroimaging methods to examine the brain mechanisms underlying altered and lost consciousness due to anesthesia (chapters 2 and 3) and brain damage (chapters 4 and 5). Of particular interest is the comparison between these brain mechanisms. This will be discussed in chapter 6. We will start, however, with an introduction to the present-day comprehension and study of consciousness.

1.2. Contemporary ideas about consciousness

Consciousness might be described as the (at least limited) ability to assess one's position in the world, and being able to manipulate external stimuli into internal thoughts about past (gathered knowledge), present (incoming stimuli), and future (projections of scenarios of possible things to come). This should form one percept. What a percept exactly is, in its qualitative sense, has not yet been possible to understand. In 1989, psychologist Stuart Sutherland (1927-1998) even went as far as to write: "Consciousness is a fascinating but elusive phenomenon… Nothing worth reading has been written on it".[12] Indeed, scientific efforts to understand consciousness have mainly focused on studying the mechanisms. What it actually *is* to feel the warmth of the sun shining on your skin, or perceive the redness of red… the 'qualia' of things, is as yet unknown.[13] We will thus focus on the mechanisms underlying consciousness.

Forming a single percept based on the wide range of stimuli the brain receives at any moment depends on a high degree of information integration. It has been found that the brain is divided into many highly specialized processing centers, such as the regions responsible for early processing of auditory, somatosensory, and visual stimuli. Other regions are associated with integrating information from many specialized regions. This integration relies on robust and fast connections between these integration centers and different parts of the brain. It is assumed that consciousness might be generated by the integration taking place in such brain integration centers. In fact, networks have been identified that are associated with internal awareness (awareness of the self) and external awareness (awareness of the world around). Internal awareness has been associated with a brain network called the 'default mode network', while awareness of the outer world has been related to activity of the 'external control network'.[14, 15] During times when no specific attention-demanding cognitive task is being performed, but a person is in a state of mindwandering, the activity in these networks is anticorrelated. This means that at one moment, the default mode network is active, while the external control network is inactive, and vice versa. This changing occurs around once every 15 to 20 seconds, as does the accompanying internal and external awareness.[14] Furthermore, detecting salient external stimuli, like a rapidly approaching car while walking on the street, has been found to be associated with activity in the 'salience network'.[16] These brain networks enable rapid and efficient communication between distant brain regions,

and the functioning of at least one of them (the default mode network) has been found to be disturbed during states of altered consciousness, such as sleep, general anesthesia, and hypnosis.[15]

Forming a single percept does not only depend on the sending of processed information from many regions of the brain to several integration regions, but also on a strict organization in time.[17] A rose can be red, have a distinct shape, can smell nicely, may move in the wind, can produce a soft sound while swaying, may feel soft, can induce an emotion due to a past experience, good or bad. Some of these stimuli induce a more complex (and thus slightly more time-demanding) processing path. How does the brain make sure that all the different characteristics of the rose become combined in one percept at one time? The brain needs to remember which things belong together. The color red applies to the rose, but not to a butterfly you just saw passing by a second before. Since integration of processing of simple stimuli with those of complex ones suggests that the simple stimulus may have to wait for the more complex one to be processed and be ready for integration, it has been suggested that consciousness comes in blocks and that the sensation of a fluent stream of consciousness is an illusion. However, what causes this illusion? The question about a discrete or continuous consciousness remains the center of debate.[18]

It has been found that stimuli need a minimum presentation time, or are not perceived.[17] Moreover, perception of a stimulus can be influenced by presentation of another competing stimulus following shortly after it, leading to a non-perception or masking of the first stimulus.[19] Stimulus competition for awareness can also occur when one eye receives different information (other than can be explained by the difference in position of the eyes) than the other, leading to binocular rivalry. This leads to an alternating awareness of the image presented to the left eye and the image presented to the right eye. Similar findings have been reported for hearing.[20] Stimuli might even be 'noticed' by the brain, without ever reaching consciousness. An example of this is blindsight, in which persons claim to be blind, but can avoid obstacles in their way as if they were seeing.[21] Such extreme examples make us reflect on the fact that most of the stimuli entering the brain and the following brain calculations and resulting responses taking place, such as during walking, do not enter conscious awareness, or are not stored in (accessible) memory.[22] This unconscious cognition has been thought of as robust, learned neuronal behavior that works best without time-consuming processes like the generation of consciousness. It has also been suggested that consciousness exists because a higher level of

complexity exists that is unconscious of itself but conscious of the lower-level complexity.[22]

Generation of consciousness is furthermore thought to be dependent on 'brain arousal'. An aroused brain may be thought of as a brain in a state that may be roughly comparable to the result of plugging in the electricity plug of an electrical device. A state of readiness for neuronal response and generation of consciousness. In general, this is thought to be dependent on the activity of the ascending reticular arousal system, which originates in the brainstem.[23] A remarkable state of arousal without consciousness is thought to exist in patients with the unresponsive wakefulness syndrome (previously known as the vegetative state).[24] These patients may eventually recover (partial) consciousness.[24]

From an evolutionary point of view, one might expect some kind of consciousness to exist in non-human animals with relatively complex brain morphology. An animal equivalent of the previously mentioned default mode brain network, thought to be a biomarker of internal awareness, has indeed been detected in several animal species.[25-27] Further evidence seems to suggest forms of self-awareness in some birds, mammals and cephalopods.[28, 29]

Interestingly, some human patients with only one half of the brain functioning are conscious, while patients with a split brain (isolation of the right and left hemisphere from each other through surgery in order to stop severe epileptic seizures) report having two separate consciousnesses.[30, 31] Near-death experiences, in which a patient afterwards often reports visions of tunnels, heaven, flashbacks of life, a floating out-of-body experience, can result from brain insult (such as hypoxia during cardiac arrest).[32] Scientists have recreated such experiences in healthy subjects by electrically or magnetically stimulating specific brain regions.[33] Extreme human cases of consciousness are observed in children without a cerebrum, having only a brainstem and a cerebellum. These anencephalic children might have never developed a cerebrum, or it was degraded during development. After birth, anencephalic children may not present conspicuous symptoms until weeks or months after birth, when they begin missing developmental milestones. With the right kind of care, these children can live for decades and although literature on this condition is rare, reactivity associated with consciousness has been found in such patients.[34] The children have been described as being awake and alert, responding to their surroundings with an emotional or orienting reaction. Reactivity to stimuli is usually limited to sound stimuli. However, some children have some remaining visual cortex

and optic nerve and also respond to salient visual stimuli. They laugh and cry depending on the situation and can show preferences for certain situations and stimulations over others (such as toys, tunes, or video programs). Could this mean that the (upper) brainstem, one of the brain structures appearing early in evolutionary history, is a main center of consciousness generation?[35] How does the cerebral cortex generate more complex cognition and more recognizable (self-) awareness? Have mechanisms of consciousness generation adapted to the minimal neuronal machinery available in these children?

1.3. Measuring brain structure and activity

The experiments described in this thesis were conducted using a neuroimaging technique called magnetic resonance imaging. Different versions of this technique can be used to look at brain structure and function. It is based on the natural phenomenon of nuclear magnetic resonance, which involves atomic nuclei in a magnetic field absorbing and remitting electromagnetic radiation. Following work of Isidor Rabi (1898-1988), Joseph Larmor (1857-1942), Felix Bloch (1905-1983), and Edward Purcell (1912-1997), Hermann Carr (1924-2008) created the first magnetic resonance image in the early 1950s, which was one-dimensional. Paul Lauterbur (1929-2007) developed a technique to locate the position of atoms in three-dimensional space and produced the first three-dimensional image of a living mouse, which was published in 1973. In the late 1970s, Peter Mansfield (born in 1933) devised a mathematical method to make images clearer and the imaging process faster (from hours to seconds).[36]

In 1993, Seiji Ogawa (born in 1934) published his discovery that specific changes in the magnetic resonance signal could be used to get a measurement of the amount of oxygenated blood present in regions of the brain (the blood oxygenation level-dependent signal, or BOLD signal), which in turn could be associated with neuronal activity (the foundations for this idea were laid by Linus Pauling (1901-1994) in the 1930s).[37, 38] Therefore, it was named functional magnetic resonance imaging, which is now a neuroimaging method of choice for examining brain responses to stimuli. More recently, it has also been used, under the name of resting state functional magnetic resonance imaging, to examine task-independent spontaneous brain activity.

Examining brain structural integrity

In patients with brain damage, voxel-based morphometry can be used to find structural brain damage that may explain the alterations in behavior. It is a mostly automatic alternative to visual inspection of structural brain scans, and can improve detectability of changes in gray and white matter integrity. Voxel-based morphometry uses structural magnetic resonance images to examine the brain's integrity voxel by voxel (a voxel is a three-dimensional pixel; a cube). To

enable group comparisons, such as between healthy control subjects and patients with brain damage, measures are taken to make sure the brains of different patients and control subjects can be compared per voxel. This means correcting for different brain sizes, positioning of the brain, possible problems with image quality, morphing and accompanying downweighting of voxel intensities, and data smoothing. In the final step, the resulting brain images from a patient group and those from a number of healthy control subjects are statistically contrasted, meaning that the signal intensity of each brain voxel of the patient is weighted against a voxel in the same position in the healthy control subjects. This will pinpoint regions of brain damage in patients.

Examining functional brain connectivity

Traditional functional magnetic resonance imaging activation studies look at the difference in the intensity of the BOLD signal (thought to be a representation of neuronal activity) at different places in the brain between a condition in which a task of interest is conducted and a task-free condition. It follows a so-called block design, in which a period (block) of task performance alternates with a task-free period. This is usually repeated several times. The differences in BOLD signal are then usually attributed to the task conducted.

More recently, it has been discovered that the brain exhibits task-independent fluctuations in the BOLD signal.[39] The frequency of such fluctuations is considered to be in the low-frequency range, between 0.007 and 0.1 Hertz. Analyzing these spontaneous fluctuations has offered valuable insight into the way in which the brain works. It has been found that areas of the brain, in a task-free condition, have a comparable pattern of BOLD signal increase and decrease. It is thus assumed that brain regions with a similar pattern of BOLD signal change work closely together in a network. As the task-free paradigm is called the resting state (where the scanned subject is awake but does not perform a specific attention-demanding task, but is mindwandering), these networks are called resting state networks. Observing them requires different analysis techniques from those used with the traditional block design.

There are two main ways of finding resting state networks. With seed-based analysis, the changes in time of the BOLD signal can be measured in a specific part of the brain (the seed region, the location of which depends on the interest of the

researcher). Then, the changes in BOLD signal in all other regions of the brain are measured, and those that have a high similarity with the temporal pattern of the seed region are said to be connected to that seed region. Alternatively, with independent component analysis, the whole brain signal is divided into a set number of components, in a way that the components are as different from each other as possible, but regions clustered within each component have a temporal behavior comparable to each other.[40] Certain resting state networks can be robustly detected in nearly all healthy subjects (figure 1.1). Such networks include those with long-range connectivity and associated with higher-order, consciousness-related processes (default mode network, bilateral external control networks, and salience network), and those with more short-range connectivity (auditory network, sensorimotor network, and visual network).[41]

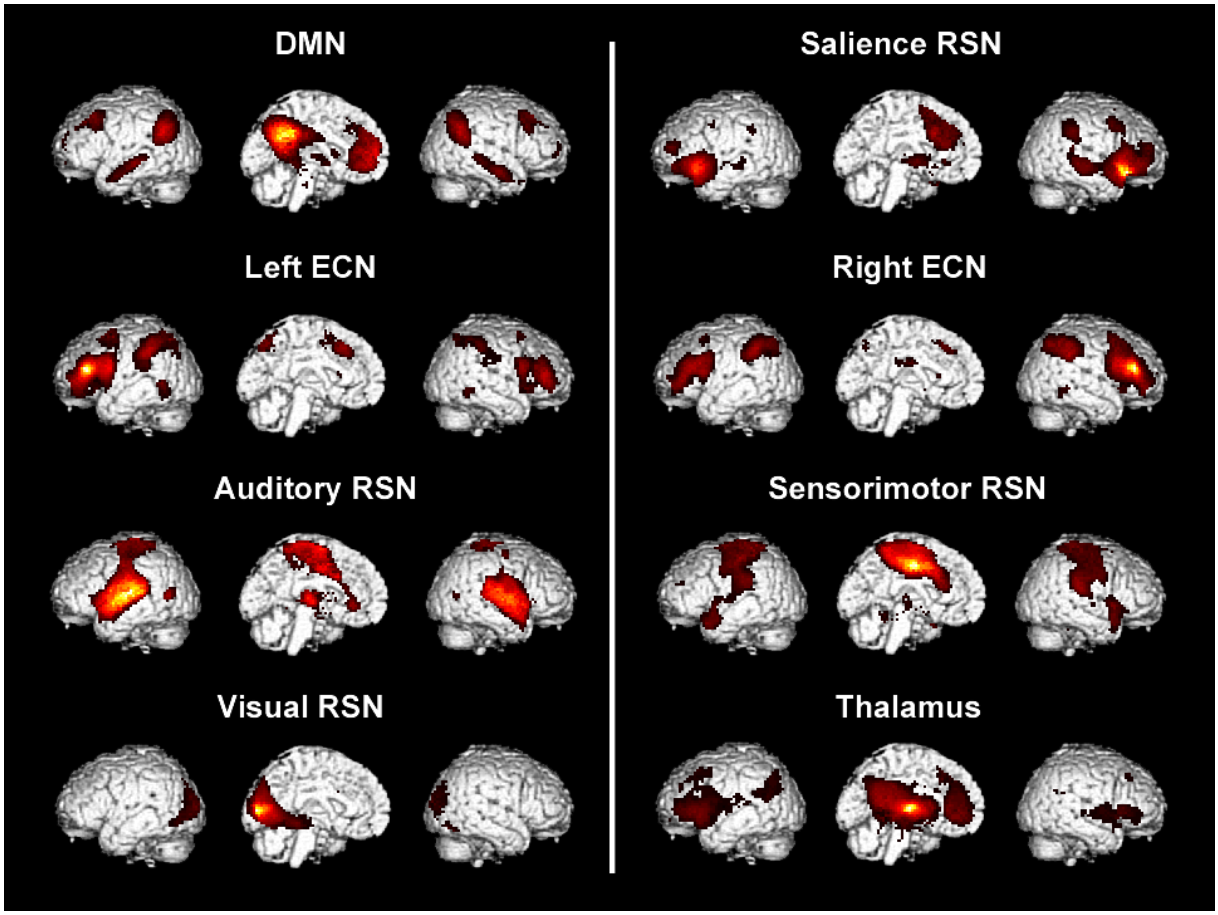

Figure 1.1. The default mode network (DMN), salience network, left and right external control networks (ECN), auditory network, sensorimotor network, visual network, as well as a thalamic network (adapted from [42]).

1.4. Anesthesia

General anesthetics are drugs used to temporarily completely deplete consciousness, mostly applied for conducting highly invasive medical procedures. One of the first public demonstrations of general anesthesia was in the Massachusetts General Hospital, in 1846. In this famous operation performed by dentist William Morton (1819-1868), a patient was operated after he had lost consciousness as a result of diethyl ether administration. Morton was famously quoted as saying: “Gentlemen, this is no humbug!”.[43] However, there is evidence that experiments with consciousness-reducing medicine have been part of human history for millennia.[44]

Nowadays, propofol is one of the most often used general anesthetics in both the clinical and experimental setting,[45] and this is the anesthetic we examined in the experiments described in this thesis. Several earlier studies have used neuroimaging to examine propofol-induced brain connectivity changes, and it is of importance to distinguish between results obtained during sedation, in which consciousness still persists, and results obtained during total loss of consciousness. Using resting state functional magnetic resonance imaging, it was found that sedation with propofol induced a change in the connective repertoire of the posterior cingulate cortex/precuneus to include (stronger) functional connections to motor/ somatosensory cortices, the reticular activating system, and the anterior thalamic nuclei.[46] When consciousness was lost due to propofol, strong default mode network and external control network disconnections occurred.[47] This also included disconnection of these networks with the thalamus and brainstem.[47] Interestingly, while connectivity within two lower-order networks (the visual and auditory networks) did not appear to be reduced, connectivity between these networks did decrease.[47] Furthermore, anticorrelation between the default mode network and external control network, a natural state during wakefulness, was found to decrease.[47]

Positron emission tomography experiments have also emphasized the important role of higher-order networks, thalamus, and brainstem regions, in loss of consciousness.[48-52] Studies employing electroencephalography have shown that during alert wakefulness, alpha wave activity is prominent in the occipital and parietal cortices, while propofol-induced unconsciousness results in an increase of

highly coherent alpha waves in the frontal cortex in a process called anteriorization.[53] Alpha anteriorization resembling that produced by propofol has also be found during sevoflurane-, isoflurane- and thiopental-induced loss of consciousness.[54-57] Furthermore, a similar anteriorization can be found in alpha coma.[58] Recent research shows that alpha activity might well be a hallmark of selective inhibition of brain activity in a region in order to maintain, strengthen or shift attentional focus established by other brain regions.[59-63]

In this thesis, we describe analyses we performed to examine the effect of propofol on brain connectivity, with a special emphasis on the salience network, thalamus, and brainstem (chapter 2). Furthermore, using novel analysis methods, we described more global brain connectivity changes and their corresponding temporal patterns (chapter 3). Finally, the effect of propofol sedation on patients with disorders of consciousness, applied in an effort to reduce patient movement in the scanner, was analyzed (chapter 4).

1.5. Disorders of consciousness

Since the early 1950s, patients with severe acute brain damage leading to coma have had an increased chance of survival due to new ways of intensive care that were developed during the Copenhagen polio epidemic of 1952.[64] This has led to an increased population of patients with coma or related disorders.[24]

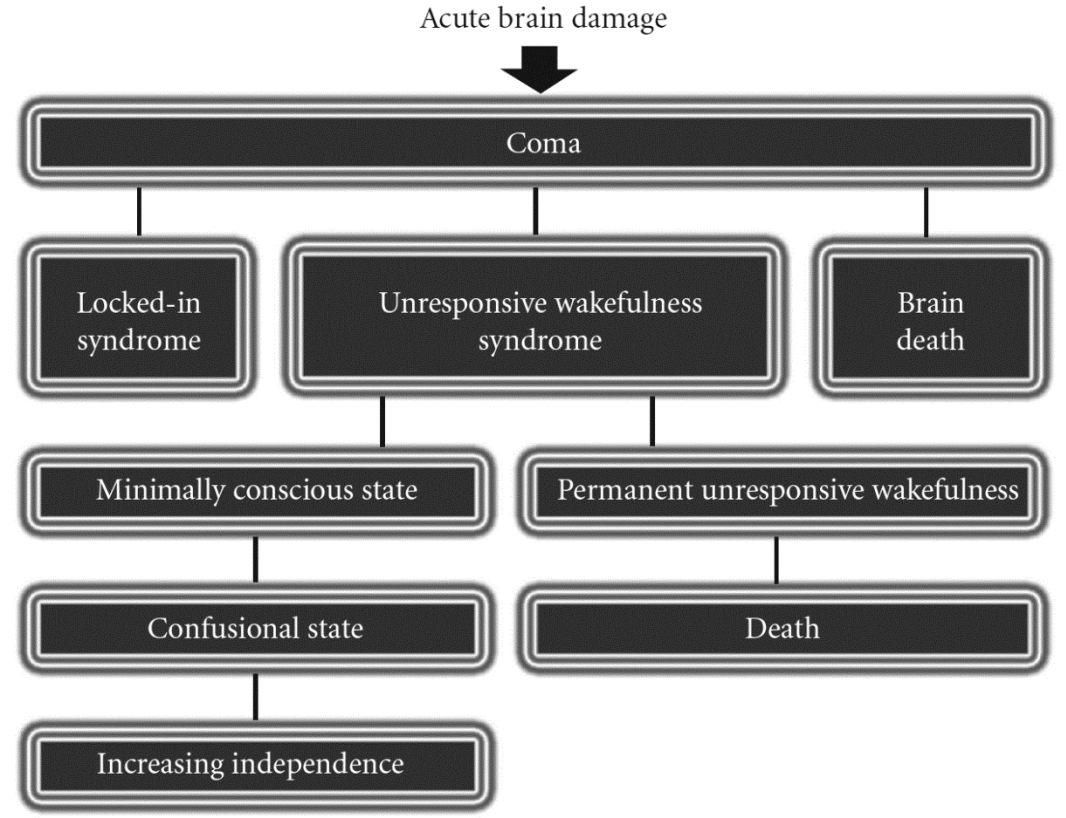

Figure 1.2. Flowchart of disorders of consciousness.[11]

Coma patients are not conscious. However, in time, patients may partly or fully recover consciousness. They may evolve to a vegetative state (recently renamed the unresponsive wakefulness syndrome; VS/UWS), in which no consciousness is detected, but eye opening, reflex movements, and periods of apparent sleep are visible. A patient may then proceed to a minimally conscious state (MCS) and, in some cases, recover high levels of consciousness (figure 1.2).[24] On rare occasions, full consciousness after coma may be present, while possibilities for communication are restricted to eye movement and blinking. These patients have the classical variant of the locked-in syndrome. Complete locked-in syndrome (where even the possibility of

eye movement and blinking is absent) and incomplete locked-in syndrome (where the patient might be able to move a hand or leg) can also occur.[65]

Neuroimaging techniques, like positron emission tomography and functional magnetic resonance imaging, can readily distinguish patients with the locked-in syndrome from those with VS/UWS.[24, 65] However, the combined effort of standardized behavioral and neuroimaging examinations for distinguishing between MCS and VS/UWS is still in need of improvement.[11] Discriminating these two states is important for prognostic, therapeutic, and ethical reasons. The prognosis of patients in MCS is thought to be relatively better than that of patients in VS/UWS.[66-69] Besides prognosis, a key question is the potential for suffering in the two states. Patients in MCS may show oriented behavioral pain responses, while those in VS/UWS do not. Whether the pain reaction in the MCS is purely reflexive or has a subjective component is not clear, but evidence from neuroimaging studies suggests the latter.[70] It is reasonable to assume that interventions such as social and physical care and adapted analgesia treatment may help to improve the quality of life and alleviate suffering of these patients. However, such care is resource consuming, emotionally taxing on the relatives, and may be considered futile. It might therefore be neglected in cases of VS/UWS where the prospects of awakening are poor.

Neuroimaging for differential diagnosis in patients with disorders of consciousness has been applied in three different categories: examination of spontaneous brain activity, brain activity as a result of a stimulus (passive paradigms), and brain activity induced by the patient conducting a cognitive task (active paradigms; figure 1.3).

Figure 1.3. Three different approaches for assessing the presence of consciousness in patients with disorders of consciousness (adapted from [11]).

Even when a subject is not performing a particular task, the brain shows vivid activity. This spontaneous activity, as well as brain structure, can be measured and compared to that of healthy control subjects, and has the advantage of not being dependent on patient cooperation. It is also possible to provide a stimulus to the

brain (such as a sound, or pain), and then measuring how the brain responds to it. Similarly, no patient cooperation is necessary, although brain damage (such as injury leading to aphasia) can interfere with the usefulness of this method. These two methods can give an indication of the chance that a patient has some preserved consciousness. However, the clearest evidence for consciousness comes from the third method. With active paradigms, a patient is asked to perform a mental task. By measuring the resulting brain activity and comparing it to the brain activity found in healthy control subjects performing that task, given enough cognitive power, a yes-no or more advance communication can be established. Thus, it can be discovered if the patient is performing the task. However, only few patients with disorders of consciousness have so far been able to perform the tasks in this type of paradigm.[71] Therefore, patient diagnosis is in general still awaiting advances in our understanding of spontaneous and stimulus-induced brain activity.

With the experiments described in this thesis, we examined changes in the brain's spontaneous activity (chapter 4) and its structure (chapter 5) associated with disorders of consciousness. Several studies have shown a disruption of functional connectivity in the default mode network in disorders of consciousness.[72] However, little is known about likely changes occurring in other resting state networks.[73] Much uncertainty also remains about how to interpret structural brain damage in disorders of consciousness.[74] Damage in the thalamus and brainstem, as well as extensive cerebral damage, are among the most frequent observations in disorders of consciousness in post mortem[75-80] and magnetic resonance imaging studies.[81-84] Furthermore, decreased structural connectivity between the thalamus and default mode network regions has been shown to play an important role in disorders of consciousness.[83] Other unanswered questions are about brain atrophy secondary to the injury causing disorders of consciousness, damage patterns distinguishing between etiologies and between VS/UWS and MCS, and between patients in MCS with and without a partially preserved language understanding.

1.6. Thesis overview

The neuroimaging-based experiments described in this thesis have been performed with the aim of increasing our understanding of the mechanisms by which the brain creates, sustains, and suppresses consciousness. These findings might be used to better estimate the level of remaining consciousness in patients with disorders of consciousness. In chapters 2 and 3, new dynamics of propofol-induced brain connectivity changes are explored. Chapter 4 describes how propofol sedation in patients with disorders of consciousness, frequently necessary to reduce patient movement and acquire good quality magnetic resonance data, could affect the patterns of brain connectivity used to estimate the level of consciousness. In chapter 5, patterns of structural brain damage in these patients are examined to better understand the functional connectivity changes observed. Eventually, a comparison between pathological and pharmacological loss of consciousness is made in the general discussion (chapter 6). Future examinations are also suggested to better understand our findings and to put them in a wider context of lost consciousness.

Chapter 2

PROPOFOL-INDUCED LOSS OF CONSCIOUSNESS:

CONNECTIVITY CHANGES ASSOCIATED WITH THE THALAMUS, BRAINSTEM AND SALIENCE NETWORK

Corresponding article:

Thalamus, Brainstem and Salience Network Connectivity Changes During Propofol-Induced Sedation and Unconsciousness

P. Guldenmund[1], A. Demertzi[1,2], P. Boveroux[1,3], M. Boly[1,2], A. Vanhaudenhuyse[1,2], M.-A. Bruno[1,2], O. Gosseries[1,2], Q. Noirhomme[1], J.-F. Brichant[3], V. Bonhomme[1,3,4], S. Laureys[1,2], A. Soddu[5].

(1) Coma Science Group, Cyclotron Research Center, University of Liège, Liège, Belgium. Departments of (2) Neurology and (3) Anesthesia and Intensive Care Medicine, CHU Sart Tilman Hospital, University of Liège, Liège, Belgium. (4) Department of Anesthesia and Intensive Care Medicine, CHR Citadelle, University of Liège, Liège, Belgium. (5) Physics & Astronomy Department, Mind & Brain Institute, Western University, London, Canada.

Brain Connectivity 2013

2.1. Abstract

In this functional magnetic resonance imaging study, we examined the effect of mild propofol sedation and propofol-induced unconsciousness on resting state brain connectivity, using graph analysis based on independent component analysis and a classical seed-based analysis. Contrary to previous propofol research, which mainly emphasized the importance of connectivity in the default mode network (DMN) and external control network (ECN), we focused on the salience network, thalamus, and brainstem. The importance of these brain regions in brain arousal and organization merits a more detailed examination of their connectivity response to propofol. We found that the salience network disintegrated during propofol-induced unconsciousness. The thalamus decreased connectivity with the DMN, ECN, and salience network, while increasing connectivity with sensorimotor and auditory/insular cortices. Brainstem regions disconnected from the DMN with unconsciousness, while the pontine tegmental area increased connectivity with the insulae during mild sedation. These findings illustrate that loss of consciousness is associated with a wide variety of decreases and increases of both cortical and subcortical connectivity. It furthermore stresses the necessity of also examining resting state connectivity in networks representing arousal, not only those associated with awareness.

2.2. Introduction

Consciousness is a phenomenon that has so far evaded detailed description. With the advent of modern brain imaging techniques, it has become possible to better locate changes in brain activity associated with altered consciousness. In the healthy awake brain, structured brain activity occurs even in the absence of a specific task. This spontaneous activity is organized into resting state networks (RSNs).[41] Each RSN consists of brain regions that have a comparable temporal pattern of spontaneous neuronal activity, which are said to be functionally connected. Resting state functional magnetic resonance imaging (resting state fMRI) is an established method used to examine changes in the brain's connectivity when consciousness is altered, assuming that low frequency changes in blood oxygenation reflect neuronal activity. It has been demonstrated that especially higher-order RSNs show decreases in connectivity when consciousness is reduced or lost. The default mode network (DMN), external control network (ECN), and salience network are considered to represent the major portion of higher-order RSNs.

The DMN is known to show changes in the spatial pattern during altered states of consciousness like deep sleep, vegetative state, and general anesthesia.[15, 47, 72, 85, 86] More recent studies also show substantial disintegration of the ECN, an RSN with spontaneous neuronal activity that is anticorrelated to that of the DMN, with decreasing consciousness.[14, 47] However, although the DMN and ECN are associated with the mediation of internal and external awareness, respectively, and are thus logical networks of interest for anesthesia studies, these are not the only brain networks showing changes during loss of consciousness. For instance, little is known about connectivity of the salience network during mild sedation and unconsciousness. The salience network is an RSN that consists of the bilateral frontal insulae, anterior cingulate cortex, and presupplementary motor area.[87] Activity in the salience RSN is associated with the detection of novel, salient stimuli, and is thought to play a role in coordinating an adequate response by recruiting appropriate brain networks. Therefore, some authors suggest it might play a role in coordinating between DMN and ECN activity.[16, 88]

Furthermore, although some resting state fMRI literature discusses changing connectivity between higher-order, highly integrative networks, and the thalamus, much remains to be discovered about changing connectivity between thalamus,

brainstem and lower-order networks (like the auditory and sensorimotor RSNs). The propofol study by Boveroux *et al*. (2010)[47] showed an involvement of the thalamus and brainstem regions in propofol-induced unconsciousness. However, no separate seed-based analysis with these loci as seed regions was performed to document their connectivity changes in detail. The brainstem pontine tegmental area (PTA), mesencephalon, and thalamus are brain structures closely associated with brain arousal via the ascending reticular arousal system.[89, 90] In fact, microinjection of pentobarbital in the mesopontine tegmental region in rats has been shown to result in a condition resembling general anesthesia.[91] Furthermore, the thalamus is regarded as one of the key loci for information integration and brain RSN coordination.[92-96]

In general, propofol-induced unconsciousness is thought to result from increased GABA-ergic transmission in the cortex and at inhibitory projections from the preoptic area of the hypothalamus to arousal regions in the brainstem.[97] Physiological effects of propofol, such as atonia and apnea, can also be traced back to the drug's actions on the brainstem.[97] These findings stress the potential importance of brainstem, thalamus and salience RSN activity in propofol-induced mild sedation and loss of consciousness. Therefore, we further examined their functional connectivity with resting state fMRI. Potential thalamic and brainstem involvement in the DMN and auditory RSN was first tested using a recently developed analysis method based on independent component analysis (ICA). Next, we used a classical seed-based technique to further examine connectivity changes with regions in the salience network, thalamus, and brainstem. A seed was also placed in the hippocampus, to examine expected changes in connectivity with the DMN other than the previously described frontoparietal disconnection.[47] Given its role in the detection of salient stimuli and thus direction of attention, we expected decreases in salience network connectivity with unconsciousness, while the PTA, mesencephalon and thalamus, being involved in brain arousal and information integration, are also likely to show a propofol-induced change in connectivity.

2.3. Materials and Methods

Subjects

We used previously published fMRI data from 20 healthy right-handed volunteers.[47, 86] One subject was excluded from the analysis due to the occurrence of hyperventilation, while data from two other subjects were left out as they were acquired during pilot sessions. Data from the remaining 17 volunteers (13 women and 4 men; mean age: 21.9 ± 1.9 years; none was under medication or pregnant) were used for our analysis. The study was approved by the Ethics Committee of the Faculty of Medicine of the University of Liège, Belgium, and subjects gave written informed consent.

Sedation protocol

Subjects fasted for at least six hours for solids and two hours for liquids before the sedation. They wore headphones and earplugs in the scanner. Propofol infusion, using a target controlled infusion device (Diprifusor-algorithm, Pharmacokinetics and Pharmacodynamics Software Server, Department of Anesthesia, Stanford University, USA) to obtain constant effect-site concentrations, occurred via an intravenous catheter placed into a vein of the right forearm or hand. During all four levels of consciousness, the blood pressure, electrocardiogram, breathing frequency, and pulse oxymetry (Sp02) were continuously monitored. For the whole duration of the experiment, subjects were breathing spontaneously, while additional oxygen was delivered at 5 L/min via a loosely fitting plastic facemask. The level of consciousness was assessed using the Ramsay scale.[98] The subject was asked twice per consciousness level assessment to strongly squeeze the hand of the investigator. The awake states before sedation and after recovery of consciousness were Ramsay 2 (strong squeezing of the hand), mild sedation was Ramsay 3 (clear but slow squeezing), and propofol-induced unconsciousness was Ramsay 5–6 (no response). In addition, a reaction time task was also given to the subject before and after each session to help define the level of consciousness. This reaction task consisted of a block of 20 beeps delivered via the headphones, and the subjects were asked to press a keypad as fast as they could. After reaching the desired effect-site concentration, a 5 min equilibration period was established. Mean propofol plasma concentrations for

wakefulness, mild sedation, unconsciousness, and recovery were 0 ± 0 μg/mL, 1.71 ± 0.72 μg/mL, 3.02 ± 1.03 μg/mL, and 0.59 ± 0.28 μg/mL, respectively. These propofol measurements were based on arterial blood samples taken directly before and after each scan. Two certified anesthesiologists and complete resuscitation equipment were present throughout the experiment (for supplementary protocol information, see [47]).

fMRI data acquisition

Functional images were acquired on a 3T Siemens Allegra scanner (Siemens AG, Munich, Germany; Echo Planar Imaging sequence using 32 slices, repetition time = 2460 ms, echo time = 40 ms, field of view = 220 x 220 mm^2, voxel size = 3.45 x 3.45 x 3 mm^3, matrix size = 64 x 64 x 32). Ten minute acquisitions were made (mean: 253 ± 74 scans) during four different states of consciousness: normal wakefulness, mild propofol sedation, propofol-induced unconsciousness, and recovery. The temporal order of mild sedation and propofol-induced unconsciousness sessions was randomized. A high-resolution T1 image was also made for each subject for coregistration purposes. Total scan time per condition was around 30 min.

ICA-based analysis

The first analysis method we used was an automated ICA-based process combined with graph theory. This approach was used to analyze propofol-induced connectivity changes of whole networks: the DMN and the auditory RSN. These RSNs were chosen as they, and regions anticorrelating with the DMN and auditory RSN, are well-described and robust. This is important for the selection of regions of interest (ROIs) representing the RSNs, a vital part of our selection procedure as will be described below. Furthermore, these two RSNs are thought to be good representatives of a ‘‘higher-order,’’ highly integrative RSN and a sensory ‘‘lower-order’’ RSN, respectively. Structural and functional magnetic resonance images were realigned, normalized, smoothed (8 mm kernel), and corrected for 3D motion using BrainVoyager QX software (R. Goebel, Brain Innovation, Maastricht, The Netherlands). ICA with 30 components yielded statistically independent RSNs and possible artifacts.[99, 100] Independent components corresponding to the DMN were selected using a previously published automated selection technique.[101, 102] For this technique, using an average DMN template calculated on the basis of resting state

fMRI scans from 12 healthy subjects (4 women, 8 men; mean age: 21 ± 3 years),[103] who were scanned for a previous study on a 3T scanner (10 min resting state with eyes closed), we defined 14 ROIs (10 x 10 x 10 mm^3) that were considered to be most representative of the DMN based on previous research (supplementary material 2.1).[104, 105] These ROIs were employed in the automatic selection process to choose the component that showed the highest level of total connectivity between these nodes, thereby being most likely to be the DMN component.

A connectivity graph was created for each of the 30 independent components produced by ICA. For a given graph, edges between each pair of ROIs represented how the corresponding time course was predicting the blood oxygenation level-dependent (BOLD) signal in that pair. To be certain that the global signal was not chosen as the best representative of the DMN, a method was devised to remove the independent component representing the global signal from the automatic selection process.[101] For this, beta values from regions that are known to anticorrelate to the DMN were introduced as a weight. The value of this weight was dependent on the amount of anticorrelation with the regions that are known to anticorrelate with the DMN, becoming stronger when less anticorrelation is present. As the global signal does not anticorrelate with these regions and the DMN does, this made sure the independent component representing the DMN was selected rather than the global signal. To ensure that neuronal independent components were selected rather than artifacts, temporal characteristics of the independent components were added to the selection process, by comparing the components to an average component fingerprint (obtained from 12 controls scanned for a previous study).[103, 106] This fingerprint is a collection of characteristics of each independent component, including information about frequency behavior, clustering, skewness, kurtosis, spatial entropy, one lag autocorrelation, and temporal entropy. Specific values of these characteristics imply that a component is truly neuronal.[106] The automated selection process used these values to favor selection of a more neuronal component fitting the spatial pattern (goodness of fit) above non-neuronal components. This process yielded one selected connectivity graph per subject per consciousness condition representing DMN connectivity. These graphs were then averaged across all subjects, resulting in one graph per condition. Connectivity graph contrasts representing connectivity differences between different consciousness conditions were constructed using the four averaged graphs. Graph connections with p-values that survived Bonferroni correction for the average across subjects were represented by thick lines, while uncorrected p-values were drawn as thin lines. In addition to the

connectivity graphs, beta maps were generated by regressing the BOLD signal with the DMN time course (keeping all the other components' time courses as confounds).

The obtained beta maps were subsequently used in a random effects analysis to construct a t-test spatial map per consciousness condition. Contrast t-test spatial maps were also calculated. The auditory RSN was examined in a similar way as the DMN. This well-described robust sensory network was selected to have a way of comparing the effect of propofol on the DMN with its effect on a sensory RSN. Eleven ROIs were chosen to represent the auditory RSN, based on the same 12 subjects as those used to determine DMN ROIs (supplementary material 2.1).[103] For illustrative purposes, we superimposed on the connectivity graphs of each condition of the DMN (figure 2.1) and auditory RSN (figure 2.2) nodes between which connectivity changed significantly between conditions as seen when performing t-tests (thick blue circles for decreased connectivity in the DMN and thick red circles for increased connectivity in the auditory RSN).

Seed-based analysis

Although our automatic ICA method is a robust tool for analyzing the well-described DMN and auditory RSN, seed analysis was chosen for further analysis of the connective repertoire of ROIs arising from previous research in the context of consciousness. Regions selected for the seed-based analysis were the right anterior insular cortex (33, 22, 6), thalamus (-7, -16, 6 and 7, -16, 6 combined), mesencephalon (-2, -24, -8), PTA (-3, -18, -27), and hippocampus (25, -16, -15). Literature confirms strong relationships of these regions with cognition and consciousness: the PTA, mesencephalon, and thalamus are of interest because of their roles in cortex activation and coordination,[93, 107, 108] while the hippocampus has a pivotal role in memory processing and has a close association with the DMN, providing additional information about DMN integrity.[109] The right anterior insular cortex has been associated with the making of go/no-go decisions[110, 111] and is part of the salience network, which is thought to enable switching between internally-oriented thought (DMN-driven) and externally-oriented activity (ECN-driven).[87]

For the same 17 subjects that we used for our ICA-based analysis, and for all four consciousness conditions, we used SPM8 software (statistical parametric mapping, Wellcome Trust Centre for Neuroimaging, www.fil.ion.ucl.ac.uk) to realign, normalize, smooth (8 mm kernel), and analyze the data. Results were thresholded at

family-wise error corrected p-value < 0.05 at the whole brain level or in a 10 mm radius spherical small volume around *a priori* coordinates taken from previous studies.[47, 103, 104, 112-114] For display purposes, data are presented at p < 0.001 (uncorrected). Although whole brain family-wise error correction, and to lesser extent whole brain false discovery rate correction, are often employed in studies where relatively great changes in brain activity can be expected (such as sensory and motor processes in classical fMRI studies), more subtle changes will go unnoticed. In fMRI research, there is a trend towards dramatically trying to minimize the chance of finding false positives (type I errors), resulting in an increase in type II errors (missing true effects). However, a great number of highly reproducible studies have used p < 0.001 uncorrected thresholds.[115] This threshold is generally considered to be a good balance between the chance of finding type I and II errors.[115] Nevertheless, carefulness is advised with the interpretation of clusters consisting of less than 10 voxels. The employment of knowledge of the region's behavior in comparable experimental setups outlined in previous studies, used for applying small volume correction at a family-wise error of p < 0.05 in this study, is a commonly employed procedure in the field of fMRI and further aids in minimizing potential type I errors.

2.4. Results

ICA of the DMN

During wakefulness before administration of propofol, DMN connectivity could be observed in all subjects (figure 2.1.A). The DMN consisted of medial prefrontal cortex, posterior cingulate cortex/precuneus, and bilateral inferior parietal cortices.[41, 116] With mild propofol sedation, no significant changes were observed in DMN connectivity strength as compared to wakefulness (figure 2.1.B, see supplementary material 2.2, DMN, for contrasts). The scalar contrast map showed that anticorrelation between the bilateral anterior insular cortices and the DMN had decreased from wakefulness to mild sedation (supplementary material 2.2, DMN).

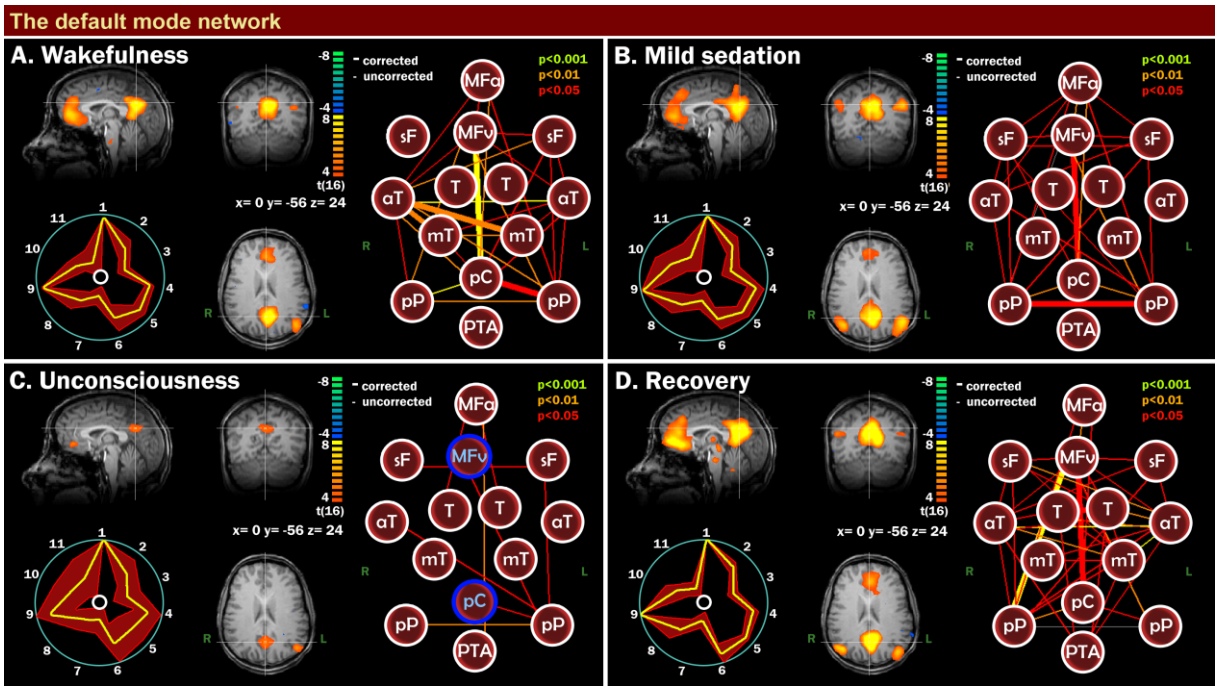

Figure 2.1. Default mode network (DMN) integrity during wakefulness, mild sedation, unconsciousness, and recovery. Scalar maps (left in each panel), fingerprints (bottom left in each panel) and connectivity graphs (right in each panel) in four conditions: wakefulness (the right inferior parietal region of the DMN is just below the z-axis of the image) (A), mild sedation (B), unconsciousness (C), and recovery (D). Scalar map legend: the yellow/orange regions (yellow/orange color scale) represent DMN regions; blue/green regions (blue/green color scale) are anticorrelated to the DMN regions. P < 0.001 uncorrected, cluster size corrected. Fingerprint legend: 1, Clustering; 2, Skewness; 3, Kurtosis; 4, Spatial entropy; 5,

One lag autocorrelation; 6, Temporal entropy; 7, 0–0.008 Hz; 8, 0.008–0.02 Hz; 9, 0.02–0.05 Hz; 10, 0.05–0.1 Hz; 11, 0.1–0.25 Hz. Connectivity graph legend: MFa, medial frontal cortex anterior; MFv, medial frontal cortex ventral; sF, superior frontal cortex; T, thalamus; aT, anterior temporal cortex; mT, medial temporal/parahippocampal cortex; pC, precuneus; pP, posterior parietal; PTA, pontine tegmental area. R, right; L, left. Thick lines are functional connections that survive multiple comparisons. Blue-bordered circles represent DMN regions between which connectivity has dropped in that consciousness state as compared to wakefulness, based on a two-sample t-test between conditions (supplementary material 2.2).

During propofol-induced unconsciousness (figure 2.1.C), the only difference found with the graph analysis between wakefulness and unconsciousness that survived Bonferroni multiple comparisons correction was the loss of frontoparietal connectivity (figure 2.1.C & supplementary material 2.2, DMN). Disconnection of the frontal part of the DMN was seen on the scalar map. As with mild sedation, the bilateral anterior insular cortices were less anticorrelated to the DMN as compared to wakefulness (supplementary material 2.2, DMN). Recovery of consciousness was accompanied by the reestablishment of frontoparietal connectivity (figure 2.1.D). No significant differences were observed between wakefulness before sedation and recovery, apart from weaker anticorrelation of the right anterior insular cortex with the DMN during recovery, as seen on the contrast scalar map (supplementary material 2.2, DMN). On the scalar map, two brainstem areas (the PTA and a region of the mesencephalon) showed up as being functionally connected to the DMN, whereby the mesencephalon demonstrated a significant increase in connectivity to the DMN during recovery from unconsciousness (supplementary material 2, DMN). We also found the thalamus and the cerebellum to be connected to the DMN during recovery (figure 2.1.D). The fingerprints from the chosen components of all four conditions were similar to the average fingerprint obtained from healthy, non-sedated controls,[103, 106] and were thus likely to be neuronal. Movement parameters showed that there were no significant differences in patient movement between patients, or between scanning sessions.

ICA of the auditory RSN

The identified auditory RSN during wakefulness consisted of bilateral insular regions, the (supplementary) motor area and thalamus (figure 2.2.A). An increase in connectivity between thalamus and insula was observed during mild sedation (figure 2.2.B). No other significant differences were observed during either of the four consciousness conditions (figures 2.2.C, D; supplementary material 2.2, auditory

RSN). During wakefulness, we observed on the scalar maps an anticorrelation between the auditory RSN and two bilateral homotopic parts of the secondary visual cortex, while during mild sedation; connectivity was seen between the auditory RSN and a medial part of the secondary visual cortex.

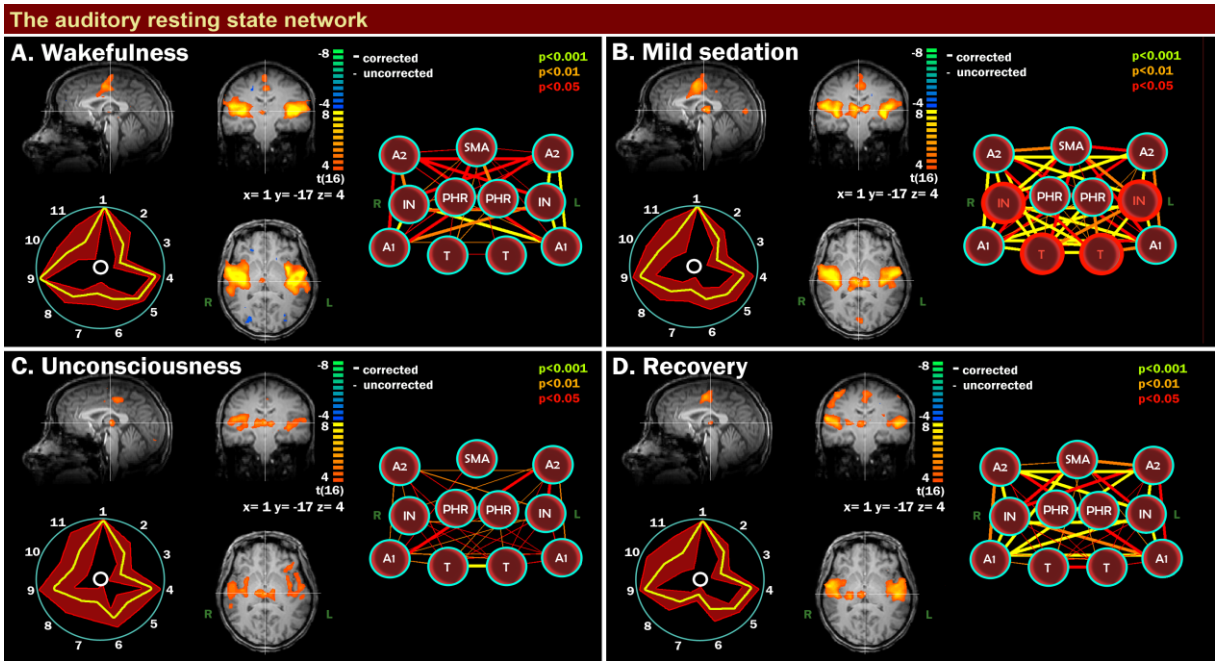

Figure 2.2. Auditory resting state network (RSN) integrity during wakefulness, mild sedation, unconsciousness, and recovery. Scalar maps (left in each panel), fingerprints (bottom left in each panel), and connectivity graphs (right in each panel) in four conditions: wakefulness (A), mild sedation (B), unconsciousness (C), and recovery (D). Scalar map legend: the yellow/orange regions (yellow/orange color scale) represent auditory RSN regions; blue/green regions (blue/green color scale) are anticorrelated to the auditory RSN regions. P < 0.001 uncorrected, clustersize corrected. Fingerprint legend: 1, Clustering; 2, Skewness; 3, Kurtosis; 4, Spatial entropy; 5, One lag autocorrelation; 6, Temporal entropy; 7, 0–0.008 Hz; 8, 0.008–0.02 Hz; 9, 0.02–0.05 Hz; 10, 0.05–0.1 Hz; 11, 0.1–0.25 Hz. Connectivity graph legend: SMA, supplementary motor area; A2, secondary auditory cortex; PHR, parahippocampal region; IN, insula; A1, primary auditory cortex; T, thalamus. R, right; L, left. Thick lines are functional connections that survive multiple comparisons. Red-bordered circles represent auditory RSN regions between which connectivity has increased in that consciousness state as compared to wakefulness, based on a two-sample t-test between conditions (supplementary material 2.2).

Seed-based analysis

1. The first seed was placed in the anterior insular cortex (supplementary material 2.3). Decreased connectivity between the anterior insular cortex and bilateral inferior parietal cortices, precuneus, secondary sensorimotor area, and primary auditory cortex was found during mild sedation. Proceeding from mild sedation to unconsciousness, the anterior insular cortex also disconnected from the salience network, thalamus, and superior temporal gyrus.

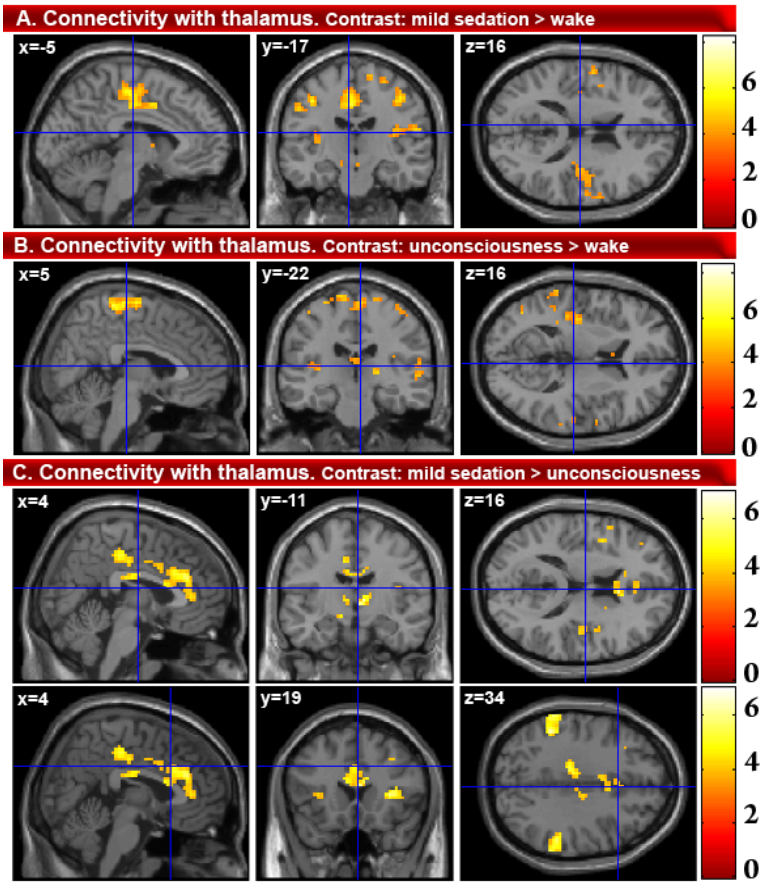

Figure 2.3. Changes in connectivity with the thalamus. (A) Mild sedation > wake, showing an increase in connectivity to the bilateral insulae and sensorimotor cortex; (B) unconsciousness > wake, also showing increased thalamus-insula and thalamus-motor cortex connectivity; (C) mild sedation > unconsciousness. From mild sedation to unconsciousness, a decrease in connectivity between thalamus and inferior parietal lobules and salience RSN regions (insular and anterior cingulate cortices) is observed ($p < 0.001$, see supplementary material 2.4 for whole brain and small volume corrections).

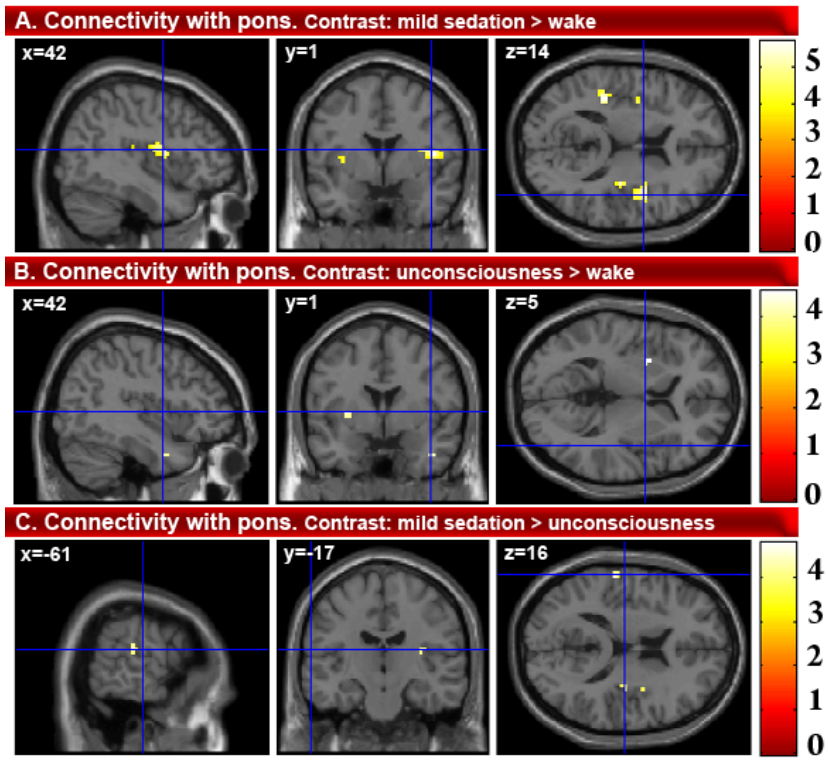

Figure 2.4. Changes in connectivity with the PTA. (A) Mild sedation > wake, showing increased connectivity of the PTA with bilateral insulae; (B) unconsciousness > wake, showing an increase in PTA-putamen connectivity; (C) mild sedation > unconsciousness. From mild sedation to unconsciousness, the increased PTA-insula connectivity found with mild sedation decreases to a pre-anesthesia level ($p < 0.001$, see supplementary material 2.4 for whole brain and small volume corrections).

2. The second seed region of our analysis was the thalamus (figure 2.3 & supplementary material 2.3). With mild sedation, an increase in connectivity between the thalamus and the auditory cortex, insular cortex, primary somatosensory cortex, primary motor cortex, and supplementary motor area was observed. Decreased connectivity was found between thalamus and cerebellum. Compared to mild sedation, unconsciousness was accompanied by a decrease in thalamic connectivity with insular regions. Connectivity between thalamus and both the salience network regions and bilateral inferior parietal lobules was found to decrease from mild sedation to unconsciousness. Thalamic connectivity with regions overlapping with those of the DMN decreased during unconsciousness as compared to wakefulness. Connectivity between thalamus and supplementary motor and primary motor areas remained stronger than during full wakefulness.

3. In the mesencephalon seed region (supplementary material 2.3), mild sedation was associated with decreased connectivity with the posterior cingulate

cortex/precuneus and the mesencephalon itself. Proceeding from mild sedation to unconsciousness, the seed region decreased connectivity with the posterior cingulate cortex/precuneus and left inferior parietal cortex. Compared to wakefulness, unconsciousness was associated with decreased connectivity with the posterior cingulate cortex/precuneus, inferior parietal cortices, and anterior cingulate cortex.

4. The fourth seed region was the PTA (figure 2.4 & supplementary material 2.3). During mild sedation, the PTA became more connected to the auditory and other insular regions. From mild sedation to unconsciousness, a decrease in connectivity compared to mild sedation was observed between PTA and auditory/insular areas, until pre-anesthesia levels of connectivity. Compared to wakefulness, during unconsciousness, a decrease in PTA connectivity with the posterior cingulate cortex/precuneus and right superior frontal cortex was found, while connectivity between PTA and putamen increased. During both mild sedation and unconsciousness, a decreased connectivity between PTA and thalamus was found.

5. The fifth seed region was the hippocampus (supplementary material 2.3). With mild sedation, we found a connectivity decrease between hippocampus and both posterior cingulate cortex/precuneus and primary/secondary visual cortex. From mild sedation to unconsciousness, a decrease in connectivity between hippocampus and the inferior parietal region was observed.

2.5. Discussion

We examined the changing connectivity of the thalamus, brainstem and salience network during mild propofol sedation and propofol-induced unconsciousness. The results of this analysis complement the research performed by Boveroux *et al*. (2010),[47] who focused on DMN and ECN connectivity changes associated with a decreasing level of consciousness. This previous research found propofol-induced decreased frontoparietal connectivity in the DMN, decreased anticorrelation between DMN and ECN, and decreased connectivity between thalamus and both DMN and ECN. Furthermore, they reported decreased connectivity between visual and auditory RSNs, while connectivity within the auditory and visual RSNs did not change significantly. We here present results from our analyses focusing on propofol-induced salience network, thalamus, and brainstem connectivity changes.

Salience network

Disconnection within the salience network and between salience network regions and thalamus was found with the thalamus and anterior insular cortex seeds. This disconnection has not been previously described in anesthesia and could play a major role in loss of consciousness. The influence of correct salience network functioning on brain connectivity was shown in a study with patients with cognitive impairment following mild traumatic brain injury.[88] The patients were performing a stop-signal task. Rapid deactivation of DMN regions was associated with efficient inhibitory control. Failure of this deactivation correlated with white matter damage in tracts connecting the salience network nodes. Menon and Uddin (2010) therefore propose that the salience network organizes DMN and ECN activity to account for an appropriate response to salient stimuli.[16] Disrupted salience network functioning has also been associated with a multitude of other cognitive disorders, among which are schizophrenia,[117] psychosis,[118] bipolar disorder,[117] autism,[16] and frontotemporal dementia.[119, 120] Further research should elucidate how the disruptions in DMN and ECN functioning during propofol anesthesia relate to disrupted salience network functioning.

Thalamus

Seed analysis from the thalamus showed decreases in connectivity between thalamus and regions overlapping with the DMN and ECN, similar to those found in the study of Boveroux *et al*. (2010),[47] as well as the salience RSN. Therefore, unconsciousness seems to correlate with disintegration of all three major higher-order networks, as well as their connectivity with the thalamus. Using positron emission tomography, thalamic metabolism has been shown to decrease significantly during anesthesia-induced unconsciousness.[51] Furthermore, a model has been suggested in which the thalamus orchestrates the commonly observed increased and coherent alpha frequency activity in the frontal cortex during propofol-induced unconsciousness.[53, 121] The authors suggest that this steady thalamic alpha rhythm could impede conduction and thus responsiveness to external stimuli. The fact that such a relatively active thalamus during unconsciousness has not been described for positron emission tomography and fMRI experiments could be because the signals obtained with these imaging methods are thought to be mostly associated with high-frequency activity, rather than alpha activity.[122]

It is not unlikely that links might exist between increased frontal cortex alpha activity and the disconnection of frontal cortex components of the DMN and salience network described in this paper. Indeed, new evidence supports the view that alpha activity in a certain brain area might be associated with inhibition in that area.[59] In the awake brain, alpha activity is thought to serve maintenance and change of attentional focus by inhibition of distracters.[60-63] In the unconscious brain, alpha activity might reflect inhibition of perception.[121] We observed increased connectivity between thalamus and both sensorimotor and auditory/insular cortices during mild sedation (figure 2.5.A). Although increased thalamic connectivity with these regions has previously been observed during mild sevoflurane sedation,[112] to our knowledge, no previous resting state fMRI reports exist on the persistence of such increased connectivity during unconsciousness (figure 2.5.B). One possible partial explanation for this connectivity increase might be that brain disturbance by propofol favors functional connectivity between brain regions that make up an above average contribution to the functional and possibly structural connective repertoire of the central thalamus. This is the case for the sensorimotor cortices.[123] However, further research should elucidate the origin of this increased connectivity.

Brainstem

The brainstem contains a major part of the ascending reticular arousal system.[108, 124] Using our ICA of the DMN, we detected involvement of the mesencephalon within the DMN with recovery from unconsciousness. With seed analysis, we found propofol-induced decreased connectivity between DMN regions, especially the posterior cingulate cortex/precuneus, and both PTA and mesencephalon. The posterior cingulate cortex/precuneus is one of the most active regions in the human brain during wakefulness, and diminished activity here has been associated with loss of consciousness due to anesthesia and disorders of consciousness.[50, 125] The importance of the PTA in the ascending reticular arousal system is well illustrated in the case of brainstem coma, a state in which there is a total absence of brain arousal and awareness,[125] where bilateral damage in the PTA alone can induce coma.[126] Recovery of brainstem functioning during recovery from coma shows similarities with recovery from anesthesia.[94] The mesencephalon has been shown to have solid connections with the posterior cingulate cortex/precuneus and anterior cingulate cortex in a multitude of studies and is considered to be a key region in pain saliency processing.[127]

Moreover, two nuclei in the mesencephalon, the periaquaductal gray matter and the parabrachial nucleus, are thought to have a prominent role in modulating global brain activity. Projections have been found from these nuclei to the brain arousal areas of the reticular nuclei and basal forebrain, as well as intralaminar thalamic nuclei.[126] Considering the brain arousal modulating capacities of the pontine and mesencephalic nuclei, their decreased connectivity with DMN regions during unconsciousness and the increasing connectivity between DMN and mesencephalon during recovery suggest brainstem-driven changes in brain arousal to partly underlie propofol-induced DMN connectivity decreases. These DMN decreases include disconnection of the frontal cortex and the hippocampus.

A decreased connectivity between thalamus and PTA was also found; two pivotal entities in brain arousal that are known to work closely together.[108] Decreased connectivity between them could potentially also represent a change in coordination of brain arousal. We observed increased connectivity between PTA and insular cortices with mild sedation. These PTA connectivity changes have not been previously described and further research should indicate whether they could potentially underlie changes in brain processing associated with the insulae, such as auditory processing, salience detection, and self-perception.[16, 108, 128] No increased PTA

connectivity with the insular cortex was found during unconsciousness as compared to wakefulness. This suggests a nonlinear behavior during decreasing levels of consciousness, with increased connectivity during mild sedation but not unconsciousness. The reason for the absence of this increased connectivity between PTA and insulae during unconsciousness might be related to the state of general depression in the brain during unconsciousness, impeding salience detection and execution of behavior.

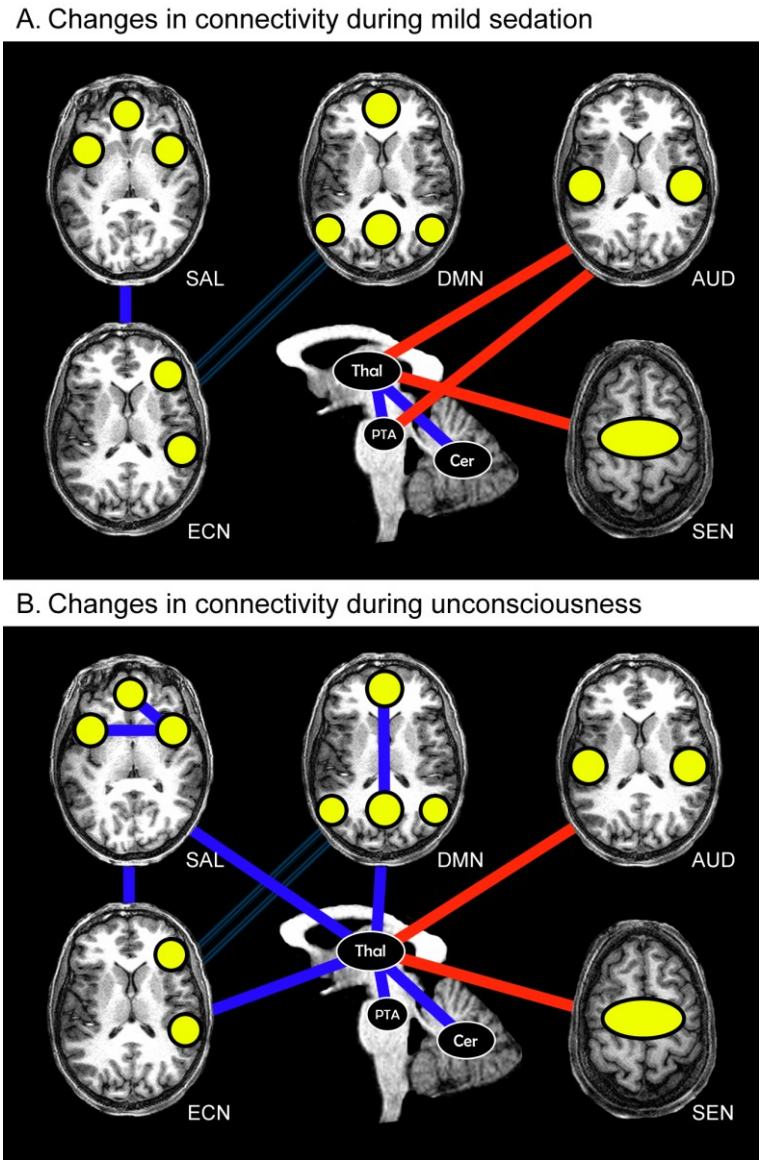

Figure 2.5. Summary of propofol-induced connectivity changes. (A) Connectivity increases (red lines) and decreases (blue lines), as well as decreased anticorrelation (thin blue double lines) during mild sedation as compared to wakefulness. (B) Connectivity increases (red lines) and decreases (blue lines), as well as decreased anticorrelation (thin blue double lines) during unconsciousness as compared to wakefulness. SAL, salience network; AUD, auditory network/insular cortex; ECN, external control network; Thal, thalamus; Cer, cerebellum; SEN,

sensorimotor cortex. Yellow blobs represent network nodes. Lines represent resting state connectivity between regions and/or networks.

Methodological considerations

In our study, we used both ICA- and seed-based methods to try to examine connectivity decreases and increases during mild sedation and unconsciousness. For this, we used resting state fMRI, which assumes that low frequency changes in blood oxygenation reflect neuronal activity. ICA is an established data-driven method that is an adequate tool for exploring data and discriminating neuronal activity from artifact.[99] It relies on the method of maximum discrimination of brain activity frequencies within a dataset given a certain number of components. However, potential bias might occur during the component selection step, as well as from the assumption that in every consciousness condition, remnants of the RSN of interest (e.g., DMN) are still present. The seed-based technique does not have these kinds of biases. However, given that proper preprocessing has been conducted, seed-based techniques might still suffer from the bias of ROI selection. Seed-based analysis shows the total connective repertoire of a chosen ROI. It looks at the degree of similarity of brain activity with all frequency patterns found in the ROI. Therefore, the techniques might be considered to be complementary, although comparing findings obtained using ICA with those gathered with seed-based methods requires some caution, especially when using different software packages for each method. However, we consider our results as being robust, as both the ICA- and seed-based methods found increased connectivity between thalamus and insular/auditory areas during mild sedation.

Inspection of component fingerprints[106] showed that it is possible to reliably find and study RSNs during propofol-induced unconsciousness. Anesthesia could potentially affect the number of RSNs present in the brain. If this number changes, and we still only divide into 30 independent components with ICA, possibly RSNs are grouped together that would normally not be incorporated in the same independent component, or RSN regions could stop being associated with a certain RSN and become associated with another RSN in another independent component. A seeming disconnection or connectivity increase may thus be the result of a changing number of discriminable RSNs available in the brain. However, previously published research using seed-based methodology also showed propofol-induced disconnection of the frontal part of the DMN.[47]

Increased connectivity in the auditory RSN seen during mild sedation with ICA was also found with our seed-based method. Therefore, although it is imaginable that propofol might confound by changing discriminability of RSNs, we do not expect that this will affect our results greatly. A possible explanation for the increased connectivity between thalamus and primary sensorimotor areas might be increased body movement during propofol sedation. Although we did not observe significant head motion, we did not perform electromyography to exclude significant body movement. However, a recent high-density electroencephalography study with propofol[129] examined subjects at Ramsey 3 (mild sedation) and 5 (unconsciousness) levels of sedation; comparable to the sedation levels used in our study. Using electromyography, they found no significantly increased body movement during sedation stages. However, they report an increase in spindle (12–15 Hz) and beta (15–25 Hz) power during mild sedation, while increased gamma (25–40 Hz) power was observed in both mild sedation and unconsciousness. The authors excluded the possibility that these increases originated from ocular or muscular sources. Using electroencephalography source reconstruction, another report showed increased thalamic excitability during mild sedation and unconsciousness.[130]

A further point of caution is the discrimination between connectivity and correlated activity. Although the central thalamic nuclei are often regarded as part of a vital brain arousal pathway with a broad connective range,[93, 94] our findings cannot single out the possibility that increased connectivity with sensorimotor/insular regions might rather be a form of coincidental correlation. An in vivo cell recording study in rats with lesions in the central lateral intralaminar nucleus, destroying thalamic afferent connections, showed that brain arousal of local cortical networks might not be associated with thalamic afferent input.[131] Synchronous activity of thalamus and sensorimotor/insular cortices could therefore also be a result of both regions receiving similar input from another brain region, or being connected via that other region. However, other studies have shown significant decreases in brain arousal associated with central thalamic injury and significant deafferentation of its neurons due to diffuse brain insults in humans.[132, 133] Furthermore, sevoflurane-induced unconsciousness has been reversed by microinjection of nicotine, a cholinergic agonist, into the rat central thalamus.[134]

These results emphasize the close direct relationship of the thalamus with the cortex, suggesting propofol influences direct connectivity between thalamus and cortical regions. It is possible that complementary arousal pathways provide an indirect connection between thalamus and cortical regions. An example would be the

part of the ascending arousal pathway that does not run through the thalamus, but is influenced by it.[108] Further research should elucidate the exact role of thalamic nuclei in cortical excitation during states of altered consciousness. Another possible reason for carefulness when interpreting fMRI data might be the potential influence of pCO2 levels on the BOLD signal. However, it has been shown that pCO2 levels do not seem to change the BOLD response to neuronal activity.[135, 136] Furthermore, for our analysis, we are interested in correlations rather than specific regional effects and are therefore confident pCO2 levels do not significantly influence our results.[137]

2.6. Conclusion

Our study shows that propofol-induced mild sedation and unconsciousness is associated with decreased connectivity within the salience network, in addition to previously reported DMN and ECN breakdown. Thalamic connectivity with these three higher-order RSNs was also found to be reduced. Furthermore, brainstem connectivity with DMN-related regions decreased. In contrast, connectivity increases were observed between the thalamus and sensorimotor/insular/auditory cortices, as well as between the PTA and insular/auditory cortices. These findings give insight into how connectivity changes in DMN and ECN internal and external awareness networks might be related to salience network integrity and arousal components located in the thalamus and brainstem. It emphasizes the necessity of examining resting state connectivity of brain regions associated with both brain arousal and awareness together to make inferences upon mechanisms responsible for loss of consciousness.

2.7. Supplementary material

2.1. ROIs used in the automated ICA-based method

Network	Region	Coordinates (x,y,z)
DMN	ventral medial prefrontal cortex (MFv)	-3, 39, -2
	medial prefrontal cortex anterior (MFa)	2, 59, 16
	posterior cingulate cortex/precuneus (pC)	-3, -55, 21
	left posterior parietal lobe (pP)	-49, -60, 23
	right posterior parietal lobe (pP)	45, -61, 21
	left superior frontal gyrus (sF)	-19, 32, 51
	right superior frontal gyrus (sF)	23, 29, 51
	left middle temporal gyrus anterior (aT)	-61, -11, -10
	right middle temporal gyrus anterior (aT)	57, -11, -13
	left parahippocampal/mesiotemporal cortex (mT)	-23, -17, -17
	right parahippocampal/mesiotemporal cortex (mT)	25, -16, -15
	left thalamus (T)	-5, -11, 7
	right thalamus (T)	4, -11, 6
	pontine tegmental area (PTA)	-3, -18, -27
Auditory RSN	left primary auditory cortex (A1)	-57, -19, 15
	right primary auditory cortex (A1)	54, -18, 14
	left thalamus (T)	-8,-17, 9
	right thalamus (T)	8, -17, 9
	left insula (IN)	-44, -5, 3
	right insula (IN)	44, -6, 2
	left secondary auditory cortex (A2)	-52, 6, 1
	right secondary auditory cortex (A2)	52, 6, 1
	supplementary motor area (SMA)	0, -8, 49
	left parahippocampal region (PHR)	-25, -7, -5
	right parahippocampal region (PHR)	22, -7, -10

2.2. Contrast images for the DMN and the auditory RSN

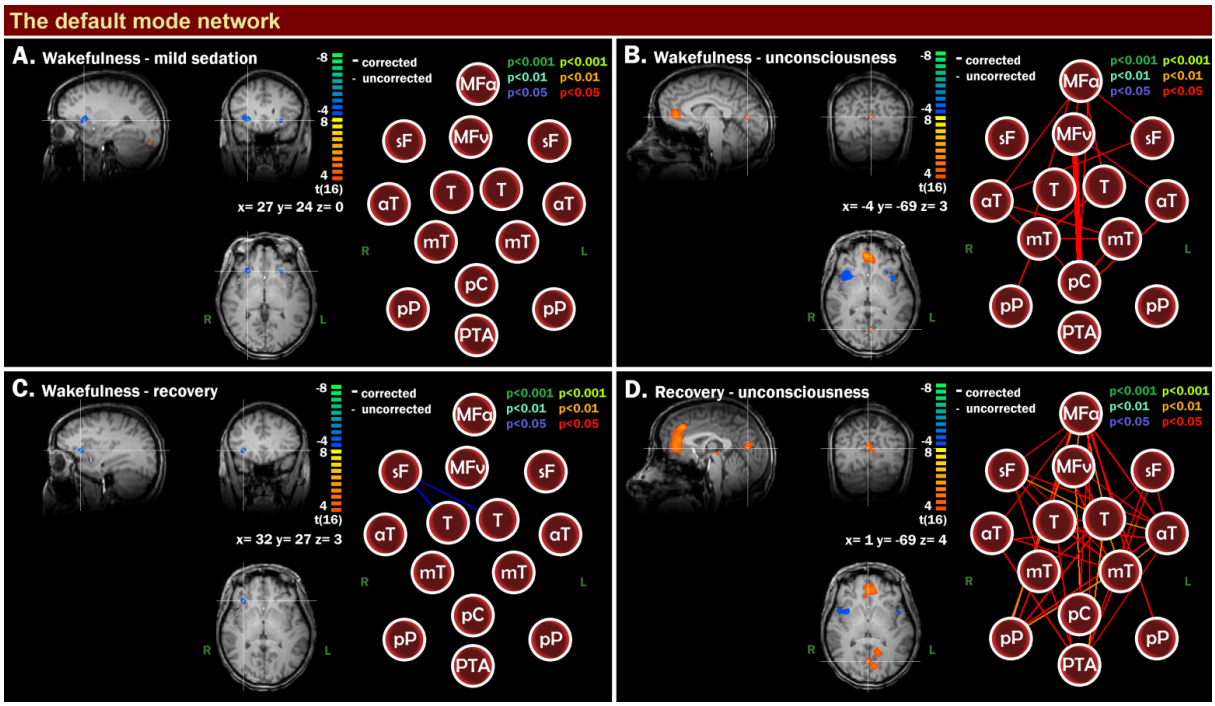

Default mode network integrity: contrast images.
<u>Scalar map legend:</u> In these contrast images, presence of red areas (yellow/orange colorscale) represents decreased connectivity of these regions within the DMN, while presence of blue areas (blue/green colorscale) represents decreased anticorrelation of these regions with the DMN; p < 0.001 uncorrected, clustersize corrected. <u>Fingerprint legend:</u> 1. Clustering, 2. Skewness, 3. Kurtosis, 4. Spatial entropy, 5. One lag autocorrelation, 6. Temporal entropy, 7. 0-0.008 Hz, 8. 0.008-0.02 Hz, 9. 0.02-0.05 Hz, 10. 0.05-0.1 Hz, 11. 0.1-0.25 Hz. <u>Connectivity graph legend:</u> MFa = medial frontal cortex anterior, MFv = medial frontal cortex ventral, sF = superior frontal cortex, T = thalamus, aT = anterior temporal cortex, mT = medial temporal/parahippocampal cortex, pC = precuneus, pP = posterior parietal, PTA = pontine tegmental area. R = right. L = left. Thick lines are functional connections that survive Bonferroni correction.

(A) wakefulness – mild sedation. No significant changes observed, except for a decrease in anticorrelation between anterior insular cortex (blue regions) and DMN. Connectivity graph: yellow, orange and red lines represent connections that decrease from wakefulness to mild sedation. (B) wakefulness – unconsciousness. A significant decrease is observed between pC and MFv. Furthermore, anticorrelation of the anterior insular cortex with the DMN decreases. Connectivity graph: yellow, orange and red lines represent connections that decrease from wakefulness to unconsciousness. (C) wakefulness – recovery. The anterior insular cortex is less anticorrelated to the DMN during recovery. Connectivity graph: green, turquoise and

blue lines represent connections that are stronger during recovery than during wakefulness. (D) recovery – unconsciousness. Connectivity graph: yellow, orange and red lines represent connections that are higher during recovery than during unconsciousness.

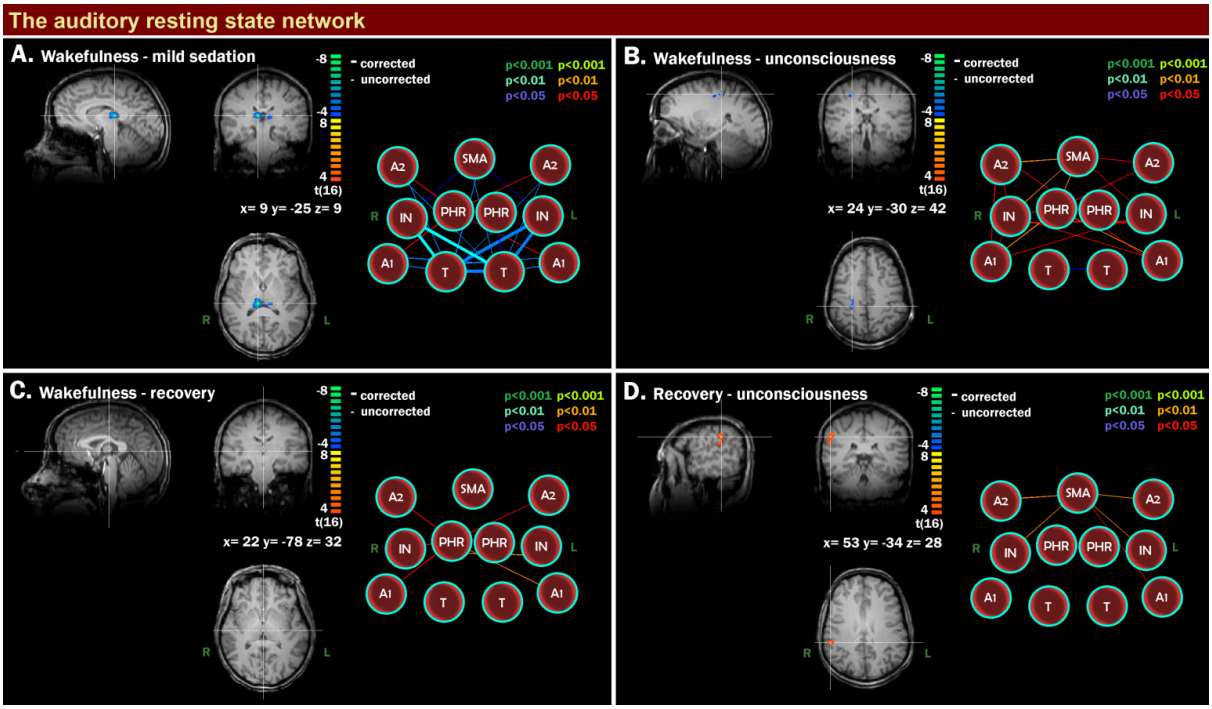

Auditory resting state network integrity: contrast images.
<u>Scalar map legend:</u> In these contrast images, presence of red areas (yellow/orange colorscale) represents decreased connectivity of these regions within the auditory RSN, while presence of blue areas (blue/green colorscale) represents decreased anticorrelation of these regions with the auditory RSN; p < 0.001 uncorrected, clustersize corrected. <u>Fingerprint legend:</u> 1. Clustering, 2. Skewness, 3. Kurtosis, 4. Spatial entropy, 5. One lag autocorrelation, 6. Temporal entropy, 7. 0-0.008 Hz, 8. 0.008-0.02 Hz, 9. 0.02-0.05 Hz, 10. 0.05-0.1 Hz, 11. 0.1-0.25 Hz. <u>Connectivity graph legend:</u> SMA = supplementary motor area, A2 = secondary auditory cortex, PHR = parahippocampal region, IN = insula, A1 = primary auditory cortex, T = thalamus. R = right. L = left. Thick lines are functional connections that survive Bonferroni correction.

(A) wakefulness – mild sedation. An increase in connectivity between thalamus and insulae is seen with mild sedation. Connectivity graph: yellow, orange and red lines represent connections that decrease from wakefulness to mild sedation. Green, turquoise and blue lines represent connections that are greater during mild sedation than during wakefulness. (B) wakefulness – unconsciousness. No significant changes are observed. Connectivity graph: yellow, orange and red lines represent connections that decrease from wakefulness to unconsciousness. Green, turquoise and blue lines represent connections that are greater during mild sedation than during wakefulness. (C) wakefulness – recovery. No significant

changes are observed. Connectivity graph: green, turquoise and blue lines represent connections that are stronger during recovery than during wakefulness. (D) recovery – unconsciousness. No significant changes are observed. Connectivity graph: yellow, orange and red lines represent connections that decrease from recovery to unconsciousness.

2.3. Further seed regions

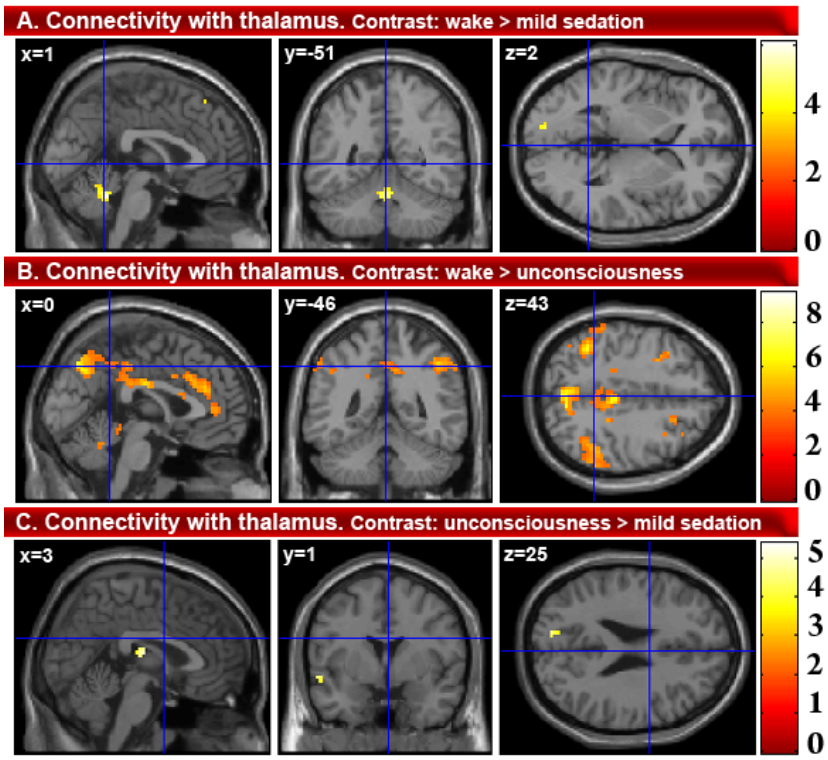

Figure I. Changes in connectivity with the thalamus. (A) wake > mild sedation, showing a decrease in connectivity between thalamus and cerebellum; (B) wake > unconsciousness, showing a decrease in thalamus-precuneus connectivity, and between thalamus and salience (insulae and anterior cingulate cortex) and external control network-associated regions (inferior parietal lobules); (C) unconsciousness > mild sedation, showing an increase in connectivity between medial thalamus and posterior thalamus, as well as to the secondary visual cortex. P < 0.001, see supplementary material 2.4 for whole brain and small volume corrections.

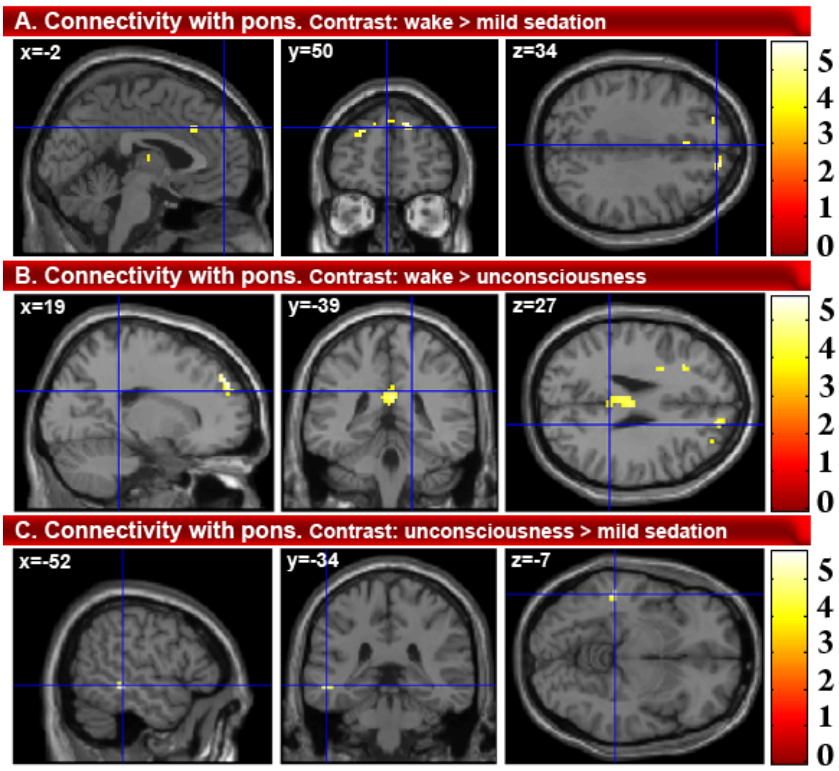

Figure II. Changes in connectivity with the pons. (A) wake > mild sedation, showing a decrease in connectivity between pons and anterior cingulate cortex and supplementary motor area; (B) wake > unconsciousness, showing a decrease in connectivity between pons and prefrontal cortex, supplementary motor area and thalamus, and between pons and posterior cingulate cortex; (C) unconsciousness > mild sedation, showing an increase in connectivity between pons and the inferior temporal cortex. P < 0.001, see supplementary material 2.4 for whole brain and small volume corrections.

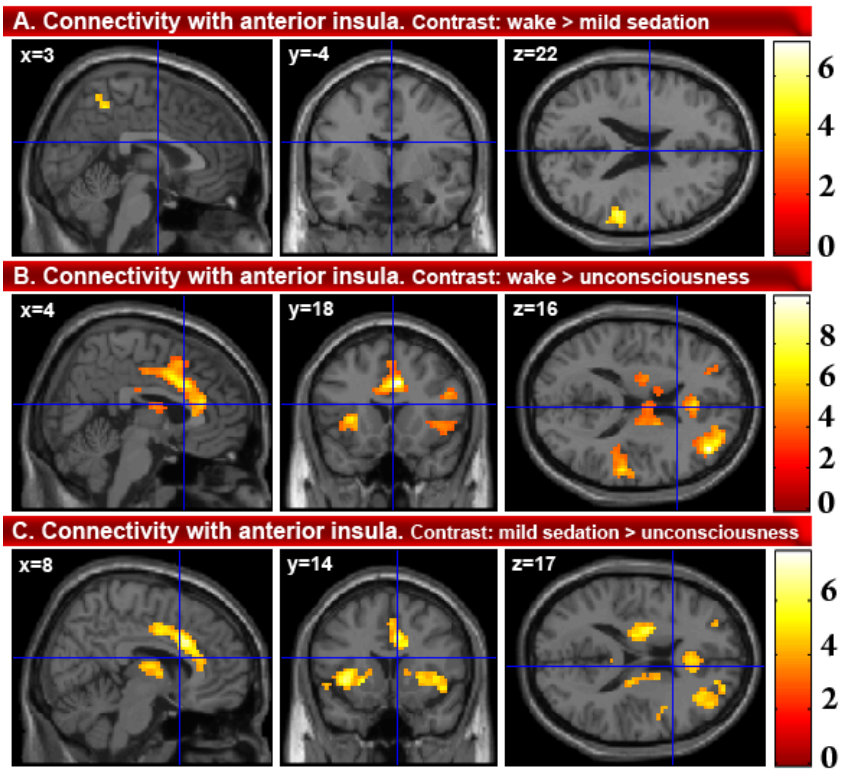

Figure III. Changes in connectivity with the right anterior insular cortex. (A) wake > mild sedation, showing a reduction in connectivity between the anterior insular cortex and posterior external control network associated regions; (B) wake > unconsciousness, showing decreased connectivity between anterior insular cortex and thalamus, salience network and external control network associated regions; (C) unconsciousness > mild sedation, with a reduction of connectivity between anterior insular cortex and salience network and thalamus. P < 0.001, see supplementary material 2.4 for whole brain and small volume corrections.

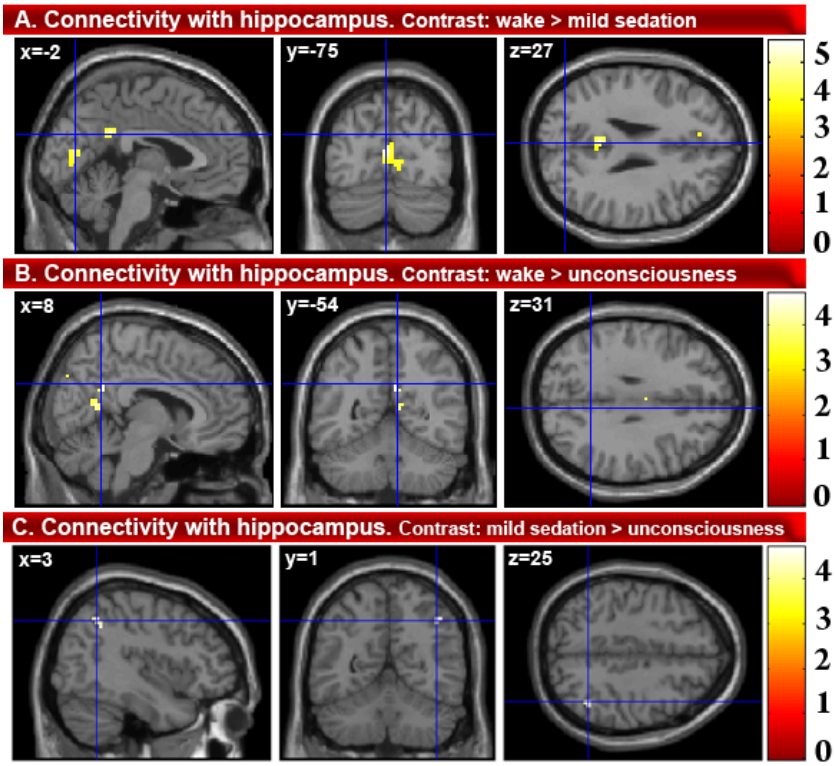

Figure IV. Changes in connectivity with the hippocampus. (A) wake > mild sedation, showing a reduction in connectivity between hippocampus and posterior cingulate cortex/precuneus and secondary visual cortex; (B) wake > unconsciousness, showing a reduced connectivity between hippocampus and posterior cingulate cortex/precuneus; (C) unconsciousness > mild sedation, showing a reduction in connectivity between hippocampus and inferior parietal lobule. P < 0.001, see supplementary material 2.4 for whole brain and small volume corrections.

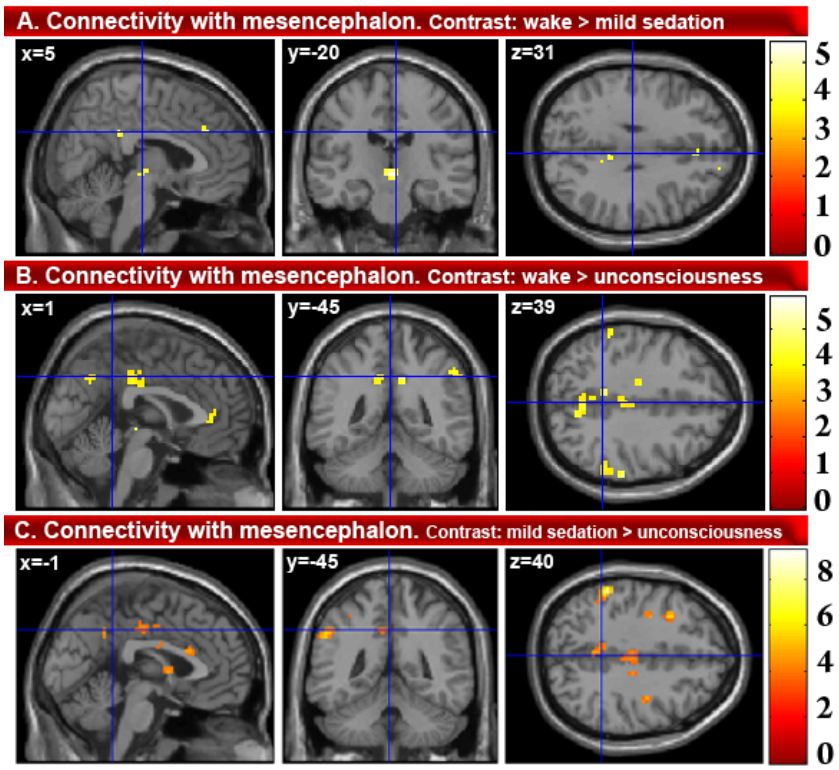

Figure V. Changes in connectivity with the mesencephalon. (A) wake > mild sedation, showing a reduction in connectivity between mesencephalon and precuneus and anterior cingulate cortex; (B) wake > unconsciousness, showing a reduced connectivity between posterior cingulate cortex/precuneus, medial prefrontal cortex, and temporoparietal areas; (C) unconsciousness > mild sedation, showing a connectivity reduction between mesencephalon and precuneus, temporoparietal areas, anterior cingulate cortex. P < 0.001, see supplementary material 2.4 for whole brain and small volume corrections.

2.4. Whole brain and small volume FWE corrections

Accompanying figures 2.3 and 2.4 of the article:

Image	Seed region	Contrast	Coordinates (x,y,z)	Name of connected region	P-values whole brain ('*') or small volume corrected
Fig. 3	Medial thalamus	mild sedation > wake	0 -22 49	Premotor/supplementary motor cortex	< 0.001 *
			36 -22 61	Primary motor cortex	< 0.001 *
			0 -22 49	Supplementary motor area	< 0.001
			-51 -19 40	Primary somatosensory cortex	0.014 *
			-33 -19 7	Insula	0.014
			60 -13 19	Insula	< 0.001
			-54 -4 22	Premotor cortex	0.038 *
			42 -4 13	Secondary auditory cortex	0.015
			-36 -1 10	Secondary auditory cortex	0.010
			-39 -16 46	Primary motor cortex	0.008 *
			60 -13 19	Primary somatosensory cortex	0.001 *
	Medial thalamus	unconsciousness > wake	-42 -31 19	Primary auditory cortex	0.001
			60 -22 13	Primary auditory cortex	0.014
			21 -25 4	Posterior thalamus	0.009
			-33 -16 7	Insula	0.011 *
			-48 -13 52	Primary motor area	0.050 *
			30 -10 67	Pre-/supplementary motor area	< 0.001 *
	Medial thalamus	mild sedation > unconsciousness	-51 -46 40	Inferior parietal lobule	< 0.001 *
			54 -40 40	Inferior parietal lobule	0.001 *
			54 -40 40	Inferior parietal lobule	0.001 *
			-60 -37 37	Inferior parietal lobule	0.004

			6 -25 25	Posterior cingulate gyrus	< 0.001 *
			-6 -7 43	Pre-/supplementary motor area	0.015
			39 5 10	Secondary auditory cortex	0.002
			-33 8 7	Secondary auditory cortex	0.047
			39 11 7	Insula	0.001 *
			33 20 7	Anterior insula	0.001
			-39 29 7	Anterior insula	0.004
			-33 32 25	Middle frontal gyrus	0.017 *
			0 38 7	Anterior cingulate	0.008
Fig. 4	Pontine tegmental area	mild sedation > wake	-39 -31 13	Primary auditory cortex	0.004
			42 -4 10	Insula	0.047
			-39 -1 10	Insula	0.029
			42 2 10	Secondary auditory cortex/ Broca's area	0.012 *
	Pontine tegmental area	unconsciousness > wake	-30 2 4	Putamen	0.017
	Pontine tegmental area	mild sedation > unconsciousness	3 -64 49	Precuneus	0.045
			-60 -22 16	Primary auditory cortex	0.011
			33 -16 13	Insula	0.024
			-36 -1 10	Insula	0.045

Accompanying supplementary figures I to VI:

Image	Seed region	Contrast	Coordinates (x,y,z)	Name of connected structure	P-values whole brain ('*') or small volume corrected
I A	Medial thalamus	Wake > mild sedation	-3 -55 -20	Cerebellum	0.007
			12 -37 26	Posterior cingulate gyrus	0.001 *
I B	Medial thalamus	Wake > unconsciousness	3 -55 -20	Cerebellum	0.046

			-12 -55 31	Posterior cingulate cortex/precuneus	0.019
			42 -55 46	Inferior parietal lobule	0.002
			-39 -52 40	Inferior parietal lobule	0.002 *
			63 -37 37	Inferior parietal lobule	< 0.001 *
			6 -19 31	Posterior cingulate gyrus	< 0.001 *
			6 32 25	Anterior cingulate gyrus	< 0.001 *
			-42 41 10	Middle frontal gyrus	< 0.001 *
			0 44 4	Medial prefrontal cortex ventral	0.004
			3 44 7	Medial prefrontal cortex anterior	0.011
			42 47 7	Anterior middle frontal gyrus	< 0.001 *
I C	Medial thalamus	Unconsciousness > mild sedation	-12 -85 28	Secondary visual cortex	0.033
			3 -16 13	Posterior thalamus	0.005
II A	Pontine tegmental area	Wake > mild sedation	-3 -13 7	Thalamus	0.011
			-33 23 49	Supplementary motor area	0.047
			-24 50 31	Superior frontal gyrus	0.014
			15 50 37	Superior frontal gyrus	0.029
II B	Pontine tegmental area	Wake > unconsciousness	3 -67 49	Precuneus	0.020
			0 -37 22	Posterior cingulate cortex	0.003 *
			-3 -13 7	Thalamus	0.011
			-33 23 49	Supplementary motor area	0.047
			-24 50 31	Superior frontal gyrus	0.014
			18 50 37	Superior frontal gyrus	0.023 *
II C	Pontine tegmental area	Unconsciousness > mild sedation	-51 -34 -8	Parahippocampal gyrus	0.044
III A	Right anterior insular cortex	Wake > mild sedation	3 -49 52	Precuneus	0.024
			9 -37 49	Secondary sensorimotor area	0.018 *

			54 -34 28	Inferior parietal lobule	< 0.001 *
			-45 -31 13	Inferior parietal lobule	0.031
			-45 -31 10	Primary auditory cortex	0.023
			48 -25 13	Primary auditory cortex	0.007
III B	Right anterior insular cortex	Wake > unconsciousness	-9 -52 49	Precuneus	0.029
			39 -34 13	Insula	0.016
			-45 -31 10	Primary auditory cortex	0.027
			-57 -31 22	Inferior parietal lobule	0.037
			57 -28 19	Inferior parietal lobule	< 0.001 *
			3 -10 13	Thalamus	0.029
			-6 -10 10	Thalamus	0.048
			-57 -4 4	Superior temporal gyrus/ Wernicke's area	0.029 *
			6 2 43	Pre-/supplementary motor area	< 0.001
			-30 11 7	Inferior frontal gyrus pars orbitalis	0.012 *
			9 17 34	Anterior cingulate gyrus	< 0.001 *
			-33 20 4	Inferior frontal cortex	0.008
			-3 26 7	Medial prefrontal cortex ventral	0.020
			3 32 19	Frontal cortex	0.002
			-24 44 16	Frontal cortex	0.042
			39 44 16	Frontal cortex	< 0.001 *
III C	Right anterior insular cortex	Mild sedation > unconsciousness	-42 -52 40	Inferior parietal lobule	0.009 *
			3 -7 13	Thalamus	0.036
			-8 -4 7	Thalamus	< 0.001
			-24 2 10	Inferior frontal gyrus pars orbitalis	< 0.001 *
			39 8 4	Inferior frontal gyrus pars orbitalis	0.009

			6 5 40	Pre-/supplementary motor area	< 0.001
			12 20 28	Anterior cingulate cortex	< 0.001
			-33 20 1	Inferior frontal cortex	< 0.001
			12 20 28	Frontal cortex	< 0.001 *
			-24 47 19	Frontal cortex	0.014
			21 50 16	Frontal cortex	0.020
			0 26 10	Medial prefrontal cortex ventral	0.001
			39 44 19	Middle frontal gyrus	< 0.001 *
IV A	Hippo-campus	Wake > mild sedation	15 -88 2	Primary visual cortex	< 0.001 *
			0 -76 7	Secondary visual cortex	0.003
			-3 -49 28	Posterior cingulate cortex/precuneus	0.019
IV B	Hippo-campus	Wake > unconsciousness	6 -55 25	Posterior cingulate cortex/precuneus	0.035
			-3 -16 13	Thalamus	0.011
IV C	Hippo-campus	Mild sedation > unconsciousness	42 -55 46	Inferior parietal lobule	0.038
V A	Mesen-cephalon	Wake > mild sedation	3 -61 55	Precuneus	0.047
			6 -40 28	Posterior cingulate cortex	0.044
			3 -19 -2	Mesencephalon	0.020
V B	Mesen-cephalon	Wake > unconsciousness	-6 41 -2	Anterior cingulate cortex	0.003
			-6 -52 31	Posterior cingulate cortex/precuneus	0.020
			39 -49 43	Inferior parietal cortex	0.023
			-30 -55 49	Inferior parietal cortex	0.045
V C	Mesen-cephalon	Mild sedation > unconsciousness	-33 -49 52	Inferior parietal cortex	0.008
			-0 -52 37	Posterior cingulate cortex/precuneus	0.010

Chapter 3

PROPOFOL-INDUCED LOSS OF CONSCIOUSNESS:

FRONTAL CORTEX DISCONNECTION

Corresponding article:

Propofol-induced Frontal Cortex Disconnection: a Study of Resting State Networks, BOLD Oscillatory Frequencies and their Generalized-Ising Model Interpretation.

T. Das*[1], S. Gantner*[2], P. Guldenmund*[2], K. Baquero[3], S. Khajehabdollahi[1], A. Sosnowski[1], B. Ge[4], A. Demertzi[2,5], P. Boveroux[6], V. Bonhomme[6,7], A. Vanhaudenhuyse[8], M.-A. Bruno[2,5], O. Gosseries[2,5], Q. Noirhomme[2], M. Kirsch[2,6], M. Boly[9], A.M. Owen[10], S. Laureys[2,5], F. Gómez+[11], A. Soddu+[1].

*Authors contributed equally.
+ Authors contributed equally.

(1) Brain & Mind Institute, Physics & Astronomy Department, University of Western Ontario, London ON, Canada. (2) Coma Science Group, Cyclotron Research Center and University Hospital of Liège, University of Liège, Liège, Belgium. (3) Computer Imaging and Medical Applications Laboratory, National University of Colombia, Bogotá, Colombia. (4) SHARCNET, University of Western Ontario, London ON, Canada. (5) Department of Neurology, CHU Sart Tilman Hospital, University of Liège, Liège, Belgium. (6) Department of Anesthesia and Intensive Care Medicine, CHU Liège, University of Liège, Liège, Belgium. (7) Department of Anesthesia and Intensive Care Medicine, CHR Citadelle, Liège, Belgium. (8) Department of Algology and Palliative Care, University Hospital of Liège, University of Liège, Liège, Belgium. (9) Department of Neurology, University of Wisconsin, Madison WI, USA. (10) Brain & Mind Institute, Psychology Department, University of Western Ontario, London ON, Canada. (11) Computer Science Department, Central University of Colombia, Bogotá, Colombia.

3.1. Abstract

Propofol is one of the most commonly used anesthetics in the world, but still much remains unknown about the mechanisms by which it induces loss of consciousness. In this resting state functional magnetic resonance imaging study, we examined qualitative and quantitative changes of resting state networks, 'total brain connectivity', and mean oscillatory frequencies of the regional blood oxygenation level-dependent (BOLD) signal, associated with propofol-induced mild sedation and loss of consciousness in healthy subjects. We discovered that detectability of resting state networks diminished significantly with loss of consciousness, and total brain connectivity decreased strongly in the frontal cortex, which was associated with increased mean oscillatory frequencies of the BOLD signal. We found that a generalized Ising model could be used to predict such behavior from the distribution of structural brain fibers. The presented methods will drastically change neuroimaging-based examination of consciousness in both the clinical and fundamental research setting.

3.2. Introduction

In the last two decades, neuroimaging has become a major addition to consciousness research. A growing number of studies have shown changes in brain functional connectivity (using resting state functional magnetic resonance imaging: resting state fMRI, as well as (high density) electroencephalography combined with transcranial magnetic stimulation), and brain metabolism (using 18F-fluorodeoxyglucose positron emission tomography; FDG-PET) during states of altered consciousness.[11, 138] With resting state fMRI, emphasis has been on analysis of separate resting state networks (RSNs),[41] and particularly the default mode network (DMN). This network is associated with internal awareness, and its intactness is therefore considered to be vital for consciousness.[15] Indeed, DMN connectivity has been shown to be decreased in deep sleep,[85] general anesthesia,[47] and in patients in coma, vegetative state/unresponsive wakefulness syndrome (VS/UWS[139]), and minimally conscious state (MCS).[72]

Anesthesia studies have also indicated the involvement of other higher-order RSNs in loss of consciousness, like the external control network (ECN; left and right ECN components are frequently mentioned separately), important for externally-oriented awareness,[47] and the salience network, which is implicated in detection of salient stimuli.[140] In contrast, lower-order RSNs (auditory, sensorimotor and visual RSNs) have not shown significant intra-network decreases during unconsciousness, although inter-network connectivity between auditory and visual RSNs has been shown to be affected.[47]

Analysis of RSNs separately using resting state fMRI gives valuable insight into the connectivity changes within each network. However, by only investigating RSNs separately, a comprehensive representation of global brain connectivity changes is lost. Analysis of the total repertoire of brain connectivity of neuronal origin ('total brain connectivity') could have significant advantages over classical resting state fMRI analysis in research and medical settings. Results may be more robust, given that analysis does not depend on predefined spatial constraints that may be inappropriate with changing brain morphology expected in brain damaged patients. Also, as all neuronal components are combined, increased signal strength is expected.

In this article, we present a method to construct total brain connectivity maps, and compare these results with results from a method examining RSN networks separately. We used resting state fMRI data from 18 healthy volunteers during wakefulness, propofol-induced mild sedation, propofol-induced unconsciousness, and recovery of consciousness. We first examined detectability of ten well-known RSNs using predefined RSN templates and a constructed neuronality classifier.[73] This would give us an idea of how well each of the ten RSNs could be automatically detected in each consciousness condition, giving an indication of detection robustness of RSNs when using a 'classical' approach that searches specifically for these ten RSNs. We then constructed total brain connectivity maps. For this, we used the neuronality classifier to select and group all RSNs of neuronal origin, without any spatial constraints.[73] This left us with a total brain connectivity map for each consciousness condition.

We also performed an analysis of the mean oscillatory frequency of the blood oxygenation level-dependent (BOLD) signal, in order to examine the relationship between propofol-induced total brain connectivity decreases and BOLD signal mean oscillatory frequency changes. Given previous resting state fMRI studies reporting on changing DMN, ECN, and salience network connectivity with propofol-induced sedation and unconsciousness,[47, 140] with an emphasis on disconnection of their frontal components, we expected brain connectivity to decrease mostly in the frontal cortex. Therefore, we theorized that such disconnection could be visible as a strong change in the BOLD signal mean oscillatory frequencies in this part of the brain.

Additionally, we introduced a generalized Ising model[141, 142] to help explain the acquired resting state fMRI results. For this, in a different group of healthy controls, resting state fMRI and diffusion tensor imaging (DTI) data were acquired during wakefulness. Structural information from DTI-tractography could be used to predict the functional connectivity patterns and the BOLD signal mean oscillatory frequencies. Assessment of the structure-function relationship has traditionally been attempted using a neuronal mass model,[143] or the Kuramoto model.[144] More recently, for assessing this relationship, the Ising model has been applied. The model assumes a chain of coupled two-state spins (neuronal firing – no firing) assumed to be in contact with a thermal bath at temperature T. This Ising model has been applied in the classical form, which assumes nearest neighbor equal couplings.[145, 146] By introducing spin couplings extracted from the structural connectivity matrix of the human brain, one can obtain a generalized Ising model where each spin corresponds to a particular region of the brain, and spins that are more coupled represent regions

of the brain that are connected via a larger number of fibers. The thermal bath temperature characterizing the generalized Ising model is the only parameter of the model, which can be used to generate different outcomes starting from the same structural fiber distribution. Different correlation matrices as well as different mean frequencies for the simulated Ising model can be obtained using different thermal bath temperatures.

Finally, this second dataset also contained FDG-PET data for the wakefulness condition. By comparing the mean oscillatory frequency of the BOLD signal with the corresponding FDG-PET values, and by further fitting the data, it was possible to extract the relationship between the BOLD signal mean oscillatory frequency and FDG-PET. Applying this found relationship to the BOLD signal mean oscillatory frequency maps of the first dataset (which had data for wakefulness, mild sedation, unconsciousness, and recovery), we could make scalar maps representing an approximation of FDG-PET maps for these four conditions, enabling a comparison with previous FDG-PET findings.

3.3. Methods

Subjects 1st data set

We used previously published resting state fMRI data of 20 healthy right-handed volunteers.[47] One subject was excluded from the analysis due to the occurrence of hyperventilation, while data from another subject was discarded as it was acquired during a pilot session. The remaining 18 volunteers (mean age: 23 ± 4 years; 14 women) were used for our analysis. The study was approved by the Ethics Committee of the Faculty of Medicine of the University of Liège, Belgium, and subjects gave written informed consent.

Subjects 2nd data set

A second set of 15 healthy subjects (mean age: 43 ± 15 years, 7 women) was studied. The study was approved by the Ethics Committee of the Faculty of Medicine of the University of Liège, Belgium, and subjects gave written informed consent.

Sedation protocol

Subjects fasted for at least six hours for solids and two hours for liquids prior to the sedation. They wore headphones and earplugs in the scanner. Propofol infusion, using a target controlled infusion device (Diprifusor©-algorithm, Pharmacokinetics and Pharmacodynamics Software Server, Department of Anesthesia, Stanford University, USA) to obtain constant effect-site concentrations, occurred via an intravenous catheter placed into a vein of the right forearm or hand. Blood pressure, pulse oxymetry and cardiac rhythm were monitored during the experiment. During all four levels of consciousness, blood pressure, electrocardiogram, breathing frequency and pulse oxymetry ($Sp0_2$) were continuously monitored. For the whole duration of the experiment, subjects were breathing spontaneously, while additional oxygen was delivered at 5 L/min via a loosely fitting plastic facemask. The level of consciousness was assessed using the Ramsay scale.[98] The subjects were asked twice per consciousness level assessment to strongly squeeze the hand of the investigator. The awake states before sedation and after

recovery of consciousness were Ramsay 2 (strong squeezing of the hand), mild sedation was Ramsay 3 (clear but slow squeezing), and propofol-induced unconsciousness was Ramsay 5-6 (no response). In addition, a reaction time task was also given to the subjects before and after each session to help define the level of consciousness. This reaction task consisted of a block of 20 beeps delivered via the headphones, and the subjects were asked to press a keypad as fast as they could. After reaching the desired effect-site concentration, a five minute equilibration period was established. Mean propofol plasma concentrations for wakefulness, mild sedation, unconsciousness and recovery were 0 ± 0 μg/ml, 1.75 ± 0.73 μg/ml, 3.06 ± 1.01 μg/ml, and 0.58 ± 0.27 μg/ml, respectively. These propofol measurements were based on arterial blood samples taken directly before and after each scan. Two certified anesthesiologists and complete resuscitation equipment were present throughout the experiment (for supplementary protocol information, see [47]).

Data acquisition for 1st subjects' set

T2*-weighted functional images were acquired on a 3T scanner (Siemens AG, Munich, Germany; Echo Planar Imaging sequence using 32 slices; matrix size = 64 × 64 × 32; repetition time = 2460 ms; echo time = 40 ms; flip angle = 90°; voxel size = 3.5 x 3.5 x 3 mm^3; field of view = 220 × 220 mm^2). Ten minute acquisitions were made during four different levels of consciousness: wakefulness, mild sedation, unconsciousness, and recovery. A high-resolution T1-weighted image was acquired for each subject (T1-weighted 3D magnetization-prepared rapid gradient echo sequence).

Data acquisition for 2nd subjects' set

T2*-weighted functional images were acquired on a 3T scanner (Siemens AG, Munich, Germany; Echo Planar Imaging sequence using 32 slices; matrix size 64 × 64 × 32; repetition time = 2000 ms; echo time = 30 ms; flip angle = 78°; voxel size: 3 × 3 × 3 mm^3; field of view = 192 × 192 mm^2). A high-resolution T1-weighted image was acquired for each subject (T1-weighted 3D magnetization-prepared rapid gradient echo sequence). For DTI, one unweighted (b = 0) volume was acquired followed by a set of diffusion-weighted (b = 1000 s / mm^2) images using 64 non-collinear directional gradients. This sequence was repeated twice, for a total of 130 volumes. FDG-PET data were acquired after intravenous injection of 300 MBq of FDG on a Philips Gemini

TF PET-CT scanner, as previously described.[147, 148] The subjects were monitored by two anesthesiologists throughout the procedure and visual monitoring assured minimal visual stimulation (e.g. eyes closed, dark room).

Data analysis for 1st subjects' set

Data were aligned, coregistered, spatially normalized into standard stereotactic Montreal Neurological Institute-space, and smoothed (8 mm full-width at half-maximum) using Statistical Parametric Mapping 8 (SPM8; www.fil.ion.ucl.ac.uk/spm). Independent component analysis (ICA) was performed with 30 components, using Group ICA (GIFT http://icatb.sourceforge.net/[149]). First, we examined the presence of ten well-known RSNs during each level of consciousness for each subject using a template matching procedure. The templates for these RSNs were built based on manual selection for each RSN in a dataset of 12 independent healthy controls. A goodness-of-fit analysis was then performed, examining the spatial fit for each RSN taking into account all 30 independent components simultaneously. The ten components with the highest overall goodness-of-fit value were selected based on two constraints: each template should be represented by one independent component, while each component could only be selected for one template.

After that, a neuronality analysis for each of the ten independent components selected was performed using a neuronality classifier obtained with binary supervised machine learning, as described in [73]. Independent components which failed to pass the neuronality test were excluded for further analysis. This meant that only independent components were included in the analysis of which the pre-set spatial and temporal criteria were met, meaning that no 'forced' detection of all 10 RSNs per subject was used. The contrast representing the level of consciousness (wakefulness: 1, mild sedation: -0.5, unconsciousness: -1.5 and recovery: 1) was then used per RSN to examine consciousness-related changes in RSN connectivity. Effect sizes for consciousness-related decreases of interest were calculated.

For the total brain connectivity map construction, no template-driven spatial goodness-of-fit selection was performed. Instead, all independent components that survived the neuronality classifier were added up by summing voxel by voxel the square root of the absolute value of the corresponding z maps as in:

$$\mathrm{fMRI}_{\mathrm{Tot}} = \sum_{i=1}^{N_{neur}} \sqrt{|z_i|}$$

where i is an index for the neuronal components. A subsequent smoothing with a kernel of 16 mm was applied. A spatial map per subject per consciousness condition was then built. Four subjects were excluded because they did not have any detected neuronal components during unconsciousness. A one-way analysis of variance compared the number of neuronal components in each consciousness condition after applying proportional scaling. The total connectivity maps of the remaining 14 subjects were averaged per condition. Furthermore, the contrast representing the level of consciousness mentioned earlier was used to examine the differences in total brain connectivity associated with decreasing consciousness.

The mean oscillatory frequency of the BOLD signal was calculated as follows. First, the mean of the temporal component per voxel was subtracted to reduce the baseline signal and focus mainly on BOLD signal changes. Second, the Fourier transform was used to detect the frequency spectrum signal per voxel. This process was applied to all voxels to generate the frequency map. These maps were generated for each subject in each of the four conditions. Furthermore, a contrast representing the inverse of the level of consciousness [wakefulness: -1, mild sedation: 0.5, unconsciousness: 1.5 and recovery: -1] was used to examine the differences in mean frequency associated with decreasing consciousness.

Data analysis for 2nd subjects' set

Data preprocessing was performed using SPM8 (www.fil.ion.ucl.ac.uk/spm). Preprocessing steps included realignment and adjustment for movement-related effects, coregistration of functional with structural images, segmentation of structural data, spatial normalization into standard stereotactic Montreal Neurological Institute-space, and spatial smoothing of the fMRI data with a Gaussian kernel of 8 mm full-width at half-maximum. Further correction for small, large, and rapid motions, noise spikes, and spontaneous deep breaths was applied using the ArtRepair toolbox for SPM (http://cibsr.stanford.edu/tools/ArtRepair/ArtRepair.htm). Segmentation of each subject's T1-weighted image was performed with Freesurfer's Desikan-Killiany atlas.[150] Further parcellation into 83 brain regions, using the "Lausanne 2008" atlas and its 1015 individually labeled regions, was done with standard functions from the

Connectome Mapping Toolkit[151-154] (parcellation was reduced to 83 regions of interest in order to reduce the simulation runtime). To facilitate the creation of both structural and functional networks, this type of parcellation was performed for both the original and spatially normalized T1 images for each subject.

Connectome construction followed a method laid out previously.[155] For fiber tractography, correction for eddy-current induced distortions was applied by coregistering all volumes to the first unweighted volume using affine transformations.[156] Tensors were fit to each voxel using linear least-squares and fractional anisotropy (FA) maps were generated. A small number of single-fiber (high FA) voxels were used to estimate the spherical-harmonic coefficients of the response function from the diffusion-weighted images.[157] Using non-negativity constrained spherical deconvolution, orientation distribution functions were obtained for each voxel.[157] For our dataset with 64 directions, we used a maximum harmonic order of 8 for both the response estimation and spherical deconvolution steps. Probabilistic tractography was performed throughout the whole brain using randomly placed seeds inside a subject-specific white matter mask and a predefined number of tracts (300.000). Affine registration with a normalized mutual information cost function was used to obtain a transformation matrix between the FA image and the subject's T1-weighted image. The set of points representing each fiber track were then transformed using the inverted transformation matrix to the subject's T1 space. Connectivity matrices were not limited to the beginning and endpoints of each track, and instead were incremented each time a track passed through any pair of regions.[155]

FDG-PET data were aligned, coregistered and spatially normalized using SPM8 (www.fil.ion.ucl.ac.uk/spm), and subsequently smoothed (full-width half-maximum of 8 mm). As with resting state fMRI data, a parcellation into 83 regions of interest was applied. This allowed for a correlation analysis in these regions of metabolism and BOLD signal mean oscillatory frequency.

Modeling

We considered a generalized Ising model with energy E given by:

$$\mathrm{E} = -\sum_{ij}^{N} J_{ij}\mathrm{s_i}\mathrm{s_j}$$

with N=83, J_{ij} the coupling between regions *i* and *j* extracted from fiber tracking counting the number of fibers between the two regions, and s_i the dynamical variable with only two states ± 1, capturing the local increase or decrease as compared to a baseline of activity measured via the BOLD signal in region *i*. A temperature T was also introduced, which represents the temperature of the thermal bath with which the Ising model is in contact. Numerical simulations were run for different temperatures and for each of the 15 subjects, for which we extracted a different coupling J_{ij}. Simulation was also run by using as couplings the values J_{ij} of the mean matrix calculated over the 15 subjects. Following [145, 158], given a certain temperature, we first made the structure driven system thermalize. Starting from an energetically hot random configuration of 83 spins, we let the system evolve to an equilibrium energy by subsequently random flipping the spins 10^6 times. At every spin flip, the newly generated configuration was accepted if either the flipping was producing a reduction of energy, $E_{fin} - E_{in} < 0$, or if the positive energy change was giving a Boltzmann factor $\exp(-(E_{fin} - E_{in})/KT)$ that was happening to be smaller than a randomly generated number between 0 and 1. Once an equilibrium configuration had been found, we started generating as many configurations of 83 spins as the number of data points we wanted to generate by testing all 83 spins for flip. 198 data points were generated for each of the spins, producing 83 time courses with a length of 198 with values either ± 1. A correlation matrix was then calculated for each different temperature. The equilibrium energy, the magnetization, the specific heat, and the susceptibility were also calculated for different temperatures. The critical temperature was extracted for each subject as the temperature corresponding to the peak in susceptibility. For each subject, we also calculated the temperature minimizing the Euclidean distance between the simulated correlation matrix and the mean correlation empirical matrix. The mean frequency was calculated for all the spin time-courses, using

$$< f > = \frac{\sum_{i=1}^{nFFT/2} P_i f_i}{\sum_{i=1}^{nFFT/2} P_i}$$

Here, P_i represents the power spectrum of spin or fMRI time-courses, and nFFT is the number of given frequency bins. This was then averaged over the 83 spins for different temperatures.

3.4. Results

We analyzed detectability of ten different RSNs for each level of consciousness, using the neuronality classifier and spatial properties for each one of the RSNs.[73] The overall average detection rate of RSNs for each condition was 81% for wakefulness, 71% for mild sedation, 46% for unconsciousness, and 80% for recovery. For seven out of ten RSNs, the number of subjects with neuronal components decreased from wakefulness to mild sedation and even further during unconsciousness, and increased again with recovery of consciousness (figure 3.1). We did not include the salience network and cerebellum in our further analysis of the effect of loss of consciousness on RSN spatial integrity, given that these RSNs could only be detected in less than half of the subjects during the wakefulness condition.

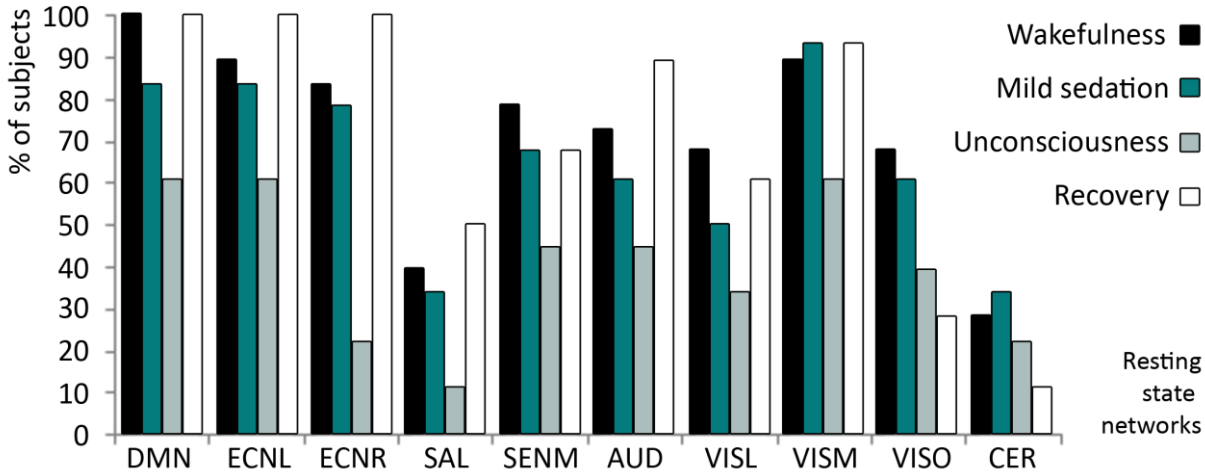

Figure 3.1. The percentage of subjects in which an RSN was detected, per RSN and consciousness condition. DMN = default mode network, ECNL = left external control network, ECNR = right external control network, SENM = sensorimotor network, AUD = auditory network, VISL = lateral visual network, VISM = medial visual network, VISO = occipital visual network.

For the remaining eight well-detected RSNs, a group-averaged scalar map was calculated per network and per consciousness condition (figure 3.2, left side). All RSNs were comparable to those described in literature,[41] although the occipital visual component showed liberal spatial and temporal variability during recovery. During each condition, fingerprints calculated for each network indicated that the detected independent components were of neuronal origin (figure 3.2, right side).[106]

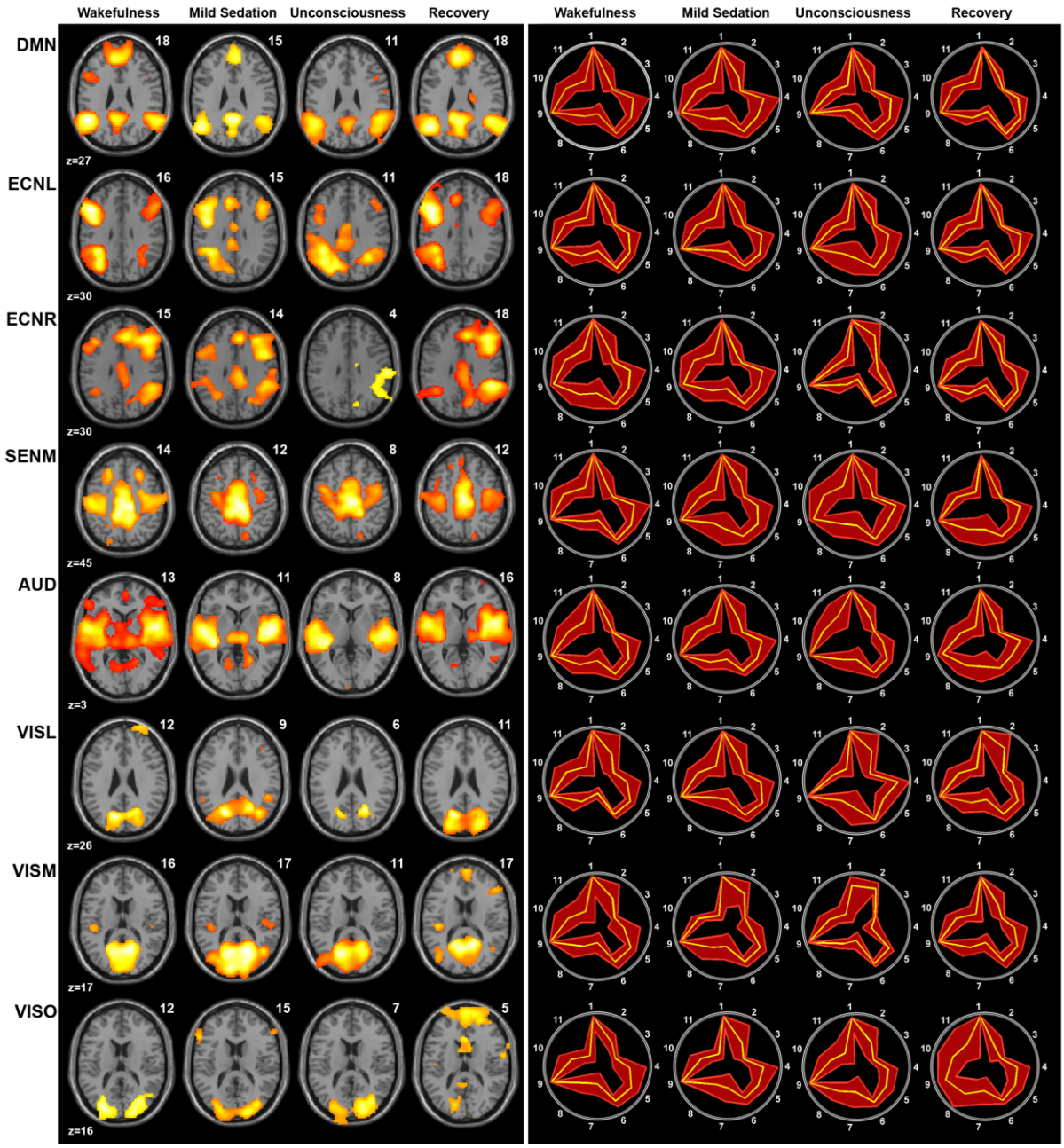

Figure 3.2. Left: spatial maps of the average of the detected RSNs per RSN and per consciousness condition (false discovery rate corrected p < 0.05). Salience and cerebellum RSNs are not depicted due to low detectability. Numbers above the brain slices indicate the number of subjects in which the RSN was detected. DMN = default mode network, ECNL = left external control network, ECNR = right external control network, SENM = sensorimotor network, AUD = auditory network, VISL = lateral visual network, VISM = medial visual network, VISO = occipital visual network. Right: accompanying fingerprints; legend: 1, clustering; 2, skewness; 3, kurtosis; 4, spatial entropy; 5, one lag autocorrelation; 6, temporal entropy; 7, 0–0.008 Hz; 8, 0.008–0.02 Hz; 9, 0.02–0.05 Hz; 10, 0.05–0.1 Hz; 11, 0.1–0.25 Hz. The yellow line represents the mean values, while the red lines represent the standard deviation.

In mild sedation, no major spatial changes in connectivity within RSN components were observed. During unconsciousness, the DMN encompassed only the posterior cingulate cortex (PCC)/precuneus and bilateral inferior parietal cortices, therefore lacking the connectivity to the medial prefrontal cortex seen during all other levels of consciousness. A decrease in functional connectivity could also be detected in bilateral inferior frontal cortices of both left and right ECNs during unconsciousness. Statistical analysis was consistent with these observed trends at a low threshold ($p < 0.001$ uncorrected, or $p < 0.05$ uncorrected), showing frontal disconnection with decreasing consciousness according to the contrast [wakefulness: 1, mild sedation: -0.5, unconsciousness: -1.5 and recovery: 1] (supplementary material figure 3.1, left side). Effect sizes for these frontal components of the DMN and bilateral ECNs, as well as frontal components of the five other RSNs, were calculated for each consciousness condition, and illustrated frontal disconnections within each RSN (supplementary material figure 3.1, right side).

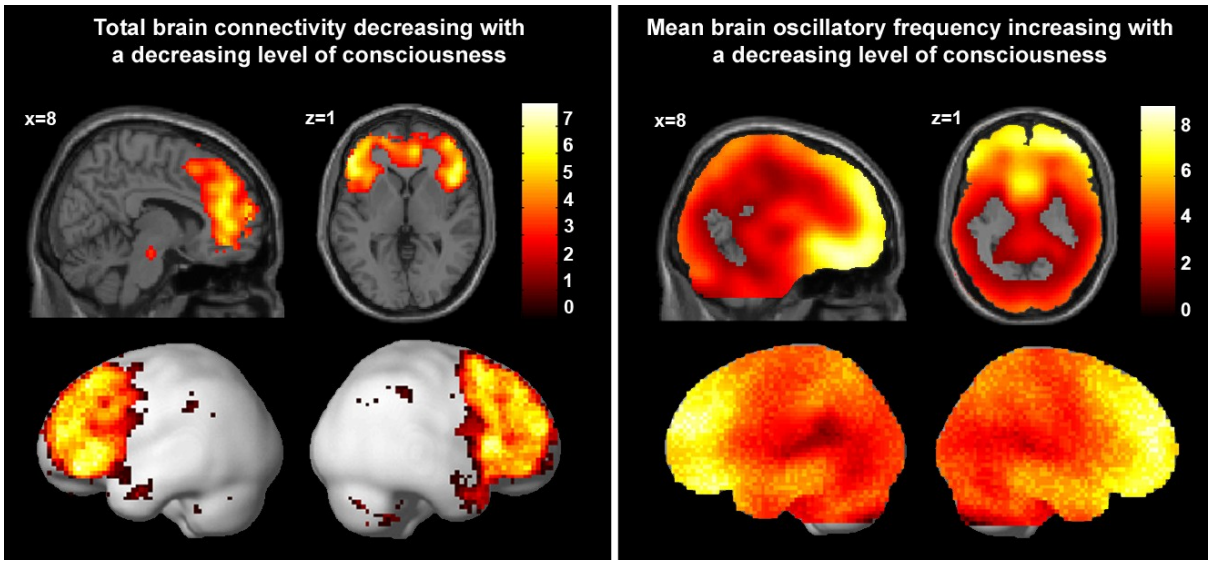

Figure 3.3. Left: brain regions in which decreased connectivity correlated with loss of consciousness, using the following contrast: wakefulness: 1, mild sedation: -0.5, unconsciousness: -1.5, and recovery: 1; at false discovery rate corrected $p < 0.05$. The total connectivity map was based on the data of 14 of the 18 subjects, as no neuronality was detected in four subjects during unconsciousness. Right: brain regions in which loss of consciousness correlated with increased mean oscillatory frequencies of the BOLD signal, according to the contrast: wakefulness: -1, mild sedation: 0.5, unconsciousness: 1.5, and recovery: -1; at false discovery rate corrected $p < 0.05$. This map was constructed using the data from all 18 subjects.

A total brain connectivity map was constructed from all of the independent components that were neuronal according to our neuronality classifier (supplementary material figure 3.2).[73] The number of detected neuronal components was significantly lower during unconsciousness than during the other three conditions. Connectivity in the medial frontal cortex, bilateral inferior/medial frontal cortices, anterior temporal and inferior parietal cortices, as well as the cerebellum and mesopontine area, decreased with loss of consciousness (false discovery rate corrected $p < 0.05$; figure 3.3, and table 3.1 of the supplementary material).

Mean oscillatory frequency analysis of the BOLD signal showed a strong, widespread increase in mean oscillatory frequency during propofol-induced loss of consciousness, with mean oscillatory frequency values approaching or surpassing 0.1 Hz (table 3.1, and figure 3.3). This effect appeared to be particularly strong in the frontal and temporal cortices.

For the generalized Ising model, when considering properties which do not imply the matching of the spin position with a particular region of interest of the brain, we found a behavior consistent with a two dimensional Ising model with equal nearest neighbor couplings. The mean energy of the system (figure 3.4a) showed an increase with the temperature T of the thermal bath with a continuous transfer of thermal energy to the system of spins. The mean magnetization (figure 3.4b) quantifying the level of order of the system decreased with temperature, showing an important transition from the ordered to the disordered phase at a temperature $T = 1.1 \pm 0.2$, which we call critical temperature T_c. The transition was also visible in the energy behavior and was strongly pronounced in figures 3.4c and 3.4d, showing respectively the specific heat and the susceptibility of the system, which presented a maximum at the critical temperature. For each temperature, a correlation matrix between the spins' time-courses simulating the BOLD signal in the corresponding region of interest was generated. In figure 3.5, the distance between the simulated correlation matrix at temperature T and the empirical correlation matrix, based on resting state fMRI data, was plotted versus temperature (the generalized Ising model, contrary to the classical form with equal couplings, allowed us to match the simulated correlation matrix with the empirical one element by element). This showed a minimum at temperature $T_{min} = 1.4 \pm 0.3$, which appeared statistically different from the critical temperature (p-value < 0.01, as tested with a t-test). Four different correlation matrices for $T < T_c$, $T = T_c$, $T > T_c$ and $T = T_{min}$, respectively, are also shown in figure 3.5, together with the empirical correlation matrix, showing a much better visual agreement with the empirical matrix for $T = T_c$ and $T = T_{min}$. In

figures 3.3 and 3.4 of the supplementary material, the linear correlation values between the left precuneus (supplementary figure 3.3) and right precuneus (supplementary figure 3.4) with all the other regions of interest are reported for $T < T_c$, $T = T_c$, $T > T_c$ and $T = T_{min}$, together with the corresponding correlation values extracted from the empirical matrix. In the same figures, the structural couplings J_{ij} between the left and right precuneus and all the other regions are also shown. Both figures 3.3 and 3.4 show a better agreement between the correlation scores of the empirical and simulated matrices at $T = T_c$ ($r = 0.48 \pm 0.04$) and $T = T_{min}$ ($r = 0.47 \pm 0.03$), as compared to the other two cases at $T < T_c$ ($r = 0.35 \pm 0.01$) and $T > T_c$ ($r = 0.38 \pm 0.04$).

With increasing temperature of the thermal bath, not only the mean energy but also the mean oscillatory frequency of the BOLD signal increased (figure 3.6a). Fitting the data with the standard Matlab 2013a curve fitting toolbox function $f(x) = \alpha(1 + \beta * \exp(-\gamma/x))$, we obtained the fitting parameters $\alpha = 0.119\ (0.117, 0.121)$, $\beta = 0.618\ (0.636, 0.692)$ and $\gamma = 0.665\ (0.620, 0.702)$. In figure 3.6b, we reported the mean oscillatory frequency of the BOLD signal over the 15 healthy subjects for each of the 83 regions of interest versus the corresponding normalized FDG-PET values. Fitting the data with the function $f(x) = \alpha(1 + \beta * \exp(-x/\gamma))$, we obtained the fitting parameters $\alpha = 0.091\ (0.090, 0.092)$, $\beta = 0.086\ (0.054, 0.119)$ and $\gamma = 0.238\ (0.032, 0.445)$ (figure 3.6b). Inverting the relationship $f(x) = \alpha(1 + \beta * \exp(-x/\gamma))$, we could obtain $f^{-1}(x) = -\gamma \log[(x - \alpha)/(\alpha * \beta)]$.

Using this inverse relationship, we generated the maps of the estimated FDG-PET values (supplementary figure 3.2b) by first calculating the BOLD signal mean oscillatory frequency scalar maps, voxel by voxel, starting from the BOLD signal for each of the four different conditions of dataset 1, and then applying the inverse relationship $f^{-1}(x)$ to generate, voxel by voxel, an estimate of the possible FDG-PET values. Supplementary figure 3.2 shows an important agreement between these maps (supplementary figure 3.2b) and the maps generated by combining all neuronal independent components (supplementary figure 3.2a).

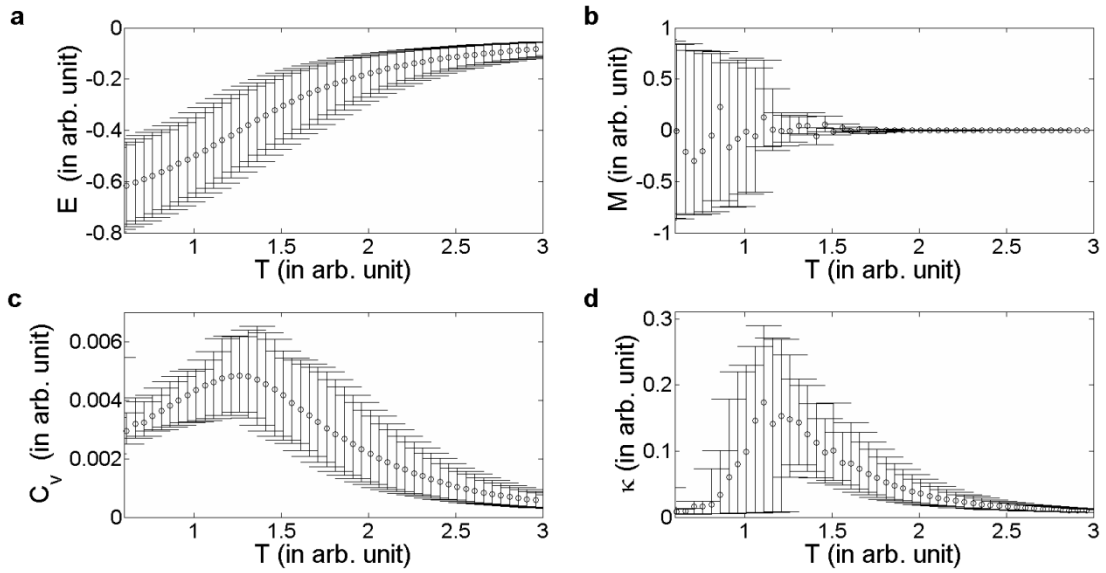

Figure 3.4. For the generalized Ising model: a) equilibrium energy vs. temperature; b) magnetization vs. temperature; c) specific heat vs. temperature; d) susceptibility vs. temperature. Error bars correspond to 90% confidence intervals.

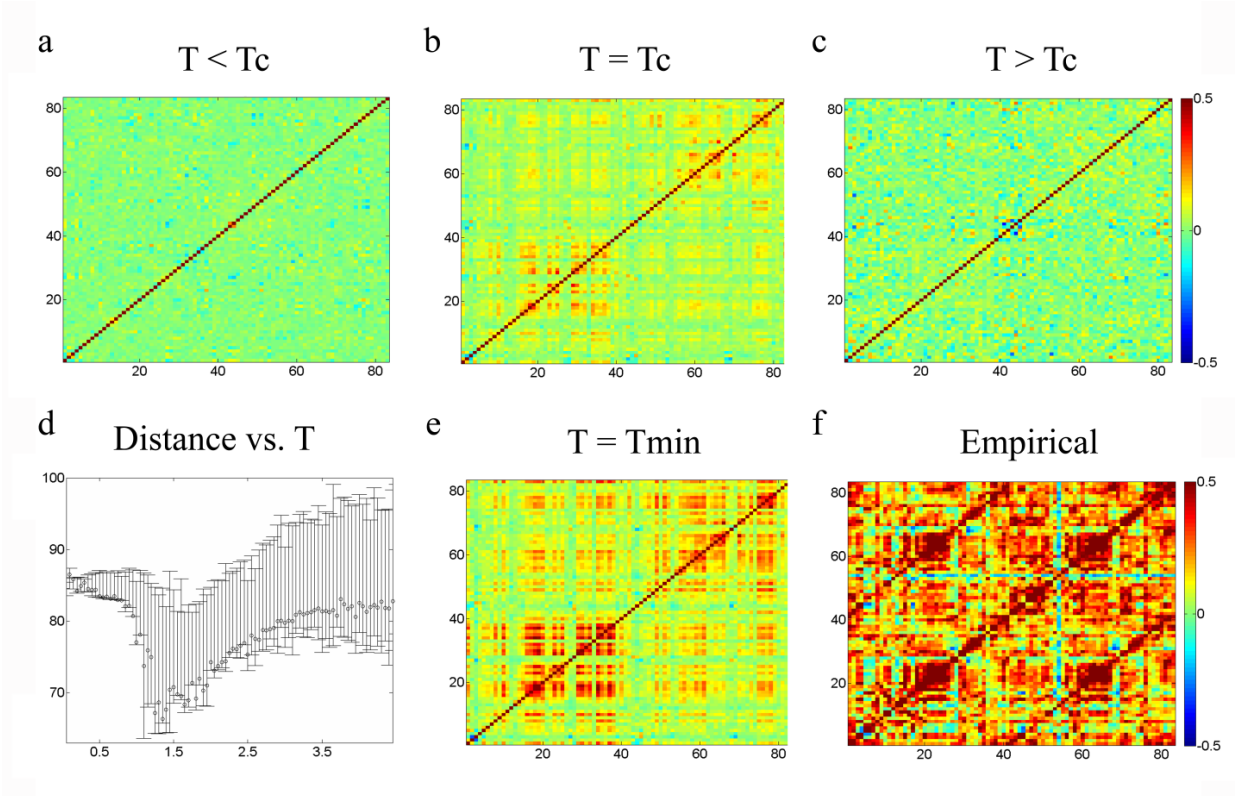

Figure 3.5. For the generalized Ising model: simulated correlation matrices with 83 regions of interest for: a) a temperature value smaller, b) equal to, and c) bigger than the critical temperature value T_c; d) distance between the simulated and the empirical correlation

matrices versus temperature; e) simulated correlation matrix for the temperature corresponding to the minimum distance; and f) the empirical correlation matrix.

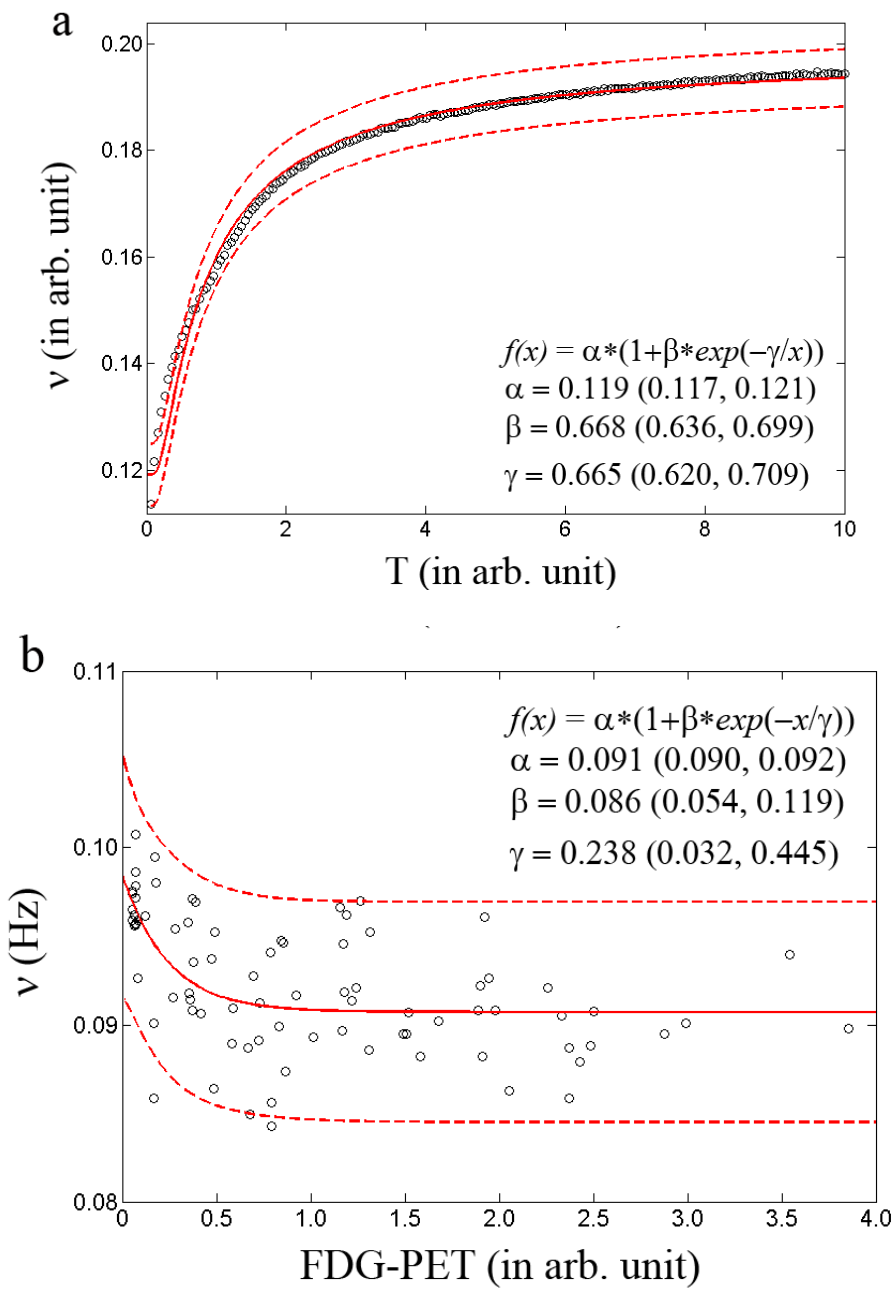

Figure 3.6. Comparison between the BOLD signal mean oscillatory frequency and FDG-PET signal. Upper panel: a) mean frequency over the 83 regions of interest and the all power spectrum for the simulated time courses as a function of temperatures. Lower panel: b) scatter plot of the mean frequency over the all power spectrum for each of the 83 regions of interest fMRI time courses versus the corresponding FDG-PET normalized value. Each data point was obtained by averaging data of the 15 healthy control subjects. Fitting curves and the corresponding fitting parameters are also presented for the two plots.

Table 3.1. BOLD signal mean oscillatory frequency analysis in DMN-associated regions.

Brain region	Coordinates (x,y,z)	Wake-fulness	Mild sedation	Loss of consciousness	Recovery	
ICA						
DMN (whole RSN)		0.053	0.054	0.063	0.052	Average mean frequency
		0.007	0.007	0.013	0.003	Standard deviation
				0.009		P-value of t-test 'mean frequency awake < loss of consciousness'
Seeds DMN regions						
Posterior cingulate cortex/precuneus	-3, -55, 21	0.064	0.069	0.075	0.067	Average mean frequency
		0.006	0.007	0.013	0.003	Standard deviation
				0.005		P-value of t-test 'mean frequency awake < loss of consciousness'
Anterior medial prefrontal cortex	2, 59, 16	0.081	0.083	0.101	0.082	Average mean frequency
		0.009	0.010	0.016	0.008	Standard deviation
				0.000		P-value of t-test 'mean frequency awake < loss of consciousness'
Ventral medial prefrontal cortex	-1, 40, 1	0.072	0.082	0.092	0.076	Average mean frequency
		0.008	0.009	0.011	0.009	Standard deviation
				0.000		P-value of t-test 'mean frequency awake < loss of consciousness'
Pontine tegmental area	-1, -18, -25	0.087	0.090	0.097	0.091	Average mean frequency
		0.007	0.006	0.011	0.005	Standard deviation
				0.005		P-value of t-test 'mean frequency awake < loss of consciousness'
Left thalamus	-5, -11, 7	0.078	0.075	0.090	0.077	Average mean frequency
		0.010	0.009	0.014	0.009	Standard deviation
				0.006		P-value of t-test 'mean frequency awake < loss of consciousness'
Right thalamus	4, -11, 6	0.075	0.073	0.088	0.075	Average mean frequency
		0.008	0.008	0.014	0.006	Standard deviation
				0.002		P-value of t-test 'mean frequency awake < loss of consciousness'
Left parahippo-campal area	-23, -17, -17	0.082	0.083	0.097	0.083	Average mean frequency
		0.009	0.008	0.012	0.010	Standard deviation
				0.000		P-value of t-test 'mean frequency awake < loss of consciousness'
Right parahippo-campal area	25, -16, -15	0.081	0.083	0.095	0.082	Average mean frequency
		0.010	0.010	0.008	0.009	Standard deviation
				0.000		P-value of t-test 'mean frequency awake < loss of consciousness'
Left inferior temporal cortex	-61, -11, -10	0.078	0.083	0.089	0.079	Average mean frequency
		0.007	0.007	0.011	0.008	Standard deviation
				0.001		P-value of t-test 'mean frequency awake < loss of consciousness'

Right inferior temporal cortex	57, -11, -13	0.076	0.081	0.092	0.078	Average mean frequency
		0.006	0.010	0.012	0.008	Standard deviation
				0.000		P-value of t-test 'mean frequency awake < loss of consciousness'
Left superior frontal cortex	-17, 28, 41	0.082	0.089	0.096	0.082	Average mean frequency
		0.006	0.007	0.010	0.005	Standard deviation
				0.000		P-value of t-test 'mean frequency awake < loss of consciousness'
Right superior frontal cortex	17, 29, 41	0.083	0.087	0.098	0.083	Average mean frequency
		0.008	0.007	0.013	0.006	Standard deviation
				0.001		P-value of t-test 'mean frequency awake < loss of consciousness'
Left lateral parietal cortex	-49, -60, 23	0.067	0.070	0.075	0.069	Average mean frequency
		0.006	0.005	0.015	0.004	Standard deviation
				0.050		P-value of t-test 'mean frequency awake < loss of consciousness'
Right lateral parietal cortex	45, -61, 21	0.066	0.070	0.076	0.070	Average mean frequency
		0.007	0.005	0.013	0.006	Standard deviation
				0.010		P-value of t-test 'mean frequency awake < loss of consciousness'
Seeds non-DMN regions						
Left medial temporal cortex	-52, -53, -5	0.044	0.044	0.036	0.044	Average mean frequency
		0.037	0.038	0.042	0.039	Standard deviation
				0.658		P-value of t-test 'mean frequency awake < loss of consciousness'
Right medial temporal cortex	52, -57, -5	0.043	0.043	0.078	0.043	Average mean frequency
		0.033	0.034	0.165	0.034	Standard deviation
				0.435		P-value of t-test 'mean frequency awake < loss of consciousness'
Supplementary motor area	2, 5, 46	0.075	0.076	0.087	0.077	Average mean frequency
		0.007	0.007	0.016	0.007	Standard deviation
				0.010		P-value of t-test 'mean frequency awake < loss of consciousness'
Left superior temporal cortex	-49, -3, 7	0.070	0.072	0.083	0.073	Average mean frequency
		0.006	0.006	0.013	0.005	Standard deviation
				0.001		P-value of t-test 'mean frequency awake < loss of consciousness'
Right superior temporal cortex	49, 1, 5	0.068	0.072	0.085	0.071	Average mean frequency
		0.009	0.007	0.013	0.006	Standard deviation
				0.000		P-value of t-test 'mean frequency awake < loss of consciousness'

3.5. Discussion

In this study, we used a recently developed method to examine total brain connectivity changes during propofol-induced mild sedation and unconsciousness and, subsequently, performed a study of the BOLD signal mean oscillatory frequency. Finally, we interpreted these results using a generalized Ising model. First, however, we examined detectability and connectivity changes for ten well-documented RSNs.[41]

Separate RSNs

In resting state fMRI, an often used analysis routine is to identify RSNs in awake, healthy controls and subsequently assume that these networks can be relatively reliably detected in different consciousness conditions and in patients with brain damage. In such an approach, an ICA component will be attributed to each known RSN, even if for certain RSNs there is no true component representing that RSN. Therefore, in our approach, we only considered RSNs that were reliably detected, based on spatial fit and temporal/data distribution information (neuronality[106]). The neuronality classifier we used was created by machine learning that resulted in a good discriminator between neuronal and non-neuronal components.[73, 106] Indeed, we found a significant difference in RSN detectability between the consciousness conditions, being lowest during unconsciousness. Although three different networks (DMN & ECN left and right) had 100% detectability during wakefulness, recovery of consciousness, or both, none of the ten RSNs could be detected in all of the subjects during any of the sedation levels. This suggests that the detectability of RSNs is highly dependent on brain state and level of consciousness, similar to findings in patients with disorders of consciousness.[73] Of the four higher-order RSNs we considered, which were the DMN, left ECN, right ECN and salience network, only the salience network had low detectability rates. Of the lower-order RSNs, the cerebellum had the lowest detectability rates. The remaining eight RSNs could be detected in above 70% of the subjects during wakefulness. They consisted of a spatial distribution similar to that described in literature.[41] Interestingly, each of the eight well-detected RSNs had at least one frontal component, with which RSN connectivity had a tendency to decrease during loss of consciousness. For the DMN and bilateral ECN, this involved core RSN structures. With lower-order RSNs, it involved a form of frontal connectivity which might be

related in part to attention modulation processes.[63] Total brain connectivity analysis gave us further insight into propofol-induced frontal cortex connectivity changes.

Total brain connectivity

For each consciousness condition, we constructed a total brain connectivity map. This map consisted of independent components that were considered to be of neuronal origin, as assessed by the neuronality classifier, without applying spatial constraints. The number of components used for this map was significantly lower during unconsciousness than during the other three conditions, suggesting a drop in neuronal low-frequency connectivity. When using a contrast to examine connectivity decreases of total brain connectivity during loss of consciousness, we found that the decreases were mostly centered within the frontal cortex and anterior temporal cortex, while sparse connectivity decreases could also be detected in the bilateral inferior parietal cortices, cerebellum, and mesopontine area.

An interesting overlap of the total brain connectivity finding of frontal disconnection is found when comparing it to electroencephalography (EEG) measurements during propofol-induced unconsciousness. EEG shows that during alert wakefulness, alpha activity is prominent in the occipital and parietal cortices, while propofol-induced unconsciousness results in an increase of highly coherent alpha-waves in the frontal cortex in a process called anteriorization.[53] Alpha anteriorization resembling that produced by propofol can also be found during sevoflurane-, isoflurane- and thiopental-induced anesthesia.[54-57] Furthermore, a similar anteriorization is seen in cases of alpha coma.[58] Recent research shows that alpha activity might be a hallmark of selective inhibition of brain activity in a region in order to maintain, strengthen or shift attentional focus established by other brain regions.[59-63] Moreover, increased alpha power has been related to a decrease in resting state fMRI connectivity.[159] A model has been proposed that describes how thalamic activity might drive propofol-induced coherent alpha-activity in the frontal lobe, inhibiting consciousness processes.[121] Possible frontal cortex deactivation is also seen during non-rapid eye movement (non-REM) sleep, where increased slow delta waves are associated with decreased frontal cortex metabolism as measured with FDG-PET.[160, 161] Furthermore, similar slow wave activity, being most prominent in frontal and inferior parietal cortices, has been observed during temporal lobe seizures.[162]

Numerous PET studies report on propofol-induced brain metabolism decreases. Regional cerebral blood flow (rCBF) PET studies have shown that propofol-induced unconsciousness is associated most with decreased blood flow in the thalamus and PCC/precuneus.[48-52] Most severe reductions in glucose use were seen in the thalamus, parietal and frontal DMN regions, and occipital lobe.[49, 163] Oxygen consumption was found to be most reduced in the occipital/precuneal cortex.[52] In general, PET studies thus associate lost consciousness mostly with metabolic reductions in the thalamus and PCC/precuneus. However, these studies show absolute decreases in metabolism. When depicting the relative decreases, the emphasis of decreased rCBF can be found in most ECN- and DMN-related regions, with only a relatively minor decrease in rCBF in the thalamus.[52] This is more similar to our total brain connectivity map. Frontal disconnection, as seen with total brain connectivity, might result in decreased activity in frontoparietal RSNs, like the DMN and ECN, which we found using network-based analysis. Studies of brain metabolism during sleep have reported that REM sleep-associated reductions could be found in regions overlapping with bilateral ECNs, while non-REM sleep also showed pronounced decreases in the thalamus, posterior cingulate and medial frontal cortex.[164] It is tentative to speculate that this results in deactivation of DMN and ECN activity in non-REM sleep, while in REM sleep, DMN functioning might be present, possibly underlying internal but not external awareness aspects associated with REM sleep. Interestingly, restoration of medial frontoparietal activity during REM sleep was associated with increased metabolism in the pontine tegmentum, thalamus and anterior cingulate cortex.[164] This hints at a role of the thalamus and frontal cortex in the restoration of REM internal awareness. Indeed, restored thalamocortical connectivity has also been associated with recovery of a patient from VS/UWS,[139, 165] while increased frontal cortex activity has been associated with Zolpidem-induced paradoxical improvements in behavioral responses of a patient in MCS.[166]

Using classical resting state fMRI with seed-voxel analysis and ICA, frontal disconnection has been found within the DMN and ECN during propofol-induced unconsciousness,[47, 140] as well as severe disintegration of the salience network.[140] Moreover, DMN frontal disconnection has been observed in non-REM sleep,[85, 167] and DMN connectivity decreases, including the frontal cortex, have been found in MCS, VS/UWS and coma.[72] Interestingly, we found that a mesopontine area was also among the regions decreasing in the total brain connectivity map. Decreased connectivity between this region and DMN structures has previously been described for propofol-induced unconsciousness.[47, 140] The brainstem contains a major part of the ascending reticular arousal system.[108, 124] This main brain arousal system is

composed of the brainstem, thalamus and basal forebrain regions,[108] and microinjection of pentobarbital in the mesopontine tegmental region in rats has been shown to result in a condition resembling general anesthesia.[91]

BOLD signal mean oscillatory frequencies

Our mean frequency analysis showed widespread increases in the mean oscillatory frequency of the BOLD signal with loss of consciousness, to around a value of 0.1 Hz. This increase appeared especially clear in the frontal, temporal and mesopontine areas; regions showing total brain connectivity disconnection during propofol-induced loss of consciousness. Mean oscillatory frequency analysis methods, comparable to those used in this analysis, might be employed as a biomarker of the brain's integrative power and level of consciousness. This could be particularly useful when dealing with the challenging diagnosis of patients with disorders of consciousness.[11, 24, 165] The main RSN examined in these patients has traditionally been the DMN, as examination of its integrity has shown its potential as a biomarker of consciousness.[15, 72] Examining mean frequencies of the BOLD signal in regions associated with the DMN (or other higher-order RSNs) in patients with disorders of consciousness, and comparing them with those found in awake healthy controls, could indicate if regions show a marked increase in mean oscillatory frequency. Strong increases in BOLD signal mean oscillatory frequencies within DMN regions might serve as a measure of disruption of the network. However, a better understanding of the mechanisms underlying mean oscillatory frequency changes is necessary.

Our results suggest that examining resting state fMRI connectivity at 'neuronal' frequencies between 0.007 and 0.1 Hz might only be part of a bigger story. As propofol-induced unconsciousness has led to increased mean oscillatory frequencies of the BOLD signal, it could be that such an increase is a common feature of decreased brain information integration. If so, such increases might be also be expected in other conditions of altered consciousness. It needs to be examined how much of the higher BOLD signal mean oscillatory frequencies might be caused by still functioning neuronal sources, and how these originate. It does however appear to be informative to also examine BOLD signal mean oscillatory frequencies that are higher than what is classically considered neuronal in conditions of altered consciousness. Furthermore, we explored indications that BOLD signal mean oscillatory frequencies might be related to metabolism, as seen with PET.

Generalized Ising model

The importance of accompanying statistical analysis, such as independent component analysis, with modeling, like the generalized Ising model, is widely recognized in the neuroscientific community. The generalized Ising model, contrary to models like the neural mass model, is very simple in its structure, having only one single fitting parameter: the thermal bath temperature. And by using the generalized form in which couplings are extracted from the fibers' distribution in the brain, and with spins representing the activity in specific regions of interest, it is possible to model the functional connectivity patterns in a relatively realistic manner. In this work, we also showed that an awake brain is described by a generalized Ising model 'sitting' at the critical temperature. We have shown that a reduction in arousal induced by propofol produces important changes in functional connectivity patterns. This change can be seen in the generalized Ising model at temperatures deviating from the critical temperature. The increase in the mean oscillatory frequency of the BOLD signal under anesthesia, consistent with an increase in mean frequency of oscillating spins with increasing temperature of the generalized Ising model, suggests that the effect of propofol can be modeled by an increase in temperature from the critical value. This motivated us to reconsider the observed increase in frequency induced by propofol as a possible change in the neuronal behavior of the BOLD signal, considering that the generalized Ising model has been simulated to capture only the neuronal component of the BOLD signal and not other artifactual sources.

3.6. Conclusion

In this study, we examined propofol-induced brain changes using different methods. Firstly, we examined the detection rate and integrity of ten well-known RSNs, showing a decreased detection rate and frontal cortex connectivity of these networks during unconsciousness. Secondly, we examined total brain connectivity changes. This showed that RSN connectivity with 'neuronal' frequencies decreased with propofol administration in the frontal, temporal and brainstem areas. Thirdly, we examined BOLD signal mean oscillatory frequency changes. Regions associated with those found disconnected with total brain connectivity analysis were found to show the highest frequency increases, although frequency increases were widespread.

The frontal cortex disconnection shows great resemblance with the anteriorization behavior of alpha brain waves as seen with EEG, which have been associated with inhibited brain activity.[59-63] The frontal cortex is thought to have an important steering role in pivotal cognitive aspects like attention and working memory,[168] and its disruption could influence activity in the whole brain. However, more research is needed to give more insight into the relationship between brain connectivity, BOLD signal mean oscillatory frequencies, metabolism, and electrical oscillatory activity. Automated RSN detection, total brain connectivity analysis, and BOLD signal mean oscillatory frequency analysis are likely to become useful additions to the neuroimaging analysis arsenal in clinical and research settings.[11] Modeling the structure-function relationship with simple models, like the generalized Ising model, can give further insight and can help to interpret RSN connectivity changes. Finally, our results suggest the usefulness of examining BOLD signal oscillatory frequencies that exceed those classically associated with neuronal resting state fMRI connectivity.

3.7. Supplementary material

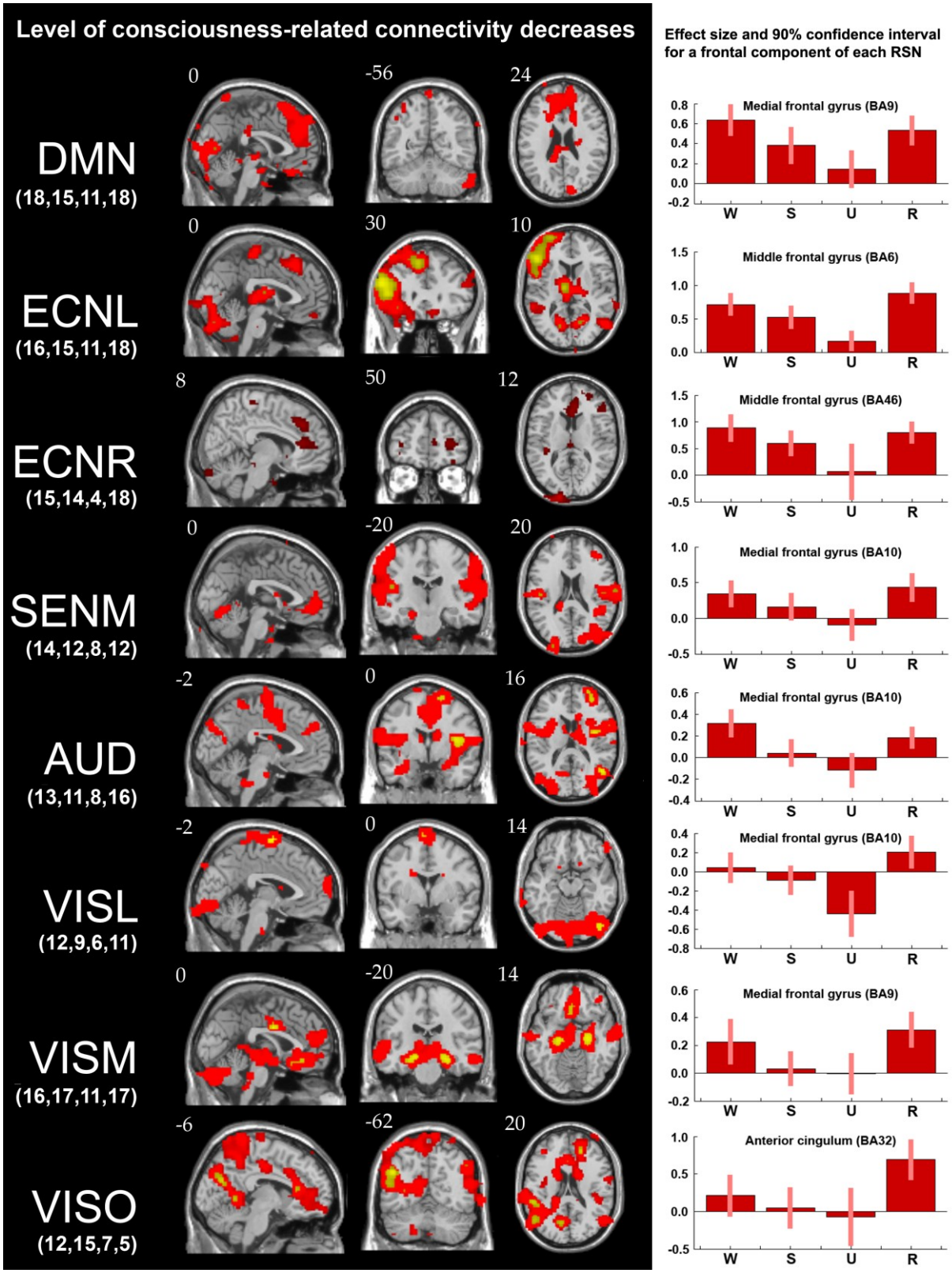

Figure 3.1. Left: areas of decreasing connectivity within each RSN correlating with loss of consciousness (contrast: wakefulness: 1, mild sedation: -0.5, unconsciousness: -1.5 and recovery: 1). For illustrative purposes, results are thresholded at p < 0.05 uncorrected (red areas) and p < 0.001 uncorrected (yellow areas). DMN = default mode network, ECNL = left external control network, ECNR = right external control network, SENM = sensorimotor network, AUD = auditory network, VUSK = lateral visual network, VISM = medial visual network, VISO = occipital visual network. Numbers under the names of the RSNs represent the number of subjects in which the component was detected (in the order: wakefulness, mild sedation, unconsciousness, recovery). Right: effect sizes and 90% confidence intervals of a frontal component of each RSN are depicted. W = wakefulness, S = mild sedation, U = unconsciousness, R = recovery. BA = Brodmann area.

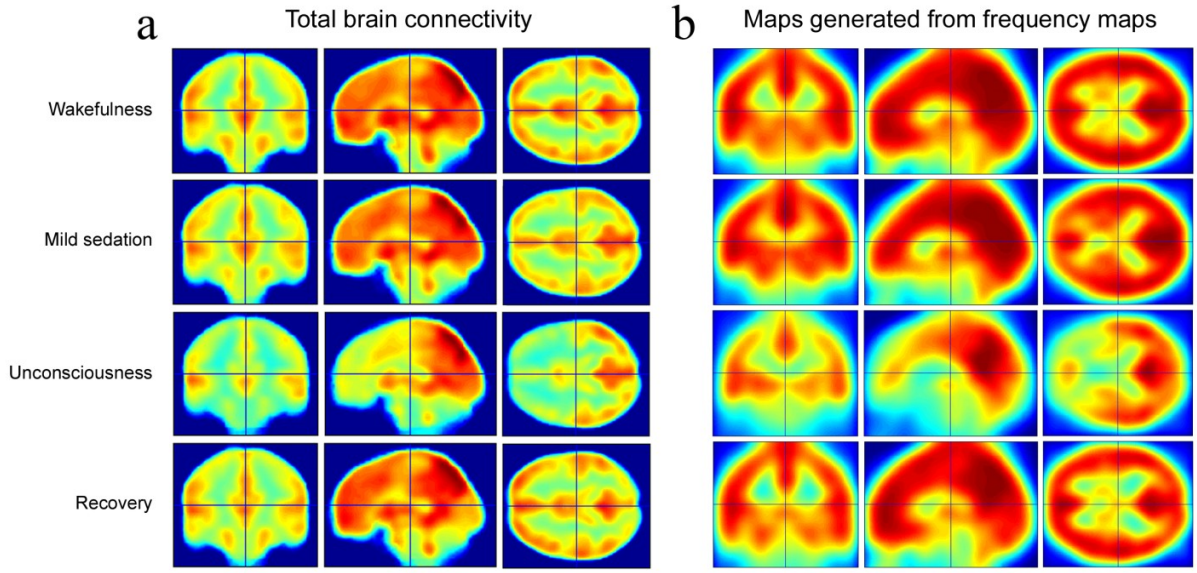

Figure 3.2. a) Total brain connectivity maps per consciousness condition. b) Simulated FDG-PET maps generated by applying the found equation of the inverse relationship between BOLD signal mean oscillatory frequencies and empirical PET values to the BOLD signal mean oscillatory frequency maps per consciousness condition.

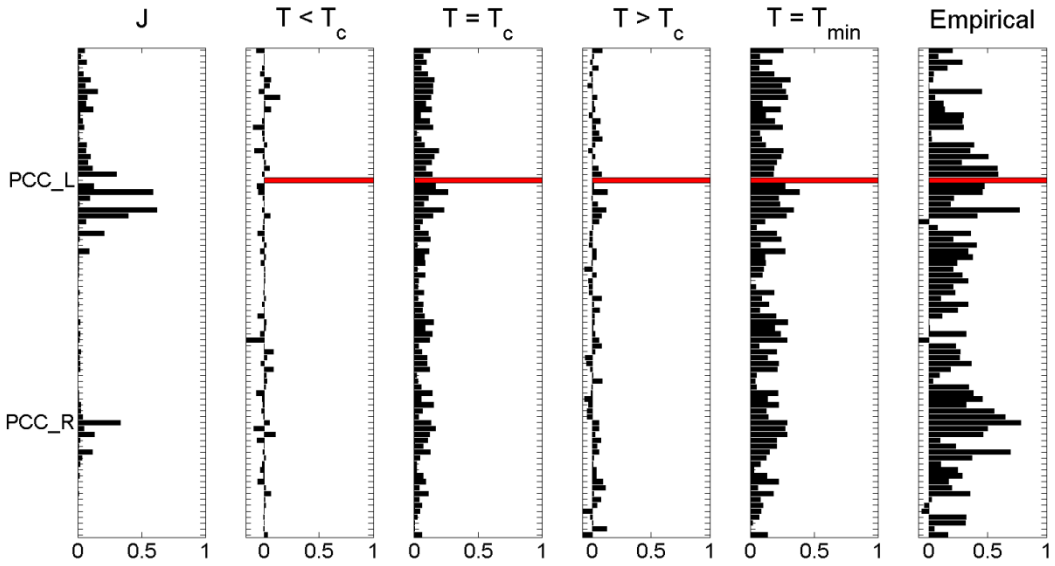

Figure 3.3. From left to right: structural coupling J_{ij} with I = PCC left, linear correlation values between the spin time course of PCC left and the 83 regions of interest for $T < T_c$, $T = T_c$, $T > T_c$ and T_{min} and the corresponding empirical correlation values.

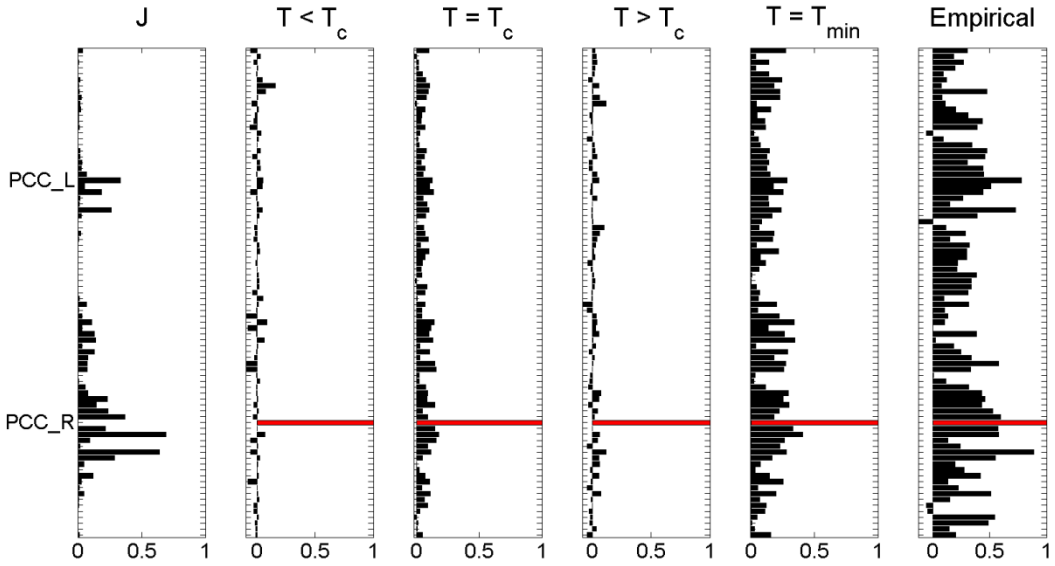

Figure 3.4. From left to right: structural coupling J_{ij} with I = PCC right, linear correlation values between the spin time course of PCC right and the 83 regions of interest for $T < T_c$, $T = T_c$, $T > T_c$ and T_{min} and the corresponding empirical correlation values.

Table 3.1. Regions in which connectivity decreases were correlated to loss of consciousness.

BA	Area	X	Y	Z	Z-value	P-value FDR
8	Superior Frontal Gyrus	33	56	16	6.02	0.000
8	Superior Frontal Gyrus	-21	32	49	5.94	0.000
10	Superior Frontal Gyrus	27	62	-8	3.17	0.008
10	Superior Frontal Gyrus	21	65	-8	2.82	0.021
10	Superior Frontal Gyrus	-6	65	-8	2.57	0.038
10	Middle Frontal Gyrus	-45	59	-11	2.61	0.036
11	Superior Frontal Gyrus	-12	47	-17	2.99	0.013
11	Middle Frontal Gyrus	-42	38	-14	5.82	0.000
11	Medial Frontal Gyrus	-6	62	-14	3.49	0.003
11	Superior Frontal Gyrus	-24	41	-17	2.78	0.023
11	Middle Frontal Gyrus	-21	38	-14	2.56	0.039
11	Middle Frontal Gyrus	-15	41	-14	2.53	0.043
11	Superior Frontal Gyrus	24	53	-29	2.56	0.040
11	Orbital Gyrus	21	50	-32	2.72	0.027
32	Anterior Cingulate	-12	29	-11	2.52	0.044
39	Angular Gyrus	51	-70	37	2.51	0.045
39	Angular Gyrus	57	-64	34	2.56	0.040
39	Angular Gyrus	60	-58	37	2.61	0.035
20	Inferior Temporal Gyrus	-45	-10	-32	2.47	0.050
20	Fusiform Gyrus	-60	-7	-26	3.37	0.004
21	Middle Temporal Gyrus	-48	2	-32	2.90	0.017
38	Superior Temporal Gyrus	-30	17	-26	2.89	0.017
38	Superior Temporal Gyrus	-33	20	-29	3.03	0.012
38	Uncus	-24	5	-38	3.42	0.004
40	Inferior Parietal Lobule	60	-49	46	2.51	0.045
40	Inferior Parietal Lobule	-63	-40	43	2.73	0.026
40	Inferior Parietal Lobule	63	-37	43	3.30	0.005
40	Supramarginal Gyrus	-66	-43	37	3.23	0.007
40	Inferior Parietal Lobule	-66	-34	31	2.78	0.023
40	Supramarginal Gyrus	-63	-55	28	2.69	0.029
13	Insula	-42	-10	13	2.59	0.037
6	Precentral Gyrus	63	-4	40	2.69	0.029
23	Cingulate Gyrus	6	-19	25	3.19	0.008
	Mesopontine area	12	-19	-17	3.16	0.008
	Inferior Semi-Lunar Lobule	30	-70	-35	2.96	0.014
	Inferior Semi-Lunar Lobule	18	-70	-35	2.92	0.016
	Inferior Semi-Lunar Lobule	39	-70	-38	2.84	0.020
	Cerebellar Tonsil	-27	-61	-35	2.91	0.017
	Cerebellar Tonsil	-45	-40	-41	2.83	0.020
	Cerebellar Tonsil	48	-43	-38	2.66	0.031
	Cerebellar Tonsil	36	-46	-44	2.99	0.013
	Cerebellar Tonsil	45	-40	-35	2.50	0.046
	Pyramis	-9	-76	-29	3.15	0.008
	Pyramis	-33	-67	-32	2.54	0.042
	Pyramis	27	-76	-32	2.70	0.028
	Uvula	-15	-70	-32	2.69	0.029

Chapter 4

PROPOFOL SEDATION IN PATIENTS WITH DISORDERS OF CONSCIOUSNESS:

EFFECTS ON REMAINING BRAIN CONNECTIVITY

Corresponding article:

Sedation of Patients with Disorders of Consciousness during Neuroimaging: Effects on Resting State Functional Brain Connectivity

M. Kirsch*[1,2], P. Guldenmund*[1], M. Bahri[1], A. Demertzi[1], K. Baquero[3], L. Heine[1,5], V. Charland[1,5], M. Thonnard[1,5], A. Vanhaudenhuyse[1,6], M.-A. Bruno[1,5], O. Gosseries[1,5], V. Bonhomme[1,2,4], J.-F. Brichant[2], C. di Perri[1], E. Ziegler[1], S. Laureys[1,5].

*Authors contributed equally.

(1) Coma Science Group, Cyclotron Research Center, University of Liège, Belgium. (2) Department of Anesthesia and Intensive Care Medicine, CHU Sart Tilman Hospital, University of Liège, Belgium. (3) National University of Colombia, Bogotá, Colombia. (4) Department of Anesthesia and Intensive Care Medicine, CHR Citadelle, University of Liège, Belgium. (5) Department of Neurology, CHU Sart Tilman Hospital University of Liège, Belgium. (6) Department of Algology and Palliative Care, University Hospital of Liège, University of Liège, Belgium.

4.1. Abstract

Detecting consciousness in post-coma patients with disorders of consciousness (DOC) is of upmost importance for caretaking and ethical reasons. Neuroimaging has become a valuable addition to behavioral assessments, with resting state functional magnetic resonance imaging (resting state fMRI) being one of the methods. Unfortunately, patients frequently move uncontrollably in the scanner, thereby dramatically decreasing image quality. This impairs detection of the patterns of brain connectivity used for differential diagnosis. Physical restraint techniques are not the full solution, nor are post-acquisition data improvement methods. Therefore, sedation with the anesthetic propofol is an often used technique to minimize patient movement. However, little is known about the effects of propofol sedation on brain connectivity patterns in the damaged brain. In this study, we aimed to assess these effects.

Using resting state fMRI, we applied a seed-based analysis method to compare long-range resting state connectivity in seven well-known resting state networks, and connectivity with the thalamus, in 20 healthy controls, 8 unsedated patients with DOC, and 8 patients with DOC sedated with propofol. The DOC groups were matched for diagnosis, age, time spent in DOC, heart rate, breathing rate, movement intensities, and pattern of brain damage (as assessed with voxel-based morphometry).

Compared to healthy controls, unsedated patients with DOC had severely impaired resting state network connectivity in all but the visual network. Thalamic connectivity to higher-order network regions was also reduced. Propofol administration in patients was associated with a minor further decrease in thalamic connectivity and connectivity in the salience network.

Our results are a first attempt to characterize the effect of propofol sedation in DOC. Although more research is needed on this topic, the findings presented here indicate that possible connectivity decreases associated with propofol sedation are relatively small compared to those already caused by DOC-associated structural brain damage. Given that typical patient motion in the MRI scanner has previously been shown to greatly decrease resting state network detectability, patient sedation might presently be considered a useful strategy for neuroimaging in patients with DOC that

display strong head movement. Future studies should further examine safety aspects associated with this procedure.

4.2. Introduction

Survivors of severe brain damage may pass into a coma: a state of absent brain arousal (level of alertness) and awareness (content of awareness).[24] Coma usually lasts no longer than three weeks, after which a patient may recover some brain arousal.[24, 169] As still no awareness can be detected, the name unresponsive wakefulness syndrome (previously known as vegetative state; VS/UWS) is used.[139] Brain awareness may return partially (minimally conscious state; MCS) or completely.[170] Coma, VS/UWS and MCS are collectively known as disorders of consciousness (DOC).

Neuroimaging in DOC is applied to improve correctness of the differential diagnosis by helping to detect signs of awareness in patients with limited or absent body control. With active task paradigms, patients can modulate brain activity in a way that is similar to that observed in healthy control subjects performing the tasks. This brain activity can be picked up with functional magnetic resonance imaging (fMRI) or electroencephalography and can even be used to establish a form of limited communication.[71, 171] However, such active brain modulation relies on high degrees of cognitive control, which is rare in patients in MCS. Passive neuroimaging paradigms, for instance the application of a salient sound such as the subject's own name, test the brain's response to the stimulus and do not need great patient cooperation. However, often occurring sensory problems like aphasia could render these paradigms uninformative. Task-free neuroimaging of the brain during the resting state (a non-sleep, mindwandering state[15, 172]) does not have these shortcomings. It is used to compare brain metabolism (with positron emission tomography) or functional brain connectivity (with resting state fMRI, or a combination of electroencephalography and transcranial magnetic stimulation) in patients with healthy controls, inferring consciousness when high similarities are found.[11, 138]

Resting state fMRI looks at spontaneous, oscillatory neuronal activity at the low-frequency range (< 0.1 Hz). Brain regions that show a comparable activity oscillation are thought to be functionally connected in a resting state network (RSN). A set of robustly detected RSNs includes the default mode network (DMN), external control networks (ECNs), and the salience network.[41, 173, 174] These higher-order RSNs are associated with internal awareness, external awareness, and saliency detection, respectively.[173] Lower-order RSNs include the auditory, visual and sensorimotor RSNs.

The integrity of higher-order RSNs, and especially the DMN, has been shown to be indicative of the level of consciousness during sleep,[85] anesthesia,[47, 86, 114, 140] and in DOC.[15, 72, 73, 101, 175-177] Current diagnostic examinations of DOC also include the other RSNs to gain a more complete picture of disturbed brain functioning.[73, 173] Additionally, thalamocortical connectivity changes have also been shown to play a role in DOC.[72, 175, 178]

Acquisition of resting state fMRI in patients with DOC is a challenging operation. One of the main problems is restraining patient head motion, as (resting state) fMRI is exceptionally sensitive to movement. This could induce false-positive 'activations' when motion artifacts are correlated with the stimulus, events of interest or neuronal activation. False-negative 'activations' can result from reduced detection sensitivity due to motion-induced noise.[179] Furthermore, head displacement leads to an altered head position in the scanner, changing slice orientation. Post-scan preprocessing steps cannot fully repair such damaged data, although this has become an active field of research.[180] The problem of movement is especially severe in patients with DOC, as around 40% of patients has been shown to exhibit severe head movement during scanning.[181] Traditional physical head restraint techniques include the placement of foam cushions around the head. Unfortunately, this precaution is often unable to cope with strong motion impulses in patients with DOC. Therefore, an often applied method for head motion reduction is sedation.[182] However, little is known about the possible effects of sedation on resting state connectivity, which is important for differential diagnosis.

In the present study, we examined the effect of sedation on long-range resting state connectivity in patients with DOC, using resting state fMRI. We chose propofol, as this is one of the most well-studied, most applied and safest anesthetic agents available.[45] It is the drug of choice for immobilization purposes in MRI research, as it has short induction and recovery times, and does usually not require additional sedatives.[183] We compared RSN integrity in 8 unsedated patients with DOC that had limited movement in the scanner with 8 patients with DOC, who had been sedated to reduce their high-intensity movement. These groups were matched for age at onset, etiology, time spent in DOC, diagnosis, movement intensities, heart rate, breathing rate, and the coma recovery scale revised (CRS-R) total score, as assessed with a t-test. Equality of structural brain damage was also assessed (using voxel-based morphometry (VBM8; http://dbm.neuro.uni-jena.de/vbm/), for SPM8 (www.fil.ion.ucl.ac.uk/spm)), as was movement intensity.[101] RSN integrity was furthermore compared with 20 age-matched healthy controls. Assessment of

differences between the effects of propofol in VS/UWS and MCS is beyond the scope of this research. We expected patients with DOC to have severely disrupted higher-order RSNs.[73, 173] Given previous examinations of the effect of mild propofol sedation on RSN connectivity in healthy controls,[47, 114, 140] and the fact that patients with DOC might already have severe disruption of RSNs,[15, 72, 73, 101, 175-177] we expected limited effects of propofol sedation on RSN integrity in patients with DOC.

4.3. Methods

Subjects

We used resting state fMRI data from 20 healthy control subjects (mean age = 46 ± 18 years), 8 unsedated patients with DOC (mean age = 44 years ± 16 years, time in DOC = 695 days ± 1169 days, 2 traumatic MCS and 8 non-traumatic VS/UWS, average CRS-R total score = 7 ± 3), and 8 patients with DOC sedated with propofol (mean age = 43 years ± 21 years, time in DOC = 867 days ± 1426 days, 2 traumatic MCS and 8 non-traumatic VS/UWS, average CRS-R total score = 7 ± 4) (table 4.1). For the patients, inclusion criteria were: patients in VS/UWS or MCS, as assessed with the CRS-R; scanning occurred more than 2 weeks after initial brain injury in stabilized patients; propofol was used as the sole sedative agent (for the sedated group); an absence of large hemorrhage effects, movement artifacts, foreign body artifacts, midline shifts, acquisition artifacts, low gray-white matter contrast, or exceptionally large brain damage, as assessed by careful visual inspection of the T1 images by an expert. Both DOC groups were matched for age at onset, etiology, time spent in DOC, diagnosis, movement intensities, heart rate, breathing rate, and CRS-R total score, as assessed with a t-test. The diagnosis of MCS or VS/UWS was based on behavioral analysis with the CRS-R,[184] a standardized scale that is currently considered to be the most trustworthy behavioral diagnosis tool for patients with DOC available.[11, 185] The study was approved by the Ethics Committee of the Medical School of the University of Liège. Informed consent to participate to the study was obtained from the subjects themselves in the case of healthy subjects, and from the legal surrogates of the patients.

Sedation protocol

The decision to sedate the patient or not was taken by an MRI scanning expert and was based on the severity of patient movement when placed in the MRI scanner. The propofol concentration was kept to a minimum. Foam cushion head restraints were placed. Before fMRI data acquisition, all subjects fasted for at least six hours for solids, and two hours for liquids. During scanning, they wore headphones and earplugs. Propofol sedation was administered through intravenous infusion, using a target-controlled infusion system (TCI, Diprifusor®, pharmacokinetic model of

Marsh[186]), to obtain constant plasma concentrations. To insure adequate ventilation, some patients received assisted mechanical ventilation through a tracheostomy or through an endotracheal tube when already in place. Additional oxygen was delivered, either through a facemask, or through the airway instrumentation device.

Table 4.1. Patient characteristics.

Patient	Diagnosis according to CRS-R	Highest CRS-R total score	Etiology	Age at onset (in years)	Time in DOC (in days)	Target Propofol concentration (µg/mL)	Airway device	Ventilation	Heart rate median (range)	Breathing frequency median (range)
U1	VS/UWS	3	nT (anoxia)	44	23	0	Endotracheal tube	Controlled	103 (102-107)	20
U2	VS/UWS	5	nT (meningitis)	54	52	0	Tracheostomy	Spontaneous	74 (60-100)	25 (14-33)
U3	VS/UWS	4	nT (anoxia)	44	20	0	Tracheostomy	Controlled	144 (140-146)	12
U4	VS/UWS	7	nT (CVA)	74	22	0	Tracheostomy	Spontaneous	94 (93-95)	12 (10-14)
U5	VS/UWS	4	nT (anoxia)	48	129	0	Tracheostomy	Spontaneous	113 (112-113)	20 (17-21)
U6	VS/UWS	6	nT (anoxia)	31	2031	0	No	Spontaneous	70 (67-74)	15 (13-18)
U7	MCS	12	T	26	3034	0	No	Spontaneous	64 (60-70)	13 (10-14)
U8	MCS	11	T	30	247	0	No	Spontaneous	67 (57-72)	15 (11-20)
avg	-	7	-	44	695	-	-	-	91	16
sd	-	3	-	16	1169	-	-	-	28	5
S1	VS/UWS	3	nT (anoxia)	73	47	1.8	Tracheostomy	Spontaneous	91 (89-92)	21 (19-21)
S2	VS/UWS	5	nT (hypoglycemia)	53	20	1.0	Endotracheal tube	Controlled	94 (93-100)	16
S3	VS/UWS	6	nT (anoxia)	48	52	2.0	Tracheostomy	Spontaneous	92 (91-93)	28 (25-28)
S4	VS/UWS	6	nT (CVA)	69	17	1.5	Endotracheal tube	Controlled	75 (74-75)	14
S5	VS/UWS	5	nT (anoxia)	16	27	2.5	Tracheostomy	Spontaneous	MD	MD
S6	VS/UWS	6	nT (anoxia)	33	456	1.5	No	Spontaneous	69 (65-72)	16 (11-17)
S7	MCS	13	T	22	2977	1.8	No	Spontaneous	59 (56-61)	16 (16-17)
S8	MCS	13	T	30	3342	1.5	No	Spontaneous	66 (64-67)	9 (8-10)
avg	-	7	-	43	867	1.7	-	-	78	17
sd	-	4	-	21	1426	0.4	-	-	14	6

12 patients in VS/UWS (all non-traumatic) and 4 patients in MCS (all traumatic); CVA = cerebrovascular accident, CRS-R = coma recovery scale revised,[184] DOC = disorders of consciousness, MCS = minimally conscious state, VS/UWS = vegetative state/unresponsive wakefulness syndrome, T = traumatic, n-T = non-traumatic, MD = missing data, U = unsedated subject, S = sedated subject, avg = group's average, sd = group's standard deviation.

Parameters of all patients were closely and continuously monitored during the procedure, including arterial blood pressure, electrocardiogram, breathing frequency, and pulse oxymetry (Sp02). All parameters remained stable during data acquisition. When administered, sedation was titrated to achieve immobility in the scanner. Once obtained, the necessary plasma concentration of propofol was kept constant throughout the procedure. Scanning started 5 minutes after having reached the

desired clinical state (immobility), hence allowing time for the equilibration of propofol concentrations between pharmacokinetic compartments. For *post hoc* confirmation of propofol plasma concentrations, a blood sample was drawn in some patients during the steady-state period of sedation (before and after the sequence). Sedation characteristics are summarized in table 4.1. Throughout the procedure, a certified anesthesiologist and complete resuscitation equipment were present.

Data acquisition

Structural MRI T1 data (T1-weighted 3D gradient echo images using 120 slices, repetition time = 2300 ms, echo time = 2.47 ms, voxel size = 1 x 1 x 1.2 mm^3, flip angle = 9^o, field of view = 256 x 256 mm^2) and resting state fMRI data (Echo Planar Imaging sequence using 32 slices, repetition time = 2000 ms, echo time = 30 ms, field of view = 192 x 192 mm^2, flip angle = 78^o, voxel size = 3 x 3 x 3 mm^3, volumes = 300) were acquired on a 3T scanner (Siemens AG, Munich, Germany).

Assessment of equality of movement intensity and brain morphology

Movement severity was assessed by calculating interscan movement and total head displacement using six rigid-body movement parameters, and a t-test was applied to examine potential differences in movement severity between patient groups.[101] Similarly, a T1-based voxel-based morphometry analysis of brain structure (VBM8 (http://dbm.neuro.uni-jena.de/vbm/) for SPM8 (www.fil.ion.ucl.ac.uk/spm)) was applied to search for potential morphological differences between both patient groups. For this analysis, we used DARTEL-based spatial normalization[187] to allow for high-dimensional spatial normalization to increase the chance of correct normalization in the severely damaged DOC brain.[188] A DOC template made from T1 images from an independent population of 61 patients with DOC was used to further aid the normalization procedure.[187, 189]

RSN analysis

We used SPM8 software (statistical parametric mapping, Wellcome Trust Centre for Neuroimaging (www.fil.ion.ucl.ac.uk)) to realign, normalize, smooth (8 mm kernel), and analyze the data. Movement artifact reduction software was applied (ArtRepair[190]) and data were temporally bandpass-filtered (0.007-0.1 Hz). We performed a seed-based analysis to investigate correlations between low-frequency blood oxygenation level-dependent signals in selected seed regions and the rest of the brain, to examine RSN connectivity. Regions selected for the analysis, based on RSNs described in literature,[41, 47, 87, 114] were the posterior cingulate cortex/precuneus (DMN; 6, -42, 32), left middle frontal gyrus (left ECN; -44, 36, 20), right middle frontal gyrus (right ECN; 44, 36, 20), right anterior insula (salience RSN; 38, 26, -10), left posterior insula (auditory RSN; -40, -22, 8), supplementary motor area (sensorimotor RSN; -2, -12, 44), and primary visual cortex (visual RSN; -4, -84, 8). Connectivity with the thalamus was also examined (-7, -16, 6 and 7, -16, 6, combined).[47, 140] 8 mm spheres around these coordinates were used as seed regions. Movement parameters, as well as white matter and cerebrospinal fluid parameters, were used for removal of sources of noise in the resting state fMRI data.[47] For analysis, patients and controls were organized into three groups: controls, unsedated patients, and sedated patients. Whole brain false discovery rate-corrected (FDR, thresholded at $p = 0.05$) spatial maps were obtained per RSN per group. The three groups were contrasted for examination of DOC-associated and Propofol-induced brain connectivity decreases. The results of these contrasts were masked with the regions of the RSN in question obtained for the control group, and were thresholded at an uncorrected p-value of 0.01 and with a cluster extent threshold of 30 voxels.

4.4. Results

Assessment of equality of movement intensity and brain morphology

A t-test showed no significant difference in movement severity between the patient groups, as assessed using speed and displacement parameters. Differences in gray matter integrity (at a threshold of FDR-corrected p = 0.05) between healthy controls and non-sedated patients with DOC were widespread (figure 4.1). No structural differences could be observed between non-sedated and sedated patients with DOC.

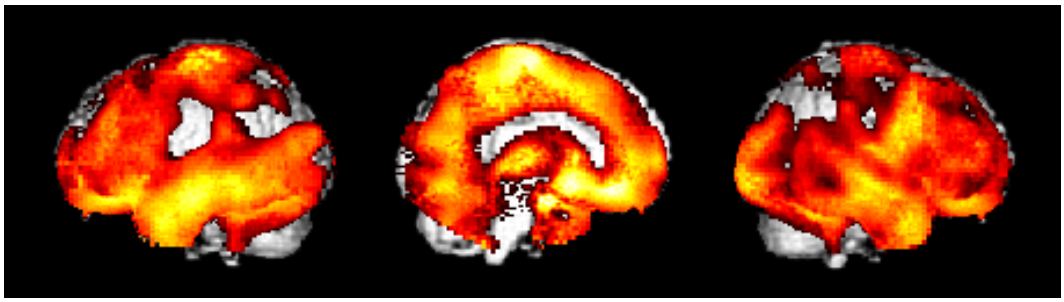

Figure 4.1. Voxel-based morphometry analysis of brain structure differences between controls and patients with DOC (DOC groups combined). DOC was associated with widespread gray matter damage, while no differences in damage could be detected between the groups of sedated and unsedated patients with DOC. Results were thresholded at FDR-corrected p = 0.05.

RSNs

All seven predefined RSNs were reliably detected in control subjects (figure 4.2). At a threshold of FDR-corrected p = 0.05, the DMN consisted of the posterior cingulate cortex/precuneus, inferior parietal lobules, medial prefrontal cortex, medial temporal lobes, dorsolateral frontal cortex, pontine tegmental area, and thalamus. In unsedated and sedated patients with DOC, connectivity was found in the posterior cingulate cortex/precuneus and inferior temporal lobe. The salience RSN consisted of anterior cingulate cortex, presupplementary motor area, and bilateral anterior insulae in controls. In sedated and unsedated DOC, no thalamus and typical salience network-associated anterior cingulate cortex and presupplementary motor area

components were observed. Instead, a more frontal anterior cingulate region was connected. In controls, the bilateral ECNs mainly consisted of the inferior parietal, dorsolateral and medial prefrontal cortices. In both sedated and unsedated DOC, connectivity of the left ECN was mostly restricted to the left dorsolateral prefrontal and inferior parietal cortices. For the right ECN, connectivity in both groups was found in the right dorsolateral prefrontal cortex. In controls, the auditory RSN consisted of bilateral insulae/superior temporal cortex, supplementary motor area, and thalamus. In sedated and unsedated DOC, it consisted of left insula/superior temporal lobe. The sensorimotor RSN consisted of sensorimotor areas in both controls and patients with DOC, although in controls, it also included regions overlapping with the auditory RSN. The visual RSN consisted of the visual cortex in all groups. The bilateral medial thalamus connected to regions overlapping with those of the DMN, ECNs, and salience network in controls, which could not be observed in the DOC groups.

RSN contrasts

Contrasts between groups were performed to assess statistical differences in RSN connectivity (figure 4.3). Patients with DOC, as compared to controls, had less connectivity in the DMN (posterior cingulate cortex/precuneus, medial prefrontal cortex, bilateral medial temporal lobes, left inferior parietal lobe and dorsolateral prefrontal cortex), salience RSN (left insula, anterior cingulate cortex, and presupplementary motor area), left ECN (bilateral dorsolateral prefrontal cortex and medial frontal cortex), right ECN (left inferior parietal lobe and left dorsolateral prefrontal cortex), auditory RSN (right insula/superior temporal lobe and sensorimotor cortex), and sensorimotor RSN (right sensorimotor cortex and left medial temporal lobe). Less connectivity with the thalamus was also found (regions overlapping with the DMN, ECNs and salience RSN). Sedated patients with DOC, as compared to unsedated patients with DOC, had less long-range connectivity (connectivity with regions distant from the seed region) in the salience network (left anterior insula: x = -24, y = 23, z = -5), and with the thalamus (posterior cingulate cortex: x = -4, y = -31, z = 34; medial prefrontal cortex: x = -8, y = 38, z = 36; left caudate: x = -12, y = 14, z = 13; right caudate: x = 15 , y = 11, z = 16; medial prefrontal cortex: x = -8, y = 41, z = 32; and left dorsolateral prefrontal cortex: x = -54, y = 20, z = 13).

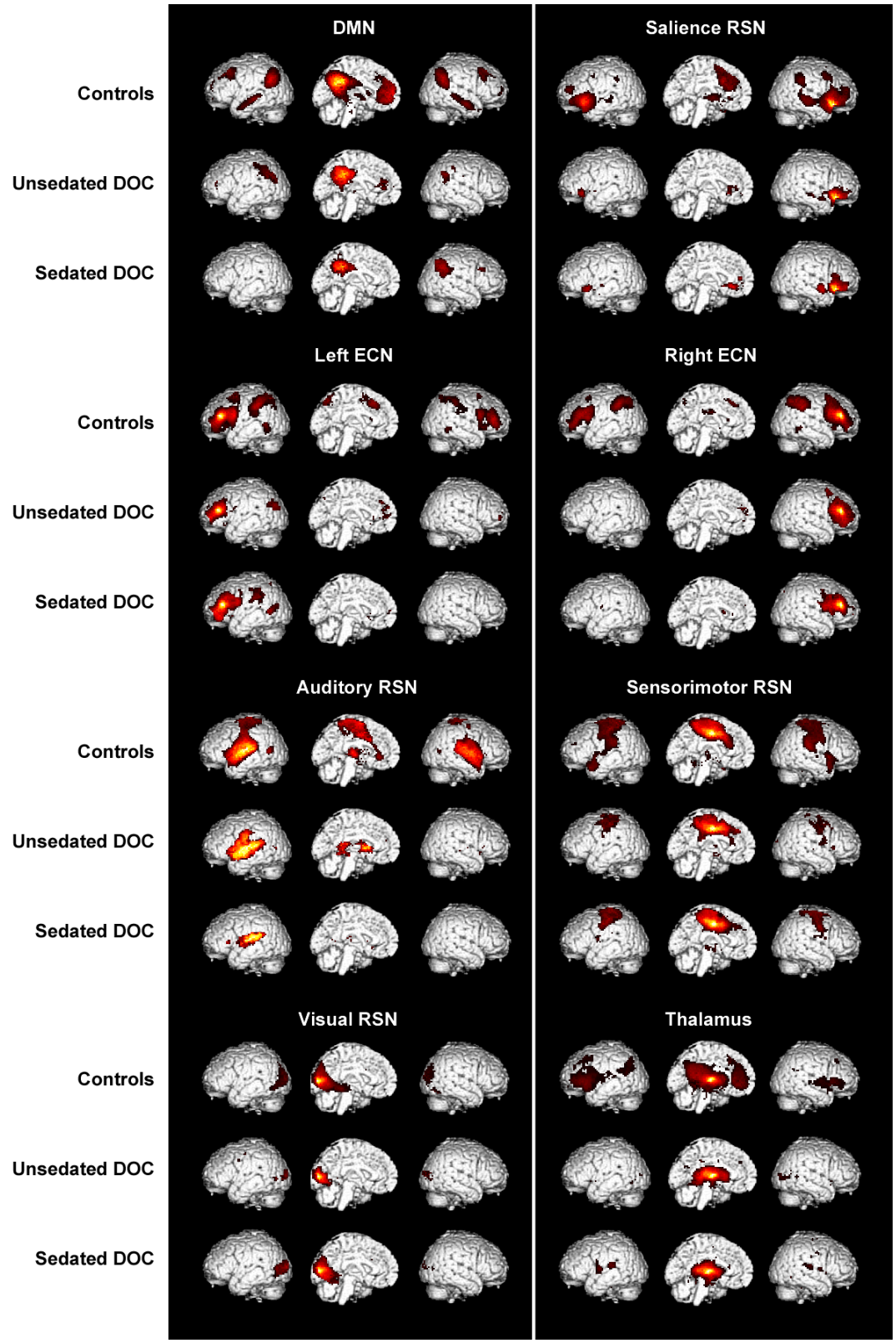

Figure 4.2. RSN connectivity in healthy controls, unsedated and sedated patients with DOC. Results were thresholded at FDR-corrected p = 0.05.

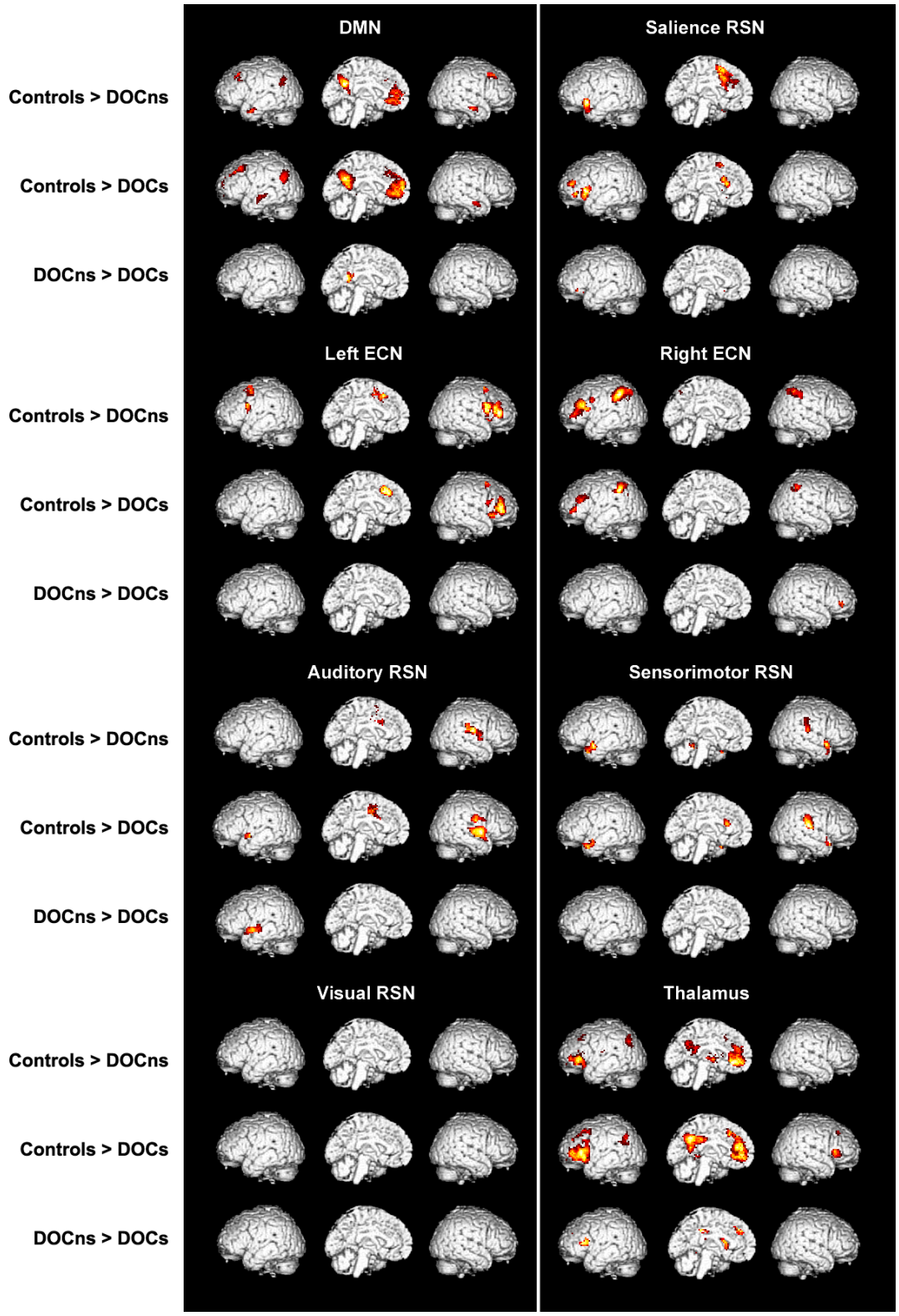

Figure 4.3. RSN connectivity decreases in patients with and without sedation, as compared to healthy controls. Unsedated and sedated DOC were also contrasted against each other. Results were masked with RSN regions obtained in the healthy controls at an FDR corrected threshold of p = 0.05, and thresholded at p = 0.01 (uncorrected; cluster extent threshold = 30 voxels).

4.5. Discussion

Methodological considerations

A clear limitation in our study is the fact that brain damage differs from one patient to the other, and consequently, to some extent, so will the effect of propofol on resting state connectivity. Therefore, although great care was taken to try to match groups of sedated and non-sedated patients for age, time in DOC, etiology, diagnosis, CRS-R total score, heart rate, breathing rate, head movement severity and brain damage, both groups were still slightly different. As such, it is extremely challenging to reliably assert which of the resting state fMRI differences found between groups were due to propofol-induced sedation, and which were due to other factors discriminating between DOC groups. Our attempt was furthermore hampered by the relatively small size and the heterogeneity of our matched study group. However, if propofol administration in patients with DOC would elicit major connectivity decreases, it would have been unlikely not to show up in our analysis. Therefore, our results should be seen as a first step in understanding the effect of sedating patients with DOC on assessment of RSN integrity.

RSNs in resting state data can be detected using two main resting state fMRI data analysis methods: independent component analysis and seed-based methods. Independent component analysis is a highly data-driven technique that groups different synchronously firing patches of neurons, as seen via the blood oxygen level-dependent signal, in a way that spontaneous activity behavior between groups is statistically independent.[101, 191] The analyst can decide on the number of components that the signal should be divided into. The seed-based analysis technique uses blood oxygenation level-dependent data from a selected region of interest as the reference to search for all other regions that show similar temporal activity behavior.[40] Although independent component analysis benefits from the fact that, compared to seed-based methods, less *a priori* (spatial) knowledge is necessary, and the fact that it is thought to excellently separate artifactual activations from neuronal activations, concerns exist about the number of components the signal should be divided into in altered states of consciousness.[40] Furthermore, the best way to discriminate between neuronal and non-neuronal independent components, as can be done by using an independent component fingerprint with information about the temporal data distribution,[106] remains uncertain. Furthermore, choosing the independent

component representing a specific RSN of interest can be challenging. Such constraints might interfere with the detection of the RSNs, especially in patients. Given proper preprocessing, seed-based analysis will more often detect remaining connectivity from an RSN core node (the seed) to other RSN and extra-RSN regions. Therefore, we applied seed-based analysis in our present analysis. Indeed, in controls, we detected RSNs resembling those mentioned in literature,[41, 173] while in DOC, we found remaining connectivity in all seven well-known RSNs. Furthermore, we detected decreases in long-range connectivity with the thalamus and the right anterior insula associated with propofol sedation, indicating that this is a valid approach for assessing propofol-induced long-range connectivity changes.

Our groups of sedated and unsedated patients had comparable heart and breathing rates. This was an important criterion for conducting a comparison between groups, as these physiological sources can induce noise in the blood oxygen level-dependent signal used for resting state fMRI.[101] Given that there were no significant differences between the groups, it may be suspected that any artifact resulting from these sources is relatively similar for both groups, thus not significantly affecting the comparison.

RSNs in controls and unsedated patients with DOC

In our healthy controls, connectivity in the seven RSNs we examined was comparable to that found in literature.[41, 173] We also added a seed analysis using the thalamus as seed region, as previous studies on the effect of propofol in healthy subjects have shown thalamus involvement.[47, 140] The thalamus was found to connect most to regions of the higher-order RSNs. This thalamocortical connectivity was lost in DOC. We furthermore found strong DOC-associated connectivity decreases in all four higher-control networks (DMN, bilateral ECN, salience RNS). Similar disruptions have been reported in previous resting state fMRI studies and link the functioning of cortical higher-order RSNs and their connectivity with the thalamus with the generation of consciousness.[11, 15, 72, 73, 101, 175-177] Brain damage in patients with DOC was found to be widespread, which is in line with findings from previous post mortem[75-80] and MRI studies.[74, 81-84] Higher-order RSNs heavily depend on long-range connectivity and these connections might thus be especially vulnerable to structural brain damage.[83, 192]

Possible effects of propofol in DOC

Although propofol-induced loss of consciousness in healthy controls has been found to lead to decreases in connectivity in higher-order RSNs, mild propofol sedation is associated with relatively minor connectivity decreases.[47, 86, 114, 140] In healthy subjects, the quantity of propofol administered to the patients with DOC in this study would have induced a state of mild sedation. However, little is known about the effect of propofol on RSN connectivity in the damaged brain. Therefore, a direct comparison between the mildly sedated state in healthy controls and the state resulting from propofol administration to patients with DOC cannot be readily made.

Comparing sedated with unsedated patients in DOC, we found reduced long-range connectivity associated with propofol sedation in the salience network and with the thalamus. Decreases in connectivity within the salience network have previously been found for propofol-induced unconsciousness in healthy subjects, where decreased connectivity between the right anterior insula and the anterior cingulate cortex, presupplementary motor area, thalamus, and left anterior insula were found.[140] Furthermore, as we found in patients with DOC, propofol-induced decreased connectivity between the thalamus and (dorsal) posterior cingulate cortex has been reported for healthy subjects.[47, 140, 193] The dorsal part of the posterior cingulate cortex, a key hub in the DMN, has been suggested to play a role in orchestrating the switch between internal and external awareness.[194, 195] In this context, the observed reduced thalamic connectivity with the dorsal and medial prefrontal cortices, overlapping with regions of the salience and external control networks, is also interesting. These connectivity changes might represent alterations in the control of interplay between higher-order RSNs. Furthermore, we found propofol-induced connectivity decreases between the thalamus and striatum, which also have been found before.[196, 197] This underlines the close association between the thalamus and these nuclei,[198] and could partially underlie differences in thalamocortical connectivity. Thalamostriatal mechanisms have been shown to be implicated in regulation of alertness and switching behaviors,[199] as well as cognitive motor control.[200]

Although the propofol-induced reductions found include connectivity in the salience network and with the thalamus, networks which might be used for neuroimaging-based diagnosis,[11, 140] the decreases were relatively minor, especially compared to those decreases caused by DOC-associated structural brain damage. Furthermore, given the fact that we here present group-level results, intersubject

variability might very well overshadow the connectivity reductions we here associated with propofol administration. It is however interesting to find that long-range thalamocortical connectivity might still be affected by propofol in patients with DOC, in which low levels or absence of consciousness is assumed.[24] Theoretically, such a response to propofol might in the future be used as a biomarker in itself, but there are several ethical problems with this idea. Most importantly, patients will only be sedated when absolutely necessary, mostly when the patients move too much to produce analyzable data, given the fact that no unnecessary potential health risks should be taken. As such, no analyzable dataset will be available for the unsedated state to compare with. In addition, the found reductions in connectivity appear to be too small to produce a reliable biomarker at the single subject level. However, the great reduction of connectivity found between thalamus and higher-order RSNs observed with our contrast between healthy controls and unsedated patients with DOC, as previously found between thalamus and DMN,[72] as well as during propofol-induced anesthesia,[47, 140] warrants a further examination of this connectivity pattern as a biomarker of consciousness.

Several factors should be taken into account when considering sedation to reduce head movement. While anesthetics may have some neuroprotective effects,[201] such as during acute cerebral ischemia,[202] anesthetics may also be theoretically toxic to the brain, as shown in laboratory models.[203, 204] In particular, uncertainty remains about the effects of anesthetics on 'fragile' brains, such as the developing,[205] the old,[206] and the pathological atrophic brain.[207] Administration of anesthetics means that extra attention should be paid to vital functions such as breathing, as these are likely to become affected, depending on the anesthetic agent used. This means that such procedures can only be performed when highly trained anesthesiologists, anesthesia equipment, and emergency personnel are present.

4.6. Conclusion

In this study, we examined how propofol sedation might affect RSN connectivity in patients with DOC. Even in our small study group, we found minor propofol-associated changes in connectivity, indicating that these patients still have a form of brain connectivity that can be modified by propofol. However, the major differences were found between controls and (un)sedated patients with DOC, which is related to the great extent of structural brain damage in DOC. Given the known negative effects of high intensity movement during resting state fMRI, which decreases detectability of RSNs, propofol sedation might presently be considered to be a good method for ensuring analyzable data in patients with DOC with strong uncontrolled head and body movement. Future studies should further examine safety aspects associated with this procedure.

Chapter 5

STRUCTURAL BRAIN DAMAGE UNDERLYING DISORDERS OF CONSCIOUSNESS:

A POTENTIAL ROLE FOR THE DEFAULT MODE NETWORK

Corresponding article:

Brain Damage in Patients with Disorders of Consciousness: a Voxel-based Morphometry Study

P. Guldenmund[1], A. Soddu[2], K. Baquero[3], A. Vanhaudenhuyse[1,4], M.-A. Bruno[1], O. Gosseries[1], S. Laureys*[1], F. Gómez*[1,5].

*Authors contributed equally.

(1) Coma Science Group, Cyclotron Research Center and University Hospital of Liège, University of Liège, Liège, Belgium. (2) Brain & Mind Institute, Physics & Astronomy Department, Western University, London Ontario, Canada. (3) Computer Imaging and Medical Applications Laboratory, National University of Colombia, Bogotá, Colombia. (4) Algology-Palliative Care Department, University Hospital of Liège, University of Liège, Belgium. (5) Computer Science Department, Universidad Central de Colombia, Bogotá, Colombia.

5.1. Abstract

Disorders of consciousness (DOC; encompassing coma, vegetative state/ unresponsive wakefulness syndrome (VS/UWS), and minimally conscious state minus/plus (MCSminus/plus)) are associated with severe structural brain damage. We attempted to characterize this damage and find structural differences between DOC groups that could help understand group-specific behavior.

We used voxel-based morphometry on structural magnetic resonance imaging scans of 61 patients with DOC to examine gray and white matter brain damage that correlated with behavioral responsiveness (using the coma recovery scale-revised), time spent in DOC, etiology, and diagnosis.

We found, using a false discovery rate-corrected threshold of $p = 0.05$, that the coma recovery scale-revised total score and time spent in DOC correlated with widespread structural brain damage, although the latter did not correlate strongly with damage in the right cerebral hemisphere. Traumatic, as compared to non-traumatic etiology, was associated with more damage in the thalamus, midbrain, hypothalamus, basal forebrain, cerebellum, brainstem and posterior corpus callosum. Differences were found between the examined non-traumatic MCS and VS/UWS at a more liberal threshold ($p = 0.01$, uncorrected) and hinted at more damage in midline default mode network-associated regions in patients in VS/UWS. Similarly, this threshold allowed us to find that patients in MCSplus had a more preserved left cerebral hemisphere than patients in MCSminus.

Our finding of widespread brain damage in patients with DOC is consistent with earlier findings and illustrates the difficulty of correctly interpreting structural brain damage in patients with DOC for diagnostic purposes. This concern was reflected in the fact that only minor potential differences in brain damage between VS/UWS and MCS were found at the group level. The high degree of atrophy occurring after initial brain damage prompts the development and use of neuroprotective techniques. Etiology influenced the pattern of brain damage, while MCSminus was associated with more damage in brain areas vital for language comprehension as compared to MCSplus. Our results show that although voxel-based morphometry holds promise as a complementary diagnostic tool, improvements are necessary for its application at the single subject level.

5.2. Introduction

Coma can result from severe brain injury and manifests itself as a condition in which a patient has the eyes closed and does not respond to any stimulus. Neither brain arousal nor awareness is thought to exist. It usually lasts no longer than three weeks, after which a patient may proceed to a vegetative state/unresponsive wakefulness syndrome (VS/UWS); a state of brain arousal without detectable awareness.[139] A patient may then enter a minimally conscious state (MCS), in which fluctuating and scattered awareness and arousal is present. The MCS has recently been divided into MCSplus and MCSminus, with patients in the latter condition showing command following, intelligible verbalization, or gestural or verbal yes/no responses to spoken or written questions.[169] These conditions are collectively known as disorders of consciousness (DOC). In some rare cases, usually due to a lesion in the upper pons, a patient can recover from a coma and become locked-in.[24, 65] The patient has recovered full consciousness, but is extremely limited in communication with the outside world due to (near-)complete body paralysis. The inability of some locked-in patients to move may lead to an incorrect diagnosis when the patients are only assessed with behavioral scales.[24]

With the advent of modern brain imaging methods, including positron emission tomography and resting state functional magnetic resonance imaging (resting state fMRI), task-free paradigms have enabled researchers to find patterns of brain activity or structure that can aid in determining whether a patient is (partially) conscious (MCS or locked-in syndrome) or not (VS/UWS).[72, 208] With task-free neuroimaging, an examiner is not dependent on patient cooperation and a patient's possibility to exhibit body movement. In resting state fMRI, examination of intactness of the default mode network (DMN) has a prominent role in DOC diagnosis, as it is known to be important for internally-oriented consciousness.[14, 15, 47, 72, 140, 175, 209] In recent years, interest has also increased for other brain regions associated with specific higher-order networks.[173] These include bilateral external control networks (ECN), important for external awareness,[14] and the salience network, which has been associated with mounting appropriate responses to salient stimuli.[16] The role of the thalamus in DOC has also been explored. Thalamic metabolism has been shown to be depressed in a way correlating with the level of consciousness, as detected with behavioral examinations.[24, 210, 211] Interestingly, restoration of thalamocortical connectivity has been associated with recovery of a patient in chronic VS/UWS.[165]

Although considerable progress has been made in the comprehension of functional and metabolic activity of the brain and its disturbance in DOC, much uncertainty remains about how to interpret structural brain damage.[74] Thalamus, brainstem and extensive cerebral damage are among the most frequent observations in DOC in post mortem[75-80] and MRI studies.[81-84] Furthermore, decreased structural connectivity between thalamus and DMN regions has been shown to play an important role in DOC.[83] Equally little is known about brain atrophy secondary to the injury causing DOC. This can result from herniations, diffuse cerebral swelling, secondary infarction, hemorrhage and long-term brain inactivity in general.[212-214] One study reported on the effects of time spent in DOC in four patients in chronic VS/UWS that had been in the VS/UWS for more than three years at the time of inclusion and were then studied over a time period of two years.[214] The patients did not recover consciousness during the study. The authors found a decrease of brain parenchyma volume of 1.8 to 4.1% within these two years. Furthermore, using spectroscopy, they detected signs of progressive neuronal dysfunction and/or loss, gliosis and membrane injury, as well as progressively decreasing functional excitability of primary cortices. Similar findings were reported in a study of 24 patients in VS/UWS, showing widespread decreased metabolism (with the exception of the frontal lobe) in chronic (> 1 month) patients, as compared to acute (< 1 month) patients.[215] Another matter of interest is the difference in the pattern of brain damage between traumatic and non-traumatic DOC. Traumatic etiology has been associated with more pronounced brainstem damage.[84] Furthermore, no clear structural differences have been found to distinguish MCS from VS/UWS. In one study,[81] thalamic volume was shown to be smaller on average in VS/UWS than in MCS. Global white matter damage as seen with diffusion tensor imaging has also been found to possibly discriminate between the patient groups.[82] Lastly, it is unknown whether an assessment of brain structure can discriminate MCSplus from MCSminus in a similar way as has been shown for positron emission tomography-based assessment of brain metabolism.[147]

In this present article, we describe gray and white matter integrity decreases of 61 patients with DOC, using voxel-based morphometry (VBM).[216, 217] An early VBM study with five chronic patients in VS/UWS[74] showed that compared to controls, patients had more damage in the inferior parietal and superior/medial frontal cortices, insula and operculum, temporal lobes, cingulum and fusiform gyrus, caudate, midbrain, dorsal pons and cerebellum. However, in contrast to other studies, little thalamic damage was found in this study. We used a newer version of VBM and a larger dataset to examine five aspects, namely: (1) brain damage correlating with behavioral assessment scores of the coma recovery scale revised

(CRS-R);[184] (2) the effect of time spent in DOC on brain gray and white matter integrity; (3) etiology-based differences in brain damage; (4) differences between VS/UWS and MCS; (5) differences between patients in MCSminus and MCSplus.

We expected widespread structural brain damage in patients with DOC, as it has previously been reported in post-mortem and diffusion tensor imaging studies.[76-81, 218] Although less frequently described, widespread damage might also correlate with the effect of time spent in DOC.[213, 214, 219-221] As white and gray matter sensitivity to traumatic and non-traumatic brain insults (mainly cerebral ischemia[222]) has been found to be comparable in severity degree, although depending on different pathological mechanisms,[222] we expected brain damage to be widespread throughout white and gray matter in both traumatic and non-traumatic etiologies. However, patients with DOC with a traumatic etiology might also have more focal damage in regions that are especially susceptible to acceleration and deceleration (near rough skull edges) and twisting and turning effects often experienced in trauma. These regions include the brainstem, thalamus, cerebellum and basal forebrain.[84, 223-225] Differences between VS/UWS and MCS might be more global than focal, based on the absence of clear structural differences mentioned in literature,[82] although thalamic damage might have especially high discriminatory power.[81] Given the found importance of the DMN, and especially the posterior cingulate cortex/precuneus, in previous neuroimaging studies,[24, 72, 83, 101] we also expected more damage in these regions in patients in VS/UWS. Based on a previous metabolic study, which found the left cerebral cortex to be more affected in MCSminus than in MCSplus, we expected structural integrity differences in the left cerebral cortex, most often associated with language functions, between MCSminus and MCSplus.[147]

5.3. Methods

Subjects and data acquisition

For our analysis, we used T1 structural magnetic resonance images acquired on a 3T scanner (Siemens AG, Munich, Germany; TR = 2300 ms, TE = 2.47 ms, T1-weighted 3D gradient echo images with 1 x 1 x 1.2 mm^3 voxels in the sagittal plane, flip angle = 9^o, matrix size = 256 x 240 x 144 mm^3, field of view = 256 x 256 mm^2) of 34 patients in VS/UWS, 62 patients in MCS, and 28 healthy control subjects. The study was approved by the Ethics Committee of the Medical School of the University of Liège. Informed consent to participate in the study was obtained from the subjects themselves in the case of healthy subjects, and from the legal surrogates of the patients. Diagnosis was based on repeated behavioral analysis with the CRS-R.[184] The CRS-R is a standardized behavioral scale that is currently considered to be the most trustworthy behavioral diagnosis tool for patients with DOC available and is therefore used in most DOC neuroimaging studies as a behavioral diagnosis reference point.[11, 185]

Of this initial group, 18 patients in VS/UWS and 17 patients in MCS were excluded from further analysis due to large hemorrhage effects, movement artifacts, foreign body artifacts, midline shifts, acquisition artifacts, low gray-white matter contrast, or exceptionally large brain damage; as assessed by careful visual inspection of the T1 images by an expert. This step, which introduced a bias into the analysis, was done in an effort to minimize the chance of severe segmentation and normalization problems occurring during the VBM procedure.[83, 187, 216, 226, 227] Visual inspection of VBM segmentation and normalization results performed to examine VBM performance did not lead to further rejection of patient data. Therefore, for further analysis, we used a database consisting of 16 patients in VS/UWS (mean age = 49 years ± 20 years, 2 traumatic, average time spent in DOC = 112 days ± 174 days), 45 patients in MCS (mean age = 41 years ± 19 years, 28 traumatic, average time spent in DOC = 792 days ± 1041 days), and 28 control subjects (mean age = 48 years ± 17 years) (table 5.1). The patient groups were matched for age.

Table 5.1. Patient data.

Subj.	Diagnosis according to CRS-R	CRS-R highest total score (and subscores*)	Etiology	Age at onset (in years)	Time spent in DOC (in days)
1	VS/UWS	6(1,0,2,2,0,1)	n-T (anoxia)	73	92
2	VS/UWS	6 (1,0,2,1,0,2)	n-T (CVA)	62	32
3	VS/UWS	3 (0,0,1,1,0,1)	n-T (anoxia)	44	22
4	VS/UWS	3 (0,0,2,1,0,0)	n-T (CVA)	73	7
5	VS/UWS	6 (1,0,1,2,0,2)	T	16	615
6	VS/UWS	7 (1,0,2,2,0,2)	T	21	196
7	VS/UWS	5 (1,0,2,1,0,1)	n-T (metabolic disorder)	53	20
8	VS/UWS	5 (1,1,1,1,0,1)	n-T (CVA)	63	32
9	VS/UWS	5 (1,0,1,1,0,2)	n-T (anoxia)	48	52
10	VS/UWS	5 (0,0,2,1,0,2)	n-T (CVA)	56	26
11	VS/UWS	6 (1,0,1,2,0,2)	n-T (anoxia)	42	104
12	VS/UWS	4 (1,0,1,0,0,2)	n-T (anoxia)	44	27
13	VS/UWS	7 (1,1,2,1,0,2)	n-T (CVA)	74	40
14	VS/UWS	5 (1,0,1,1,0,2)	n-T (anoxia)	16	27
15	VS/UWS	5 (1,0,2,1,0,1)	n-T (anoxia)	69	50
16	VS/UWS	6 (1,0,1,2,0,2)	n-T (anoxia)	31	456
17	MCS	7 (0,3,1,2,0,1)	T	30	569
18	MCS	13 (1,3,5,2,0,2)	n-T (anoxia)	30	1188
19	MCS	8 (1,3,2,0,0,2)	n-T (CVA)	59	21
20	MCS	10 (1,3,2,2,0,2)	T	19	905
21	MCS	10 (1,3,2,2,0,2)	n-T (CVA)	33	1869
22	MCS	9 (1,3,2,2,0,1)	n-T (anoxia)	50	68
23	MCS	9 (0,3,2,2,0,2)	T	34	3139
24	MCS	9 (1,3,2,1,0,2)	n-T (anoxia)	39	17
25	MCS	13 (3,5,2,0,1,2)	T	45	533
26	MCS	11 (3,3,2,1,0,2)	T	23	752
27	MCS	8 (3,1,1,1,0,2)	n-T (CVA)	64	1383
28	MCS	12 (3,3,2,2,0,2)	T	26	3034
29	MCS	15 (3,3,5,1,1,2)	T	22	3226
30	MCS	9 (3,0,2,2,0,2)	T/n-T (trauma + anoxia)	23	1538
31	MCS	12 (3,3,3,2,0,1)	T	30	583
32	MCS	5 (1,0,1,1,1,1)	n-T (CVA)	74	18
33	MCS	14 (3,5,0,3,1,2)	n-T (epilepsy)	52	20
34	MCS	11 (3,3,3,1,0,1)	n-T (CVA)	70	11
35	MCS	12 (3,4,2,1,0,2)	T	65	22
36	MCS	11 (3,3,2,1,0,2)	T	30	145
37	MCS	11 (3,2,5,0,0,1)	T	22	38
38	MCS	10 (3,3,0,2,0,2)	n-T (CVA)	39	37
39	MCS	13 (3,3,5,0,0,2)	T/n-T (trauma + anoxia)	17	2690

40	MCS	17 (3,4,5,2,1,2)	T	29	400
41	MCS	7 (3,0,2,1,0,1)	T/n-T (trauma + anoxia)	25	314
42	MCS	14 (3,5,3,1,0,2)	T	36	342
43	MCS	15 (4,5,2,0,1,3)	n-T (CVA)	87	7
44	MCS	13 (3,3,3,1,1,2)	T	22	421
45	MCS	12 (1,3,3,2,1,2)	n-T (metabolic disorder)	48	64
46	MCS	7 (4,2,0,0,0,1)	n-T (CVA)	64	7
47	MCS	18 (3,5,5,3,1,1)	T	60	51
48	MCS	7 (3,0,2,1,0,1)	T	13	257
49	MCS	16 (3,5,5,1,0,2)	T	22	1157
50	MCS	11 (0^,3,5,1,0,2)	n-T (anoxia)	72	5
51	MCS	16 (3,4,5,2,0,2)	T	54	202
52	MCS	10 (3,3,1,1,0,2)	T	17	1333
53	MCS	16 (3,3,5,2,0,3)	n-T (metabolic disorder)	54	311
54	MCS	8 (3,0,2,1,0,2)	T	31	1331
55	MCS	14 (3,3,5,2,0,1)	n-T (CVA)	71	22
56	MCS	11 (3,0,3,3,1,1)	n-T (CVA)	66	37
57	MCS	11 (3,3,2,1,0,2)	T	19	219
58	MCS	13 (3,5,2,1,0,2)	T	21	3342
59	MCS	15 (3,3,5,1,1,2)	T	45	3216
60	MCS	11 (3,3,2,1,0,2)	T	36	134
61	MCS	7 (3,0,1,2,0,1)	T	64	677

*16 VS/UWS (2 traumatic) and 45 MCS (28 traumatic) patients; CVA = cerebrovascular accident, CRS-R = coma recovery scale revised (*CRS-R subscores are, in the following order: auditory, visual, motor, verbal, communication, arousal[228]), ^ = a value of 3 has been obtained during another CRS-R assessment, DOC = disorders of consciousness, MCS = minimally conscious state, VS/UWS = vegetative state/unresponsive wakefulness syndrome, T = traumatic, n-T = non-traumatic, Subj. = subject number.*

Preprocessing

T1 structural images were automatically reoriented before preprocessing with VBM8 software (http://dbm.neuro.uni-jena.de/vbm/) for SPM8 (www.fil.ion.ucl.ac.uk/spm). We selected a warping regularization of 4, instead of the VBM8 standard 1, to mildly reduce the chance of unrealistic deformations occurring. The sampling distance was put at 1 mm, instead of the VBM8 standard of 4 mm, to increase the amount of structural data used and thus VBM8 accuracy (http://dbm.neuro.uni-jena.de/vbm/). Spatial normalization was performed using DARTEL,[187] to allow for high-dimensional spatial normalization to increase the chance

of correct normalization in the severely damaged DOC brain.[188] Furthermore, we used a DARTEL-based method implemented in VBM8 to construct a DOC template made from T1 images of our DOC population to use in the DARTEL-based normalization procedure.[187, 189] This template was used to minimize normalization difficulty,[74, 217] since it minimized the degree of warping necessary for DOC brains in the normalization step, thus potentially decreasing the chance of misclassification and normalization errors occurring during the VBM process.[189]

For de-noising purposes, a VBM8-incorporated spatial adaptive non-local means de-noising filter[229] and Markov random field weighting,[230] put at 0.15, were used. After segmentation, the images were modulated (the automatic multiplication of voxel values by the deformity parameters calculated during the normalization process) to compensate for the deformity that occurs in normalization, preserving the white and gray matter volumes considered in this analysis. After VBM preprocessing, resulting gray and white matter segments were smoothed with a 12 mm kernel. As the morphology of DOC brains is more challenging for VBM than that of controls, this larger kernel size was used rather than a more commonly employed 8 mm smoothing kernel in an effort to minimize the occurrence of possible false positive results. These could have resulted from problems in the normal distribution of error terms in the statistical model used by VBM8 to construct parametric statistical tests.[227, 231, 232] Furthermore, it helped to better minimize the influence of noise[233] and the effect of individual differences in gyral anatomy.[234] A downside of using bigger smoothing kernels is the loss of spatial detail.[231] The smoothed images were used for a statistical analysis with SPM8.

Statistical analysis

Five main analyses were performed to examine the brain damage correlating with a decreasing level of consciousness, brain atrophy correlating with the time spent in DOC, differences in brain damage between traumatic and non-traumatic etiologies, differences between VS/UWS- and MCS-related damage, and differences between brain damage in MCSminus and MCSplus.

Firstly, correlation of gray and white matter damage with the CRS-R total score was examined, including all patients in the analysis. The CRS-R score was used as a covariate and brain damage correlating to this covariate was then examined. Additionally, we performed a similar analysis for a group consisting of all patients and

control subjects, attributing the maximum CRS-R score of 23 to the control subjects.[184]

Secondly, the effect of time spent in DOC on brain atrophy for a DOC group consisting of all patients in VS/UWS and MCS was assessed. Although our dataset was limited to MRI scans acquired during one time point only, and a two time point design would have been more suited to examining the atrophy correlating to time spent in DOC, we saw the great number of patients included in our analysis as a reason to allow ourselves to make inferences upon this effect. We used the time a patient spent in the DOC at the day of scanning as a covariate (the natural logarithm of the time spent in DOC in days was used; the natural logarithm was chosen to decrease the distance between data points, as, given known biological secondary responses to primary brain injury,[212, 235-237] we expected the effect of time on brain damage to be strongest in the initial weeks). The brain damage correlating to this covariate was examined.

Thirdly, a direct comparison between brain damage in traumatic and non-traumatic patients with DOC (VS/UWS and MCS combined, 16 traumatic (mean age = 38 years ± 15 years) and 18 non-traumatic (mean age = 45 years ± 12 years)), matched for age and time spent in DOC, was also performed using a two-sample t-test.

Fourthly, we examined potential differences in brain damage between VS/UWS and MCS. For this, to remove a potential etiology effect, we only used non-traumatic patients, as only two patients in VS/UWS in our original dataset were traumatic. Of this group, a number of patients was excluded from the analysis to make matching of age and time spent in DOC possible for the remaining patients. 14 patients in VS/UWS (mean age = 53 ± 17 years) and 17 patients in MCS (mean age = 57 ± 16 years) were included in the analysis. A two-sample t-test examined brain damage differences between VS/UWS and MCS. We used a DMN spatial map constructed from resting state fMRI data from 20 healthy subjects (mean age = 47 years ± 18 years), which was comparable to the DMN as reported in literature,[41] to mask out non-DMN regions. Differences between non-traumatic patients in VS/UWS and patients in MCS that occurred in DMN regions and survived a p-value threshold of 0.01 (uncorrected) and voxel extent threshold of 30 were treated as possibly true results, although with a higher uncertainty.

Fifthly, we used the full group of patients in MCS (8 in MCSminus, mean age = 36.8 years ± 12.6 years; 37 in MCSplus, mean age = 42.1 years ± 20.7 years), matched

for age and time spent in DOC, to examine the potential structural differences between patients in MCSminus and those in MCSplus. We accepted results surviving a p-value threshold of 0.01 (uncorrected) and cluster extent threshold of 30 voxels, given our *a priori* knowledge.[147]

5.4. Results

A lower CRS-R total score was associated with widespread gray and white matter damage (figure 5.1). However, no correlation with the CRS-R total score was found when excluding the healthy controls from this analysis. Widespread gray and white matter atrophy was found to correlate with time spent in DOC, with a relative sparing of the right cortical hemisphere (figure 5.2). Comparison between the traumatic and the non-traumatic patient groups showed that in traumatic patients, more brain damage was found in the lower thalamus/midbrain (x = 0, y = -22, z = -2), hypothalamus (x = 0, y = -3, z = -5), basal forebrain (x = -6, y = 20, z = -5), cerebellum (x = 3, y = -52, z = -21), brainstem (x =-2, y = -39, z = -9), and posterior corpus callosum (x = 0, y = -30, z = 21) (figure 5.3).

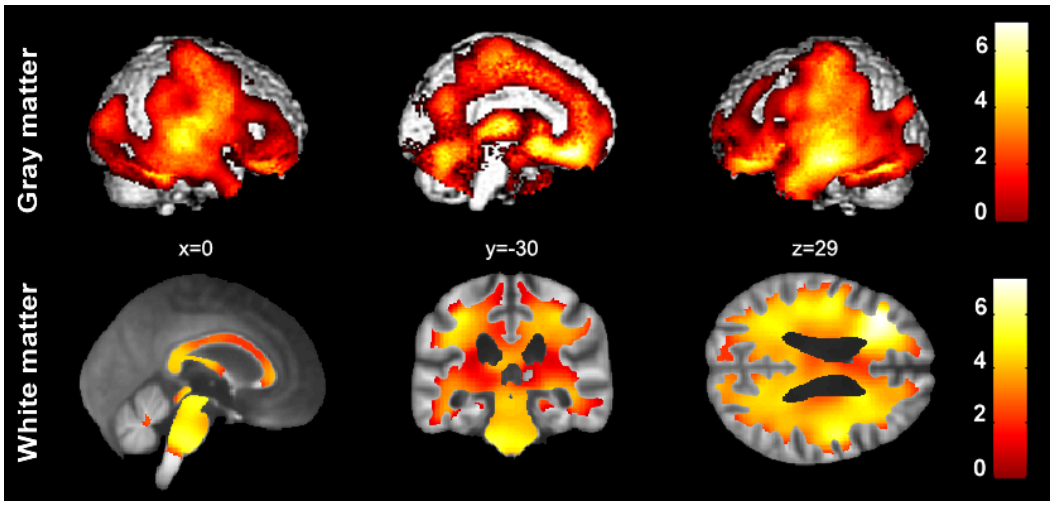

Figure 5.1. Gray matter (top) and white matter (bottom) damage correlating with the CRS-R total score (false discovery rate-corrected at p = 0.05) in 61 patients with DOC, when including healthy controls in the analysis and attributing a maximum CRS-R total score (23) to them. White matter results were superimposed on an averaged T1 that was calculated from all normalized T1´s of the DOC group.

No differences in gray or white matter damage were found between patients in VS/UWS and patients in MCS, as seen with at threshold of false discovery rate-corrected p = 0.05. However, using an inclusive spatial DMN mask and a more liberal threshold of p = 0.01 (uncorrected), we detected more damage in patients in VS/UWS in the ventromedial prefrontal cortex (x = 14, y = 50, z = -9) and the posterior cingulate cortex/precuneus (x = -15, y = -61, z = 18) when contrasting VS/UWS and MCS (figure 5.4). Contrasting patients in MCSminus with those in MCSplus, using a

liberal threshold of p = 0.01 (uncorrected), we found that patients in MCSplus had a more preserved left cerebral cortex, including the middle temporal gyrus (multimodal posterior area, x = -68, y = -55, z = 0), superior temporal gyrus (primary auditory cortex, x = -69, y = -22, z = 9; and Wernicke's area, x = -66, y = -37, z = 16), and inferior frontal gyrus (Broca's area, x = -57, y = 24, z = 16) (figure 5.5).

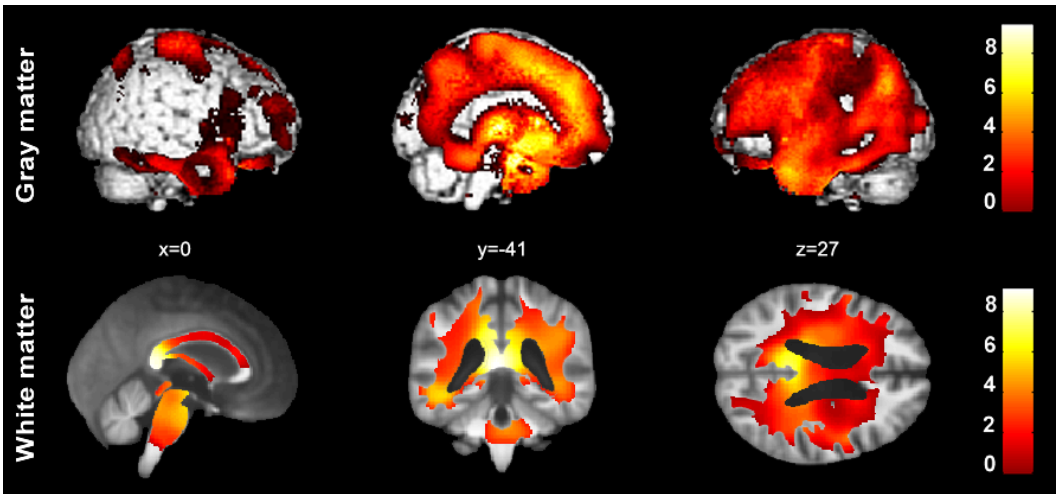

Figure 5.2. Gray matter (top) and white matter (bottom) atrophy associated with time spent in DOC (false discovery rate-corrected at p = 0.05) in 61 patients with DOC. White matter results were superimposed on an averaged T1 that was calculated from all normalized T1´s of the DOC group.

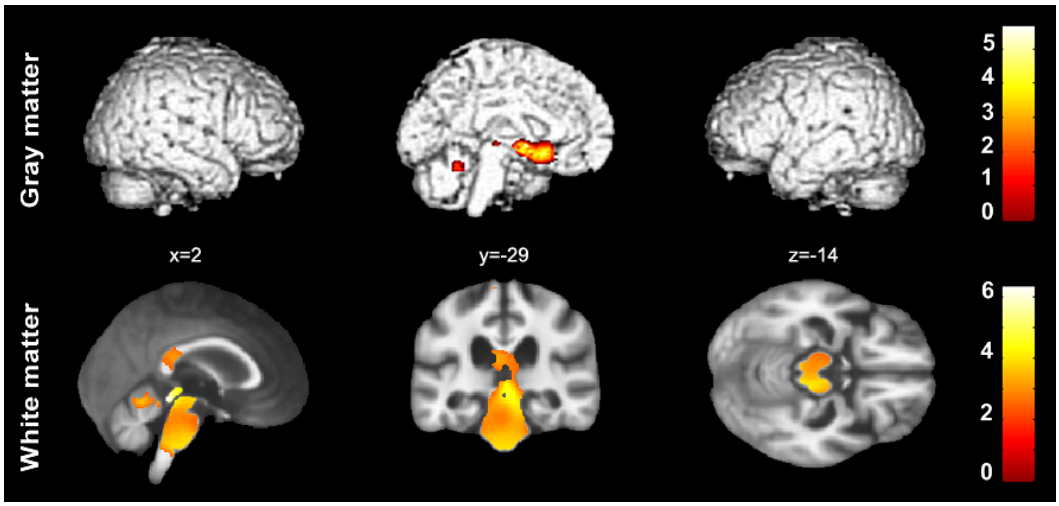

Figure 5.3. Gray matter (top) and white matter (bottom) damage more evident in traumatic than in non-traumatic DOC (false discovery rate-corrected at p = 0.05) in a group (VS/UWS and MCS combined) of 16 traumatic and 18 non-traumatic patients, matched for age and time spent in DOC. White matter results were superimposed on an averaged T1 that was calculated from all normalized T1´s of the DOC group.

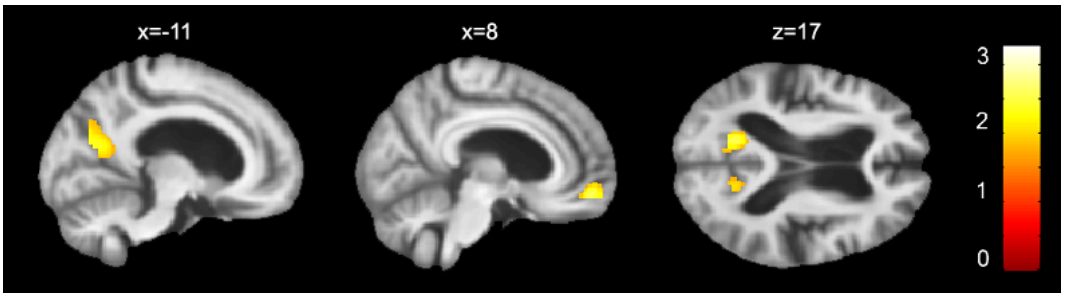

Figure 5.4. Regions of the bilateral posterior cingulate cortex/precuneus and ventromedial prefrontal cortex appeared to be more damaged in non-traumatic VS/UWS as compared to non-traumatic MCS. The groups of 14 patients in VS/UWS and 17 patients in MCS were matched for age and time spent in DOC. Results were thresholded at p = 0.05 (uncorrected) for display purposes and superimposed on an averaged T1 that was calculated from all normalized T1´s of the DOC group.

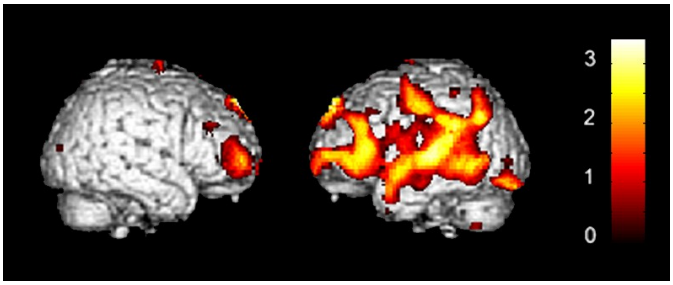

Figure 5.5. The left cerebral cortex was found to be more damaged in MCSminus as compared to MCSplus. The groups of 8 patients in MCSminus and 37 patients in MCSplus were matched for age and time spent in DOC. Results were thresholded at p = 0.05 (uncorrected) for display purposes.

5.5. Discussion

Methodological considerations

VBM, based on DARTEL, is an established and widely used technique to assess differences in brain structure and has been shown to operate well in cases of relatively mild to severe brain damage.[238, 239] In many cases, brain damage in patients with DOC belongs to the most severe class of brain damage, often showing great morphological changes like ventricle enlargement. This imposes some notes for carefulness.[238] Therefore, to minimize the chance of false results, we used a smoothing kernel of 12 mm, and employed a patient specific DARTEL template.[240] We also excluded patients with large hemorrhage effects, movement artifacts, foreign body artifacts, midline shifts, acquisition artifacts, low gray-white matter contrast, or exceptionally large brain damage. This way, data from 35 patients were discarded. This high exclusion rate introduced a bias into our examination, which we regarded as being necessary in order to obtain trustworthy segmentation and normalization.[187, 216] Our view is that further research into DOC brain morphology and VBM methods should be performed before brain scans with the abovementioned rejection criteria could be included. The results from our analyses of differences between brain damage in VS/UWS and MCS, as well as between MCSminus and MCSplus, did not survive whole brain false discovery rate correction. However, our findings are strengthened by similar findings in earlier neuroimaging studies. Finally, although VBM8 was mainly developed for examination of gray matter, a growing number of studies have also used VBM for non-diffusion tensor imaging-based examination of white matter.[188, 241-243] Therefore, while extra restraint might be advisable in its interpretation, we regard the results from our VBM-based white matter examinations reported in this paper to be trustworthy.

Brain damage correlating with the CRS-R total score

In our study, a decreasing CRS-R score was found to be correlated with widespread white and gray matter damage; consistent with findings from previous post mortem[75-80] and MRI studies.[74, 81-84] Diagnosis of DOC in our study was performed using the CRS-R, a widely accepted standardized behavioral test that looks for signs of consciousness.[11, 184, 185] Detectability of consciousness with behavioral

examinations is dependent on at least three different factors: brain arousal, internal and external awareness (perception), and the possibility to mount an appropriate response.[244] Each one of these factors can influence the CRS-R total score and the pattern of damage correlating with the CRS-R total score includes brain regions that are important not only for arousal and awareness, but also for movement initiation. These results emphasize the limits of consciousness detection using behavioral examinations, and the need for complementary neuroimaging in the diagnostic process.[11]

Time spent in DOC

The time spent in DOC correlated with widespread gray and white matter atrophy. Such secondary brain damage could influence the potential for patient recovery. Unfortunately, not much is known about its mechanisms and therefore ways to interfere with the degradative process. When brain tissue gets damaged, a whole cascade of molecular processes takes place, possibly aided by long-time brain inactivity,[212, 214] leading to events such as inflammation, apoptosis and necrosis in the neighborhood of the primary damage.[80, 213, 218, 245, 246] The potential effectiveness of drugs that are currently used with the aim of improving patient recovery chances in the short and long term, such as Amantadine and Baclofen, is subject of continuing research.[247, 248] An interesting aspect is the fact that the gray matter atrophy associated with time spent in DOC appeared to be mostly left lateralized. Left lateralized atrophy correlating with time spent in DOC has been previously described[249] and makes an association with severely impaired language processing tentative.[249, 250] A recent report also described left lateralized metabolic impairment as a pivotal discriminator between MCSminus (i.e., patients only showing non-reflex behavior such as visual pursuit, localization of noxious stimulation and/or contingent behavior) and MCSplus (i.e., patients showing comprehension of language).[147] Future research should indicate whether this left lateralized atrophy might perhaps be associated with long-term inactivity in language systems during DOC, and how this could relate to detection of consciousness.

Etiology-related damage

We found that the group of traumatic patients with DOC had more damage in the thalamus/midbrain, pons, hypothalamus, basal forebrain and cerebellum, as

compared to the group of non-traumatic patients with DOC. Traumatic insults that include rapid deceleration or acceleration cause the brain to move against the skull. As the bottom of the skull has many protuberances, fierce contact might result in damage to the basal forebrain, hypothalamus, pituitary, cerebellum and pons.[75, 223-225] Furthermore, the brainstem has less movement freedom than the higher lying parts of the brain, which results from the fact that it is connected to the base of the skull. Therefore, twists and turns might occur at the upper brainstem, thalamus and even corpus callosum.[251, 252] Specific vulnerability of the brainstem in patients with DOC with traumatic etiologies has previously been found in a diffusion tensor imaging study.[84] We did not find regions that were more damaged in non-traumatic cases. However, it must be noted that such damage may be more widespread and therefore potentially more difficult to detect using traditional statistical methods in VBM8.

Our findings show that both traumatic and non-traumatic patients with DOC have widespread damage in white and gray matter. This is in line with previous reports of severe brain injury.[222] Traumatic brain insult can lead to damage in both gray and white matter by application of severe physical pressure on neuronal cell bodies and axons, leading to disrupted cell integrity. Axonal damage can lead to Wallerian degeneration and related processes,[253] while severe white matter disturbance can also include damage to non-neuronal cells that support axonal and synaptic functioning, thereby affecting axon survival.[222] Non-traumatic insults can lead to brain damage via disruption of metabolic needs or other vital cell mechanisms in both gray and white matter.[222]

VS/UWS versus MCS

Our study did not yield structural differences between VS/UWS and MCS when correcting results for multiple comparisons. The fact that no strong differences between VS/UWS and MCS could be found in a large group of 31 non-traumatic patients, using the latest methods for examining T1 scans in a voxel-wise manner, illustrates the difficulty of differential DOC diagnosis based on structural imaging alone. This problem is emphasized when downscaling to the single subject level. It could be that conventional MRI T1 sequences cannot fully detect certain types of damage, such as more diffuse damage, that could potentially distinguish between VS/UWS and MCS. Such damage might impede whole brain information integration, while islands of cognitive processing, as reported in literature, might still exist.[254] Literature on potential structural differences between VS/UWS and MCS is scarce,

and the problem of finding robust differences between VS/UWS and MCS at the single subject level also exists for other neuroimaging modalities, such as resting state fMRI and positron emission tomography.[24, 72, 147]

However, at the group level and without correcting for multiple comparisons, our finding of the posterior cingulate cortex/precuneus and ventromedial prefrontal cortex, pivotal DMN regions, as potential discriminators is in line with earlier structural, functional and metabolic neuroimaging reports. A diffusion tensor imaging-based study showed that DMN integrity might discriminate between VS/UWS and MCS,[83] while measuring metabolism and connectivity in DMN-related areas, and especially the posterior cingulate cortex/precuneus, might also help to discriminate between VS/UWS and MCS.[24, 72, 175] Future studies should aim to find structural, functional and metabolic biomarkers that could, preferably in a multimodal setup, improve diagnosis at the single subject level.

MCSminus versus MCSplus

Although differences between MCSminus and MCSplus were found at a statistically liberal threshold, *a priori* knowledge strengthened our findings of a more severely disrupted left hemisphere of the cerebral cortex in MCSminus as compared to MCSplus: higher metabolic dysfunction in the left cerebral hemisphere in patients in MCSminus as compared to those in MCSplus has previously been reported.[147] This could be explained by the fact that most patients were right-handed and where language-related processing was thus most often associated with the left cerebral cortex.[250] An understanding of language is of great importance for successfully conducting command following, intelligible verbalization, and answering verbal and written questions, the behavioral discriminators between MCSminus and MCSplus.[11, 147] Thus, our finding of greater damage in MCSminus in Wernicke's area, Broca's area, the primary auditory cortex, and the multimodal posterior area might be associated with disrupted language processing.[255-257]

5.6. Conclusion

Our results show that reduced consciousness in DOC correlates with widespread brain damage. Traumatic etiology was found to be related to higher focal damage in regions especially vulnerable to head impact-related brain movement. Our results furthermore show the great extent of atrophy secondary to initial brain injury, with a relative sparing of the right cortical hemisphere. No clear differences in brain damage were found between VS/UWS and MCS in our large patient sample, although a potential discriminator might be the posterior cingulate cortex/precuneus. In line with previous neuroimaging findings, our findings illustrate the difficulty of using only structural MRI for differentiating between VS/UWS and MCS, especially at the single subject level. Finally, a liberal threshold allowed us to find that patients in MCSplus are likely to have a more preserved left cerebral cortex than patients in MCSminus, which could be linked to the language functions most frequently attributed to this cerebral hemisphere.

Chapter 6

GENERAL DISCUSSION

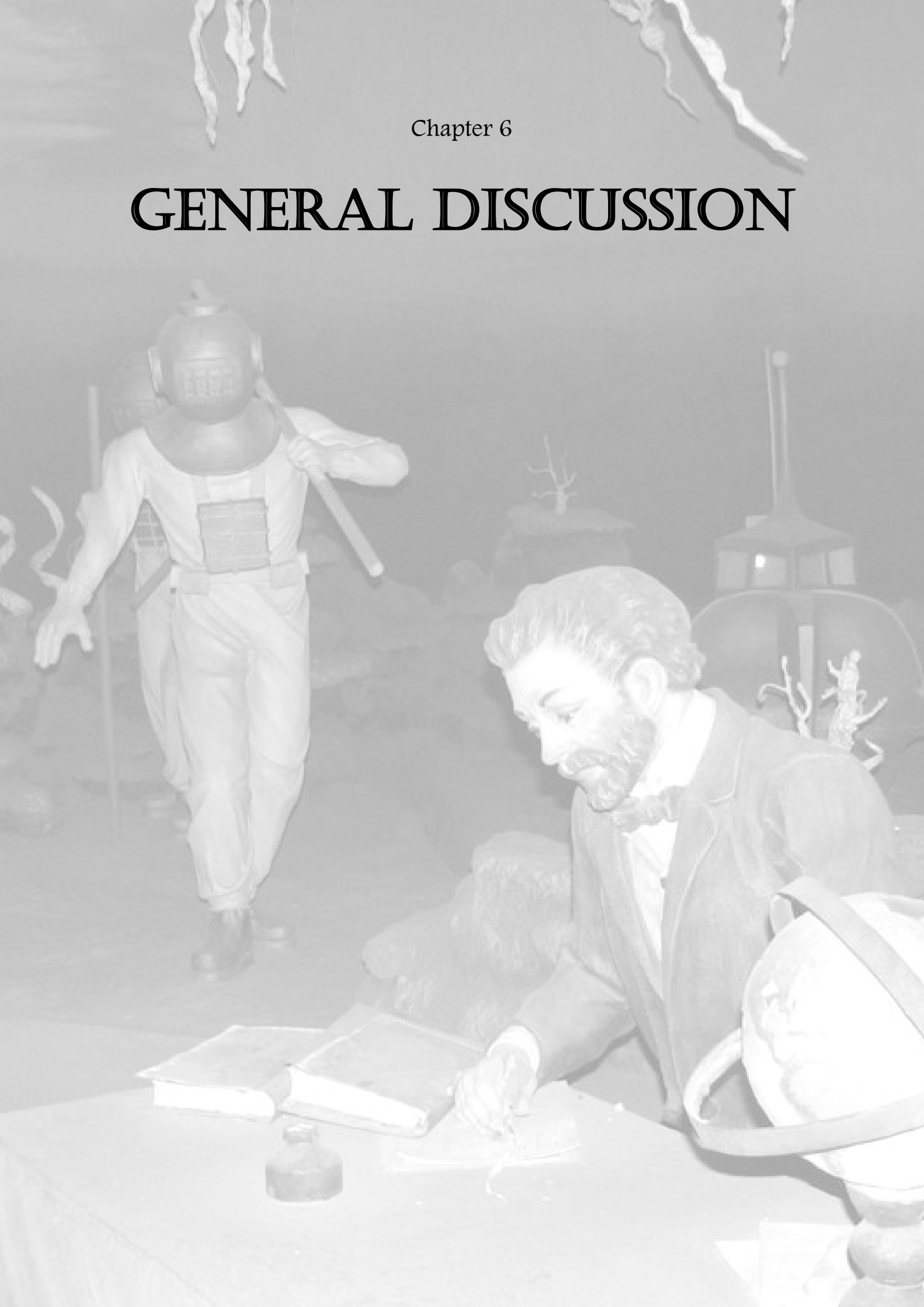

6.1. Anesthesia and disorders of consciousness: a comparison

In this thesis, we examined changes in brain functioning associated with loss of consciousness in propofol anesthesia and disorders of consciousness. One striking similarity we found between these conditions was decreased connectivity within higher-order resting state networks (default mode, external control, and salience networks). Previous studies employing positron emission tomography and functional magnetic resonance imaging have also provided evidence for disruption of the default mode network and external control network in these conditions,[15, 47, 52, 72, 73, 86, 258] and very recently also for a breakdown of the salience network in disorders of consciousness.[73] Our finding of salience network disconnection during propofol-induced unconsciousness (chapter 2)[140] completed this picture.

We also reported on the importance of disconnections occurring between higher-order networks and the thalamus with both types of loss of consciousness. For propofol-induced loss of consciousness, connectivity decreases between the thalamus and both default mode network and external control network had already been found during previous analyses,[47] which we supplemented with the finding of decreased connectivity between the thalamus and salience network. For disorders of consciousness, we found decreases between the thalamus and default mode network, as has recently also been reported using another analysis technique,[73] but we also saw evidence for disconnections between the thalamus and regions associated with the external control network and/or salience network (chapter 4).

Connectivity within the salience network regions, and possibly with the thalamus and brainstem, has been shown to be important for dynamically switching between default mode network and external control network connectivity, or internal and external awareness, respectively.[16, 259, 260] Regional cerebral blood flow in these regions has furthermore been associated with recovery from propofol- and dexmedetomidine-induced unconsciousness (dexmedetomidine is an anesthetic that has recently gained interest under anesthesiologists given the more sleep-like state of unconsciousness it appears to induce; a feature relatively unique among anesthetics).[261, 262] This shows the intimate relationship between higher-order resting state networks and the thalamus and brainstem.

Although connectivity changes during other types of loss of consciousness must be examined before a claim about general brain dynamics underlying loss of consciousness can be made, our findings are in favor of the view that loss of consciousness as a general phenomenon might be associated with disruption of both higher-order corticocortical connectivity and connectivity between the thalamus (/brainstem) and these cortical regions. The apparent mediating role of the thalamus between brainstem arousal areas, the networks for internal and external awareness (default mode network and external control network, respectively), and the salience network which orchestrates default mode network and external control network activity, might underlie why some patients in the minimally conscious state (MCS) benefit from deep brain stimulation of the thalamus.[93, 132, 263]

Interesting was that in our group of patients with disorders of consciousness, in which a low level or absence of consciousness was inferred, propofol administration was found to still diminish long-range connectivity between the thalamus and posterior cingulate cortex/precuneus (part of the default mode network), between the thalamus and a dorsolateral frontal region overlapping with the salience/external control networks, and within the salience network (chapter 4). This connectivity had already been severely disrupted due to the injuries leading to disorders of consciousness. The amounts of propofol administered would induce mild sedation in healthy subjects.[47] Behaviorally, propofol administration in these patients led to a reduction in head and body movement, making acquisition of better quality magnetic resonance images possible. Given the evidence showing the importance of connectivity within higher-order networks and between thalamus and higher-order networks for consciousness, it is intriguing to find that propofol can still reduce this connectivity in these patients.

As such, pathological and pharmacological loss of consciousness have been shown to share important traits. However, a clear difference between them is that disorders of consciousness are caused by structural brain damage, while anesthetics disturb normal brain functioning by acting on specific brain targets, usually neuronal receptors.[94] Structural brain damage in patients with disorders of consciousness was shown to be typically widespread (chapter 5), although structural integrity of default mode network regions was found to potentially discriminate between the vegetative state/unresponsive wakefulness syndrome (VS/UWS; no detectable awareness) and MCS (fluctuating low-level awareness). This, again, implies a special role for this higher-order resting state network in the generation of consciousness.[15] However, bridging the gap between structural and functional magnetic resonance imaging

findings, and then translating them to found behavioral alterations, is generally not straightforward.[264] We did find, at least at the group level, a relatively clear relationship between damage in MCSminus and MCSplus and behavior (patients with MCSplus show some preserved use/understanding of language, while those with MCSminus do not), as the greater left cortical damage found in MCSminus could be related to an inability to use/understand language, the main processing centers of which are usually located in the left cerebral cortex.[250] This furthermore stresses the importance of correctly assessing brain damage when using passive or active paradigms,[11] as severe brain damage might occur in (primary) sensory cortices and render these tests useless.

The found importance of connectivity within higher-order resting state networks and their connectivity with the thalamus and brainstem could be used to infer the level of consciousness in patients with disorders of consciousness, in order to aid differential diagnosis. However, the studies presented here are all group studies. Most literature on disorders of consciousness reports on groups, and transferring group-based knowledge (such as the correlation of default mode network connectivity with the level of consciousness in disorders of consciousness)[72] to the single subject level has so far proven to be extremely difficult with (functional) magnetic resonance imaging-based task-independent techniques. In order to improve detection sensitivity of potential discriminators between VS/UWS and MCS, finding better ways to integrate multimodal neuroimaging data is paramount. This approach should preferably include (resting state functional) magnetic resonance imaging, positron emission tomography, and transcranial magnetic stimulation-electroencephalography.[11, 138] Given the studies of this thesis, special attention during analysis should go to the thalamus, brainstem and all higher-order cortical brain regions, instead of just the default mode network. In addition, new ways of analyzing (functional) magnetic resonance imaging data (such as those presented in chapter 3), and the use of higher magnetic field strengths in the magnetic resonance imaging machines, leading to better image contrast, might lead to the discovery of new potential biomarkers for assessing the level of consciousness.

Given that neuroimaging-based differential diagnosis between VS/UWS and MCS appears to be dependent on relatively minor differences in brain connectivity and structure, a further important point is the issue of data quality. Acquisition of resting state functional magnetic resonance images in patients with disorders of consciousness is a challenging operation. One of the main problems is restraining patient movement, as (resting state) functional magnetic resonance imaging is

exceptionally sensitive to head motion. This could induce false-positive 'activations' when motion artifacts are correlated with the stimulus, events of interest or neuronal activation. False-negative 'activations' can result from reduced detection sensitivity due to motion-induced noise.[179] Furthermore, head displacement leads to an altered head position in the scanner, changing slice orientation. Physical head restraint techniques are frequently not able to cope with the uncontrolled movements displayed by patients with disorders of consciousness, and post-scan preprocessing steps cannot fully repair such damaged data, although this has become an active field of research.[180] A frequently applied technique to reduce patient movement is the application of a sedative, as mentioned in chapter 4 of this thesis. Although we did not find great decreases in resting state brain connectivity associated with the sedation-level use of propofol in these patients, continuing attempts should be made to find alternative methods.

In conclusion, our findings show that structural magnetic resonance imaging and resting state functional magnetic resonance imaging have the potential to aid in the differential diagnosis of patients with disorders of consciousness, although more research is needed to translate our results to the single subject level. Novel biomarker candidates include structural intactness of midline default mode network regions (for VS/UWS-MCS discrimination) and the intactness of the left cerebral cortex (for MCSminus-MCSplus discrimination). Functional connectivity analysis of the salience network, its connectivity with the thalamus/brainstem, as well as 'total brain connectivity analysis' and BOLD signal mean oscillatory frequency analysis (chapter 3), could further aid.

6.2. Future projects

With the experiments described in this thesis, we aimed to increase our knowledge of resting state connectivity during propofol- and brain damage-induced loss of consciousness. Their results can be followed up by experiments in a variety of directions, some of which will now be discussed.

Dexmedetomidine, propofol, sleep, and disorders of consciousness

In addition to propofol, another general anesthetic, dexmedetomidine, has recently gained interest under anesthesiologists, as it has several benefits over propofol.[265, 266] These include reduced incidence of respiratory problems and delirium.[267] Another main difference is that dexmedetomidine-induced unconsciousness is thought to be more similar to natural sleep than propofol-induced unconsciousness.[265, 266] Like during sleep, but unlike during propofol-induced unconsciousness, subjects can be readily awakened with administration of a salient stimulus.[268] This behavioral difference between the two anesthetics has been associated with different target sites in the brain. Instead of gamma aminobutyric acid receptor activation, occurring with propofol, dexmedetomidine is thought to actively target adrenergic receptors, specifically in the brainstem's locus coeruleus.[269] This region is also part of the mechanism inducing natural sleep.[10, 262, 270]

We will examine if there are differences in brain connectivity between propofol- and dexmedetomidine-induced unconsciousness, focusing on the seven resting state networks used in our study of the effect of propofol on brain connectivity in patients with disorders of consciousness (chapter 4). These are the four higher-order resting state networks (default mode, left and right external control, and salience networks), as well as the auditory, visual, and sensorimotor networks. Additionally, we will explore connectivity with the thalamus and mesopontine brainstem region, as used in our the study of the effect of propofol on connectivity in the salience network and with the thalamus and brainstem (chapter 2),[140] and the locus coeruleus, given its known importance in dexmedetomidine-induced unconsciousness.[269]

Similarities and differences between changes associated with loss of consciousness for each of the anesthetics will be explored. Similarities might be mainly associated with the main behavioral similarity: loss of consciousness. In contrast, differences might stem from another behavioral difference: dexmedetomidine-, but not propofol-induced unconsciousness, can be easily reverted with a salient stimulus.[268] Literature offers several neuroimaging-based candidates for a brain mechanism underlying this difference. Regional cerebral blood flow in the mesopontine brainstem area, thalamus, and anterior cingulate cortex has been associated with recovery from both propofol- and dexmedetomidine-induced unconsciousness.[261] The thalamus and anterior cingulate cortex/presupplementary motor area have also been implicated with perception of subtle[260] and noxious[70, 271] sensorimotor stimuli; which is interesting knowing that pain is one of the most potent stimuli capable of arousing subjects from dexmedetomidine-induced unconsciousness.

In addition to the comparison between propofol and dexmedetomidine, we will also examine connectivity changes associated with natural non-rapid eye movement sleep, which will be compared to those associated with propofol- and dexmedetomidine-induced unconsciousness. As with dexmedetomidine-induced unconsciousness, subjects in non-rapid eye movement sleep can rapidly recover consciousness after application of a salient stimulus. We will again concentrate on the connectivity within the seven resting state networks used in the other two analyses, as well as connectivity with the thalamus, mesopontine area, and locus coeruleus. This way, we can compare the three types of unconsciousness. If connectivity patterns are found in dexmedetomidine-induced unconsciousness and non-rapid eye movement sleep, but not in propofol-induced unconsciousness, we might have located connectivity patterns that could underlie the recovery of consciousness. It might be expected that the higher regional cerebral blood flow associated with recovery after dexmedetomidine- and propofol-induced unconsciousness in the thalamus and anterior cingulate cortex[261] might be dependent on relatively spared resting state connectivity between these regions during unconsciousness.

We will use previously published resting state functional magnetic resonance imaging propofol[47, 86, 140] and sleep data,[272] as well as unpublished dexmedetomidine data that has recently been acquired. For the sleep data, we have the awake state and non-rapid eye movement sleep, as assessed with electroencephalography. For propofol and dexmedetomidine, we have four states: wakefulness, mild sedation,

unconsciousness, and recovery. If a common connectivity pattern can be found that might underlie brain arousal leading to recovery of consciousness, a resting state connectivity comparison between coma (absence of brain arousal and awareness), VS/UWS (partially recovered arousal, and absence of awareness), and MCS (partially recovered arousal and awareness) might be added, using previously gathered patient data.[24, 73, 125]

Frequency and total brain connectivity analyses in dexmedetomidine-induced unconsciousness, sleep, and disorders of consciousness

In order to better understand the effect of propofol on brain dynamics, we introduced several new methods to analyze resting state functional magnetic resonance imaging data. We found that loss of consciousness was associated with increased mean oscillatory frequencies of the blood oxygenation level-dependent signal in most areas of the brain, while a predominantly frontal decrease of brain connectivity was observed (chapter 3). These methods appear to have an increased sensitivity as compared to classical approaches, and might therefore result in new biomarkers to be used in differential diagnosis in disorders of consciousness.[11] However, a better understanding of the observed values is necessary. One first step is to compare the results found for propofol with results from other states of altered consciousness, such as that induced by the anesthetic dexmedetomidine,[262] and during sleep and disorders of consciousness.

REFERENCES

1. Weiner J. Time, Love, Memory. A Great Biologist and His Quest for the Origins of Behavior. Vintage books; 1999.
2. Pandya SK. Understanding brain, mind and soul: contributions from neurology and neurosurgery. Mens Sana Monogr. 2011; 9(1): 129-49.
3. Marks LE. A Brief History of Sensation and Reward. 2011.
4. Rosenbaum DA, Chapman KM, Weigelt M, Weiss DJ, van der Wel R. Cognition, action, and object manipulation. Psychol Bull. 2012; 138(5): 924-46.
5. Haas LF. Hans Berger (1873-1941), Richard Caton (1842-1926), and electroencephalography. J Neurol Neurosurg Psychiatry. 2003; 74(1): 9.
6. Nir Y, Tononi G. Dreaming and the brain: from phenomenology to neurophysiology. Trends Cogn Sci. 2010; 14(2): 88-100.
7. Kerkhofs M, Lavie P. Frederic Bremer 1892-1982: a pioneer in sleep research. Sleep Med Rev. 2000; 4(5): 505-14.
8. Shampo MA, Kyle RA, Steensma DP. Horace Magoun--neuroanatomist and neurophysiologist. Mayo Clin Proc. 2013; 88(4): e33.
9. Levi-Montalcini R, Piccolino M, Wade NJ. Giuseppe Moruzzi: a tribute to a "formidable" scientist and a "formidable" man. Brain Res Rev. 2011; 66(1-2): 256-69.
10. Saper CB. The neurobiology of sleep. Continuum (Minneap Minn). 2013; 19(1 Sleep Disorders): 19-31.
11. Guldenmund P, Stender J, Heine L, Laureys S. Mindsight: diagnostics in disorders of consciousness. Critical care research and practice. 2012; 2012: 624724.
12. Sutherland S. International Dictionary of Psychology: The Crossroad Publishing Company; 1989.
13. Kanai R, Tsuchiya N. Qualia. Curr Biol. 2012; 22(10): R392-6.
14. Vanhaudenhuyse A, Demertzi A, Schabus M, Noirhomme Q, Bredart S, Boly M, et al. Two distinct neuronal networks mediate the awareness of environment and of self. Journal of cognitive neuroscience. 2011; 23(3): 570-8.
15. Guldenmund P, Vanhaudenhuyse A, Boly M, Laureys S, Soddu A. A default mode of brain function in altered states of consciousness. Arch Ital Biol. 2012; 150(2-3): 107-21.
16. Menon V, Uddin LQ. Saliency, switching, attention and control: a network model of insula function. Brain structure & function. 2010; 214(5-6): 655-67.
17. Bartels A, Zeki S. The temporal order of binding visual attributes. Vision Res. 2006; 46(14): 2280-6.
18. VanRullen R, Koch C. Is perception discrete or continuous? Trends Cogn Sci. 2003; 7(5): 207-13.
19. Breitmeyer BG. Visual masking: past accomplishments, present status, future developments. Adv Cogn Psychol. 2007; 3(1-2): 9-20.
20. Brancucci A, Tommasi L. "Binaural rivalry": dichotic listening as a tool for the investigation of the neural correlate of consciousness. Brain Cogn. 2011; 76(2): 218-24.
21. Brogaard B. Are there unconscious perceptual processes? Conscious Cogn. 2011; 20(2): 449-63.
22. Cleeremans A. The Radical Plasticity Thesis: How the Brain Learns to be Conscious. Front Psychol. 2011; 2: 86.
23. Saper CB, Scammell TE, Lu J. Hypothalamic regulation of sleep and circadian rhythms. Nature. 2005; 437(7063): 1257-63.

24. Laureys S, Owen AM, Schiff ND. Brain function in coma, vegetative state, and related disorders. Lancet neurology. 2004; 3(9): 537-46.
25. Mantini D, Gerits A, Nelissen K, Durand JB, Joly O, Simone L, et al. Default mode of brain function in monkeys. J Neurosci. 2011; 31(36): 12954-62.
26. Lu H, Zou Q, Gu H, Raichle ME, Stein EA, Yang Y. Rat brains also have a default mode network. Proc Natl Acad Sci U S A. 2012; 109(10): 3979-84.
27. Kyathanahally SP, Jia H, Pustovyy OM, Waggoner P, Beyers R, Schumacher J, et al. Anterior-posterior dissociation of the default mode network in dogs. Brain Struct Funct. 2014.
28. Mather JA. Cephalopod consciousness: behavioural evidence. Conscious Cogn. 2008; 17(1): 37-48.
29. Plotnik JM, de Waal FB, Reiss D. Self-recognition in an Asian elephant. Proc Natl Acad Sci U S A. 2006; 103(45): 17053-7.
30. De Sousa A. Towards an integrative theory of consciousness: part 1 (neurobiological and cognitive models). Mens Sana Monogr. 2013; 11(1): 100-50.
31. Bruno MA, Fernandez-Espejo D, Lehembre R, Tshibanda L, Vanhaudenhuyse A, Gosseries O, et al. Multimodal neuroimaging in patients with disorders of consciousness showing "functional hemispherectomy". Prog Brain Res. 2011; 193: 323-33.
32. French CC. Near-death experiences in cardiac arrest survivors. Prog Brain Res. 2005; 150: 351-67.
33. Blanke O, Mohr C, Michel CM, Pascual-Leone A, Brugger P, Seeck M, et al. Linking out-of-body experience and self processing to mental own-body imagery at the temporoparietal junction. J Neurosci. 2005; 25(3): 550-7.
34. Merker B. Consciousness without a cerebral cortex: a challenge for neuroscience and medicine. Behav Brain Sci. 2007; 30(1): 63-81; discussion -134.
35. Feinberg TE, Mallatt J. The evolutionary and genetic origins of consciousness in the Cambrian Period over 500 million years ago. Front Psychol. 2013; 4: 667.
36. Macovski A. MRI: a charmed past and an exciting future. J Magn Reson Imaging. 2009; 30(5): 919-23.
37. Pauling L, Coryell C. The magnetic properties and structure of hemoglobin, oxyhemoglobin and carbonmonoxy hemoglobin. Proceedings of the National Academy of Sciences of the United States of America. 1936; 22: 210-6.
38. Kim SG, Ogawa S. Biophysical and physiological origins of blood oxygenation level-dependent fMRI signals. J Cereb Blood Flow Metab. 2012; 32(7): 1188-206.
39. Gusnard DA, Raichle ME. Searching for a baseline: functional imaging and the resting human brain. Nat Rev Neurosci. 2001; 2(10): 685-94.
40. Margulies DS, Bottger J, Long X, Lv Y, Kelly C, Schafer A, et al. Resting developments: a review of fMRI post-processing methodologies for spontaneous brain activity. Magma. 2010; 23(5-6): 289-307.
41. Damoiseaux JS, Rombouts SA, Barkhof F, Scheltens P, Stam CJ, Smith SM, et al. Consistent resting-state networks across healthy subjects. Proceedings of the National Academy of Sciences of the United States of America. 2006; 103(37): 13848-53.
42. Kirsch M, Guldenmund P, Bahri M, Demertzi A, Baquero K, Heine L, et al. Sedation of patients with disorders of consciousness during neuroimaging: effects on resting state functional brain connectivity submitted.
43. Lopez-Valverde A, Montero J, Albaladejo A, Gomez de Diego R. The discovery of surgical anesthesia: discrepancies regarding its authorship. J Dent Res. 2011; 90(1): 31-4.
44. Holzman RS. "The History of Sedation." Pediatric Sedation Outside of the Operating Room. New York: Springer; 2012.
45. Machata AM, Willschke H, Kabon B, Kettner SC, Marhofer P. Propofol-based sedation regimen for infants and children undergoing ambulatory magnetic resonance imaging. Br J Anaesth. 2008; 101(2): 239-43.

46. Stamatakis EA, Adapa RM, Absalom AR, Menon DK. Changes in resting neural connectivity during propofol sedation. PloS one. 2010; 5(12): e14224.
47. Boveroux P, Vanhaudenhuyse A, Bruno MA, Noirhomme Q, Lauwick S, Luxen A, et al. Breakdown of within- and between-network resting state functional magnetic resonance imaging connectivity during propofol-induced loss of consciousness. Anesthesiology. 2010; 113(5): 1038-53.
48. Bonhomme V, Fiset P, Meuret P, Backman S, Plourde G, Paus T, et al. Propofol anesthesia and cerebral blood flow changes elicited by vibrotactile stimulation: a positron emission tomography study. Journal of neurophysiology. 2001; 85(3): 1299-308.
49. Schlunzen L, Juul N, Hansen KV, Cold GE. Regional cerebral blood flow and glucose metabolism during propofol anaesthesia in healthy subjects studied with positron emission tomography. Acta anaesthesiologica Scandinavica. 2012; 56(2): 248-55.
50. Xie G, Deschamps A, Backman SB, Fiset P, Chartrand D, Dagher A, et al. Critical involvement of the thalamus and precuneus during restoration of consciousness with physostigmine in humans during propofol anaesthesia: a positron emission tomography study. Br J Anaesth. 2011; 106(4): 548-57.
51. Fiset P, Paus T, Daloze T, Plourde G, Meuret P, Bonhomme V, et al. Brain mechanisms of propofol-induced loss of consciousness in humans: a positron emission tomographic study. The Journal of neuroscience : the official journal of the Society for Neuroscience. 1999; 19(13): 5506-13.
52. Kaisti KK, Langsjo JW, Aalto S, Oikonen V, Sipila H, Teras M, et al. Effects of sevoflurane, propofol, and adjunct nitrous oxide on regional cerebral blood flow, oxygen consumption, and blood volume in humans. Anesthesiology. 2003; 99(3): 603-13.
53. Cimenser A, Purdon PL, Pierce ET, Walsh JL, Salazar-Gomez AF, Harrell PG, et al. Tracking brain states under general anesthesia by using global coherence analysis. Proceedings of the National Academy of Sciences of the United States of America. 2011; 108(21): 8832-7.
54. Gugino LD, Chabot RJ, Prichep LS, John ER, Formanek V, Aglio LS. Quantitative EEG changes associated with loss and return of consciousness in healthy adult volunteers anaesthetized with propofol or sevoflurane. Br J Anaesth. 2001; 87(3): 421-8.
55. Supp GG, Siegel M, Hipp JF, Engel AK. Cortical hypersynchrony predicts breakdown of sensory processing during loss of consciousness. Current biology : CB. 2011; 21(23): 1988-93.
56. Tinker JH, Sharbrough FW, Michenfelder JD. Anterior shift of the dominant EEG rhytham during anesthesia in the Java monkey: correlation with anesthetic potency. Anesthesiology. 1977; 46(4): 252-9.
57. John ER, Prichep LS. The anesthetic cascade: a theory of how anesthesia suppresses consciousness. Anesthesiology. 2005; 102(2): 447-71.
58. Niedermeyer E. Alpha rhythms as physiological and abnormal phenomena. International journal of psychophysiology : official journal of the International Organization of Psychophysiology. 1997; 26(1-3): 31-49.
59. Jensen O, Mazaheri A. Shaping functional architecture by oscillatory alpha activity: gating by inhibition. Frontiers in human neuroscience. 2010; 4: 186.
60. Foxe JJ, Snyder AC. The Role of Alpha-Band Brain Oscillations as a Sensory Suppression Mechanism during Selective Attention. Frontiers in psychology. 2011; 2: 154.
61. Hanslmayr S, Gross J, Klimesch W, Shapiro KL. The role of alpha oscillations in temporal attention. Brain research reviews. 2011; 67(1-2): 331-43.
62. Mathewson KE, Lleras A, Beck DM, Fabiani M, Ro T, Gratton G. Pulsed out of awareness: EEG alpha oscillations represent a pulsed-inhibition of ongoing cortical processing. Frontiers in psychology. 2011; 2: 99.
63. Ben-Simon E, Podlipsky I, Okon-Singer H, Gruberger M, Cvetkovic D, Intrator N, et al. The dark side of the alpha rhythm: fMRI evidence for induced alpha modulation during complete darkness. The European journal of neuroscience. 2012.
64. Zorab J. The resuscitation greats. Bjorn Ibsen. Resuscitation. 2003; 57(1): 3-9.

65. Laureys S, Pellas F, Van Eeckhout P, Ghorbel S, Schnakers C, Perrin F, et al. The locked-in syndrome : what is it like to be conscious but paralyzed and voiceless? Prog Brain Res. 2005; 150: 495-511.
66. Estraneo A, Moretta P, Loreto V, Lanzillo B, Santoro L, Trojano L. Late recovery after traumatic, anoxic, or hemorrhagic long-lasting vegetative state. Neurology. 2010; 75(3): 239-45.
67. Giacino J, Kalmar K. The Vegetative and Minimally Conscious States: A Comparison of Clinical Features and Functional Outcome. Journal of Head Trauma Rehabilitation. 1997; 12(4): 36-51.
68. Luaute J, Maucort-Boulch D, Tell L, Quelard F, Sarraf T, Iwaz J, et al. Long-term outcomes of chronic minimally conscious and vegetative states. Neurology. 2010; 75(3): 246-52.
69. Lammi MH, Smith VH, Tate RL, Taylor CM. The minimally conscious state and recovery potential: a follow-up study 2 to 5 years after traumatic brain injury. Arch Phys Med Rehabil. 2005; 86(4): 746-54.
70. Boly M, Faymonville ME, Schnakers C, Peigneux P, Lambermont B, Phillips C, et al. Perception of pain in the minimally conscious state with PET activation: an observational study. Lancet Neurol. 2008; 7(11): 1013-20.
71. Monti MM, Vanhaudenhuyse A, Coleman MR, Boly M, Pickard JD, Tshibanda L, et al. Willful modulation of brain activity in disorders of consciousness. The New England journal of medicine. 2010; 362(7): 579-89.
72. Vanhaudenhuyse A, Noirhomme Q, Tshibanda LJ, Bruno MA, Boveroux P, Schnakers C, et al. Default network connectivity reflects the level of consciousness in non-communicative brain-damaged patients. Brain : a journal of neurology. 2010; 133(Pt 1): 161-71.
73. Demertzi A, Gomez F, Crone JS, Vanhaudenhuyse A, Tshibanda L, Noirhomme Q, et al. Multiple fMRI system-level baseline connectivity is disrupted in patients with consciousness alterations. Cortex. 2014; 52: 35-46.
74. Juengling FD, Kassubek J, Huppertz HJ, Krause T, Els T. Separating functional and structural damage in persistent vegetative state using combined voxel-based analysis of 3-D MRI and FDG-PET. Journal of the neurological sciences. 2005; 228(2): 179-84.
75. Jellinger KA. Neuropathology of prolonged unresponsive wakefulness syndrome after blunt head injury: Review of 100 post-mortem cases. Brain Inj. 2013.
76. Kinney HC, Korein J, Panigrahy A, Dikkes P, Goode R. Neuropathological findings in the brain of Karen Ann Quinlan. The role of the thalamus in the persistent vegetative state. The New England journal of medicine. 1994; 330(21): 1469-75.
77. Adams JH, Graham DI, Jennett B. The neuropathology of the vegetative state after an acute brain insult. Brain : a journal of neurology. 2000; 123 (Pt 7): 1327-38.
78. Adams JH, Jennett B, McLellan DR, Murray LS, Graham DI. The neuropathology of the vegetative state after head injury. Journal of clinical pathology. 1999; 52(11): 804-6.
79. Maxwell WL, Pennington K, MacKinnon MA, Smith DH, McIntosh TK, Wilson JT, et al. Differential responses in three thalamic nuclei in moderately disabled, severely disabled and vegetative patients after blunt head injury. Brain : a journal of neurology. 2004; 127(Pt 11): 2470-8.
80. Maxwell WL, MacKinnon MA, Smith DH, McIntosh TK, Graham DI. Thalamic nuclei after human blunt head injury. Journal of neuropathology and experimental neurology. 2006; 65(5): 478-88.
81. Fernandez-Espejo D, Junque C, Bernabeu M, Roig-Rovira T, Vendrell P, Mercader JM. Reductions of thalamic volume and regional shape changes in the vegetative and the minimally conscious states. Journal of neurotrauma. 2010; 27(7): 1187-93.
82. Fernandez-Espejo D, Bekinschtein T, Monti MM, Pickard JD, Junque C, Coleman MR, et al. Diffusion weighted imaging distinguishes the vegetative state from the minimally conscious state. NeuroImage. 2011; 54(1): 103-12.

83. Fernandez-Espejo D, Soddu A, Cruse D, Palacios EM, Junque C, Vanhaudenhuyse A, et al. A role for the default mode network in the bases of disorders of consciousness. Annals of neurology. 2012; 72(3): 335-43.
84. Newcombe VF, Williams GB, Scoffings D, Cross J, Carpenter TA, Pickard JD, et al. Aetiological differences in neuroanatomy of the vegetative state: insights from diffusion tensor imaging and functional implications. J Neurol Neurosurg Psychiatry. 2010; 81(5): 552-61.
85. Horovitz SG, Braun AR, Carr WS, Picchioni D, Balkin TJ, Fukunaga M, et al. Decoupling of the brain's default mode network during deep sleep. Proceedings of the National Academy of Sciences of the United States of America. 2009; 106(27): 11376-81.
86. Schrouff J, Perlbarg V, Boly M, Marrelec G, Boveroux P, Vanhaudenhuyse A, et al. Brain functional integration decreases during propofol-induced loss of consciousness. NeuroImage. 2011; 57(1): 198-205.
87. Seeley WW, Menon V, Schatzberg AF, Keller J, Glover GH, Kenna H, et al. Dissociable intrinsic connectivity networks for salience processing and executive control. The Journal of neuroscience : the official journal of the Society for Neuroscience. 2007; 27(9): 2349-56.
88. Bonnelle V, Ham TE, Leech R, Kinnunen KM, Mehta MA, Greenwood RJ, et al. Salience network integrity predicts default mode network function after traumatic brain injury. Proceedings of the National Academy of Sciences of the United States of America. 2012; 109(12): 4690-5.
89. Giacino J, Fins JJ, Machado A, Schiff ND. Central thalamic deep brain stimulation to promote recovery from chronic posttraumatic minimally conscious state: challenges and opportunities. Neuromodulation : journal of the International Neuromodulation Society. 2012; 15(4): 339-49.
90. Angeles Fernandez-Gil M, Palacios-Bote R, Leo-Barahona M, Mora-Encinas JP. Anatomy of the brainstem: a gaze into the stem of life. Semin Ultrasound CT MR. 2010; 31(3): 196-219.
91. Devor M, Zalkind V. Reversible analgesia, atonia, and loss of consciousness on bilateral intracerebral microinjection of pentobarbital. Pain. 2001; 94(1): 101-12.
92. Schiff ND, Fins JJ. Deep brain stimulation and cognition: moving from animal to patient. Current opinion in neurology. 2007; 20(6): 638-42.
93. Schiff ND. Central thalamic contributions to arousal regulation and neurological disorders of consciousness. Ann N Y Acad Sci. 2008; 1129: 105-18.
94. Brown EN, Lydic R, Schiff ND. General anesthesia, sleep, and coma. N Engl J Med. 2010; 363(27): 2638-50.
95. Pinault D. Dysfunctional thalamus-related networks in schizophrenia. Schizophr Bull. 2011; 37(2): 238-43.
96. Tang L, Ge Y, Sodickson DK, Miles L, Zhou Y, Reaume J, et al. Thalamic resting-state functional networks: disruption in patients with mild traumatic brain injury. Radiology. 2011; 260(3): 831-40.
97. Brown EN, Purdon PL, Van Dort CJ. General anesthesia and altered states of arousal: a systems neuroscience analysis. Annual review of neuroscience. 2011; 34: 601-28.
98. Olson DM, Thoyre SM, Auyong DB. Perspectives on sedation assessment in critical care. AACN Adv Crit Care. 2007; 18(4): 380-95.
99. Hyvarinen A KJ, Oja E Independent component analysis: John Wiley & Sons; 2001.
100. McKeown MJ, Makeig S, Brown GG, Jung TP, Kindermann SS, Bell AJ, et al. Analysis of fMRI data by blind separation into independent spatial components. Human brain mapping. 1998; 6(3): 160-88.
101. Soddu A, Vanhaudenhuyse A, Bahri MA, Bruno MA, Boly M, Demertzi A, et al. Identifying the default-mode component in spatial IC analyses of patients with disorders of consciousness. Human brain mapping. 2012; 33(4): 778-96.
102. Maudoux A, Lefebvre P, Cabay JE, Demertzi A, Vanhaudenhuyse A, Laureys S, et al. Connectivity graph analysis of the auditory resting state network in tinnitus. Brain research. 2012; 1485: 10-21.

103. Demertzi A, Soddu A, Faymonville ME, Bahri MA, Gosseries O, Vanhaudenhuyse A, et al. Hypnotic modulation of resting state fMRI default mode and extrinsic network connectivity. Prog Brain Res. 2011; 193: 309-22.
104. Fair DA, Cohen AL, Dosenbach NU, Church JA, Miezin FM, Barch DM, et al. The maturing architecture of the brain's default network. Proceedings of the National Academy of Sciences of the United States of America. 2008; 105(10): 4028-32.
105. Fox MD, Snyder AZ, Vincent JL, Corbetta M, Van Essen DC, Raichle ME. The human brain is intrinsically organized into dynamic, anticorrelated functional networks. Proceedings of the National Academy of Sciences of the United States of America. 2005; 102(27): 9673-8.
106. De Martino F, Gentile F, Esposito F, Balsi M, Di Salle F, Goebel R, et al. Classification of fMRI independent components using IC-fingerprints and support vector machine classifiers. Neuroimage. 2007; 34(1): 177-94.
107. Abulafia R, Zalkind V, Devor M. Cerebral activity during the anesthesia-like state induced by mesopontine microinjection of pentobarbital. The Journal of neuroscience : the official journal of the Society for Neuroscience. 2009; 29(21): 7053-64.
108. Saper CB, Cano G, Scammell TE. Homeostatic, circadian, and emotional regulation of sleep. J Comp Neurol. 2005; 493(1): 92-8.
109. Wang DS, Orser BA. Inhibition of learning and memory by general anesthetics. Can J Anaesth. 2011; 58(2): 167-77.
110. Aron AR, Robbins TW, Poldrack RA. Inhibition and the right inferior frontal cortex. Trends Cogn Sci. 2004; 8(4): 170-7.
111. Duann JR, Ide JS, Luo X, Li CS. Functional connectivity delineates distinct roles of the inferior frontal cortex and presupplementary motor area in stop signal inhibition. The Journal of neuroscience : the official journal of the Society for Neuroscience. 2009; 29(32): 10171-9.
112. Martuzzi R, Ramani R, Qiu M, Rajeevan N, Constable RT. Functional connectivity and alterations in baseline brain state in humans. NeuroImage. 2010; 49(1): 823-34.
113. Boly M, Tshibanda L, Vanhaudenhuyse A, Noirhomme Q, Schnakers C, Ledoux D, et al. Functional connectivity in the default network during resting state is preserved in a vegetative but not in a brain dead patient. Human brain mapping. 2009; 30(8): 2393-400.
114. Greicius MD, Kiviniemi V, Tervonen O, Vainionpaa V, Alahuhta S, Reiss AL, et al. Persistent default-mode network connectivity during light sedation. Human brain mapping. 2008; 29(7): 839-47.
115. Lieberman MD, Cunningham WA. Type I and Type II error concerns in fMRI research: re-balancing the scale. Social cognitive and affective neuroscience. 2009; 4(4): 423-8.
116. Beckmann CF, DeLuca M, Devlin JT, Smith SM. Investigations into resting-state connectivity using independent component analysis. Philos Trans R Soc Lond B Biol Sci. 2005; 360(1457): 1001-13.
117. Ellison-Wright I, Bullmore E. Anatomy of bipolar disorder and schizophrenia: a meta-analysis. Schizophr Res. 2010; 117(1): 1-12.
118. Palaniyappan L, Liddle PF. Does the salience network play a cardinal role in psychosis? An emerging hypothesis of insular dysfunction. J Psychiatry Neurosci. 2012; 37(1): 17-27.
119. Seeley WW. Anterior insula degeneration in frontotemporal dementia. Brain Struct Funct. 2010; 214(5-6): 465-75.
120. Seeley WW. Selective functional, regional, and neuronal vulnerability in frontotemporal dementia. Curr Opin Neurol. 2008; 21(6): 701-7.
121. Ching S, Cimenser A, Purdon PL, Brown EN, Kopell NJ. Thalamocortical model for a propofol-induced alpha-rhythm associated with loss of consciousness. Proceedings of the National Academy of Sciences of the United States of America. 2010; 107(52): 22665-70.
122. Lachaux JP, Fonlupt P, Kahane P, Minotti L, Hoffmann D, Bertrand O, et al. Relationship between task-related gamma oscillations and BOLD signal: new insights from combined fMRI and intracranial EEG. Human brain mapping. 2007; 28(12): 1368-75.

123. Fair DA, Bathula D, Mills KL, Dias TG, Blythe MS, Zhang D, et al. Maturing thalamocortical functional connectivity across development. Frontiers in systems neuroscience. 2010; 4: 10.
124. de Lecea L, Carter ME, Adamantidis A. Shining light on wakefulness and arousal. Biological psychiatry. 2012; 71(12): 1046-52.
125. Laureys S BM. The changing spectrum of coma. Nature Clinical Practice Neurology. 2008; 4(10): 544-6.
126. Parvizi J, Damasio A. Consciousness and the brainstem. Cognition. 2001; 79(1-2): 135-60.
127. Linnman C, Moulton EA, Barmettler G, Becerra L, Borsook D. Neuroimaging of the periaqueductal gray: state of the field. NeuroImage. 2012; 60(1): 505-22.
128. Modinos G, Ormel J, Aleman A. Activation of anterior insula during self-reflection. PloS one. 2009; 4(2): e4618.
129. Murphy M, Bruno MA, Riedner BA, Boveroux P, Noirhomme Q, Landsness EC, et al. Propofol anesthesia and sleep: a high-density EEG study. Sleep. 2011; 34(3): 283-91A.
130. Boly M, Moran R, Murphy M, Boveroux P, Bruno MA, Noirhomme Q, et al. Connectivity changes underlying spectral EEG changes during propofol-induced loss of consciousness. J Neurosci. 2012; 32(20): 7082-90.
131. Constantinople CM, Bruno RM. Effects and mechanisms of wakefulness on local cortical networks. Neuron. 2011; 69(6): 1061-8.
132. Schiff ND, Plum F. The role of arousal and "gating" systems in the neurology of impaired consciousness. Journal of clinical neurophysiology : official publication of the American Electroencephalographic Society. 2000; 17(5): 438-52.
133. Shah SA, Schiff ND. Central thalamic deep brain stimulation for cognitive neuromodulation - a review of proposed mechanisms and investigational studies. The European journal of neuroscience. 2010; 32(7): 1135-44.
134. Alkire MT, McReynolds JR, Hahn EL, Trivedi AN. Thalamic microinjection of nicotine reverses sevoflurane-induced loss of righting reflex in the rat. Anesthesiology. 2007; 107(2): 264-72.
135. Wise RG, Ide K, Poulin MJ, Tracey I. Resting fluctuations in arterial carbon dioxide induce significant low frequency variations in BOLD signal. Neuroimage. 2004; 21(4): 1652-64.
136. Birn RM, Diamond JB, Smith MA, Bandettini PA. Separating respiratory-variation-related fluctuations from neuronal-activity-related fluctuations in fMRI. Neuroimage. 2006; 31(4): 1536-48.
137. Corfield DR, Murphy K, Josephs O, Adams L, Turner R. Does hypercapnia-induced cerebral vasodilation modulate the hemodynamic response to neural activation? Neuroimage. 2001; 13(6 Pt 1): 1207-11.
138. Gosseries O, Thibaut A, Boly M, Rosanova M, Massimini M, Laureys S. Assessing consciousness in coma and related states using transcranial magnetic stimulation combined with electroencephalography. Ann Fr Anesth Reanim. 2014; 33(2): 65-71.
139. Laureys S, Celesia GG, Cohadon F, Lavrijsen J, Leon-Carrion J, Sannita WG, et al. Unresponsive wakefulness syndrome: a new name for the vegetative state or apallic syndrome. BMC medicine. 2010; 8: 68.
140. Guldenmund P, Demertzi A, Boveroux P, Boly M, Vanhaudenhuyse A, Bruno MA, et al. Thalamus, brainstem and salience network connectivity changes during mild propofol sedation and unconsciousness. Brain connectivity. 2013.
141. Marinazzo D, Pellicoro M, Wu G, Angelini L, Cortes JM, Stramaglia S. Information transfer and criticality in the ising model on the human connectome. PLoS One. 2014; 9(4): e93616.
142. Marinazzo D, Pellicoro M, Wu G-R, Angelini L, Cortes J, Stramaglia S. Information transfer of an Ising model on a brain network. BMC Neuroscience. 2013; 14((Suppl. 1)): 376.
143. Honey CJ, Sporns O, Cammoun L, Gigandet X, Thiran JP, Meuli R, et al. Predicting human resting-state functional connectivity from structural connectivity. Proc Natl Acad Sci U S A. 2009; 106(6): 2035-40.
144. Cabral J, Hugues E, Kringelbach ML, Deco G. Modeling the outcome of structural disconnection on resting-state functional connectivity. Neuroimage. 2012; 62(3): 1342-53.

145. Fraiman D, Balenzuela P, Foss J, Chialvo DR. Ising-like dynamics in large-scale functional brain networks. Phys Rev E Stat Nonlin Soft Matter Phys. 2009; 79(6 Pt 1): 061922.
146. Amit DJ. Modeling brain function: The world of attractor neural networks. . Cambridge: Cambridge University Press; 1992.
147. Bruno MA, Majerus S, Boly M, Vanhaudenhuyse A, Schnakers C, Gosseries O, et al. Functional neuroanatomy underlying the clinical subcategorization of minimally conscious state patients. Journal of neurology. 2012; 259(6): 1087-98.
148. Thibaut A, Bruno MA, Chatelle C, Gosseries O, Vanhaudenhuyse A, Demertzi A, et al. Metabolic activity in external and internal awareness networks in severely brain-damaged patients. Journal of rehabilitation medicine : official journal of the UEMS European Board of Physical and Rehabilitation Medicine. 2012; 44(6): 487-94.
149. Calhoun VD, Adali T, Pearlson GD, Pekar JJ. A method for making group inferences from functional MRI data using independent component analysis. Hum Brain Mapp. 2001; 14(3): 140-51.
150. Desikan RS, Segonne F, Fischl B, Quinn BT, Dickerson BC, Blacker D, et al. An automated labeling system for subdividing the human cerebral cortex on MRI scans into gyral based regions of interest. Neuroimage. 2006; 31(3): 968-80.
151. Gorgolewski K, Burns CD, Madison C, Clark D, Halchenko YO, Waskom ML, et al. Nipype: a flexible, lightweight and extensible neuroimaging data processing framework in python. Front Neuroinform. 2011; 5: 13.
152. Gerhard S, Daducci A, Lemkaddem A, Meuli R, Thiran JP, Hagmann P. The connectome viewer toolkit: an open source framework to manage, analyze, and visualize connectomes. Front Neuroinform. 2011; 5: 3.
153. Cammoun L, Gigandet X, Meskaldji D, Thiran JP, Sporns O, Do KQ, et al. Mapping the human connectome at multiple scales with diffusion spectrum MRI. J Neurosci Methods. 2012; 203(2): 386-97.
154. Daducci A, Gerhard S, Griffa A, Lemkaddem A, Cammoun L, Gigandet X, et al. The connectome mapper: an open-source processing pipeline to map connectomes with MRI. PLoS One. 2012; 7(12): e48121.
155. Ziegler E, Foret A, Mascetti L, Muto V, Le Bourdiec-Shaffii A, Stender J, et al. Altered white matter architecture in BDNF met carriers. PLoS One. 2013; 8(7): e69290.
156. Jenkinson M, Beckmann CF, Behrens TE, Woolrich MW, Smith SM. Fsl. Neuroimage. 2012; 62(2): 782-90.
157. Tournier JD, Calamante F, Gadian DG, Connelly A. Direct estimation of the fiber orientation density function from diffusion-weighted MRI data using spherical deconvolution. Neuroimage. 2004; 23(3): 1176-85.
158. Chialvo DR. Emergent complex neural dynamics. Nature Physics. 2010; 6(10): 744-50.
159. Scheeringa R, Petersson KM, Kleinschmidt A, Jensen O, Bastiaansen MC. EEG alpha power modulation of fMRI resting-state connectivity. Brain connectivity. 2012; 2(5): 254-64.
160. Muzur A, Pace-Schott EF, Hobson JA. The prefrontal cortex in sleep. Trends Cogn Sci. 2002; 6(11): 475-81.
161. Dang-Vu TT, Schabus M, Desseilles M, Sterpenich V, Bonjean M, Maquet P. Functional neuroimaging insights into the physiology of human sleep. Sleep. 2010; 33(12): 1589-603.
162. Blumenfeld H. Epilepsy and the consciousness system: transient vegetative state? Neurologic clinics. 2011; 29(4): 801-23.
163. Sun X, Zhang H, Gao C, Zhang G, Xu L, Lv M, et al. Imaging the effects of propofol on human cerebral glucose metabolism using positron emission tomography. The Journal of international medical research. 2008; 36(6): 1305-10.
164. Desseilles M, Vu TD, Maquet P. Functional neuroimaging in sleep, sleep deprivation, and sleep disorders. Handbook of clinical neurology / edited by PJ Vinken and GW Bruyn. 2011; 98: 71-94.

165. Laureys S, Faymonville ME, Luxen A, Lamy M, Franck G, Maquet P. Restoration of thalamocortical connectivity after recovery from persistent vegetative state. Lancet. 2000; 355(9217): 1790-1.
166. Brefel-Courbon C, Payoux P, Ory F, Sommet A, Slaoui T, Raboyeau G, et al. Clinical and imaging evidence of zolpidem effect in hypoxic encephalopathy. Annals of Neurology. 2007; 62(1): 102-5.
167. Samann PG, Wehrle R, Hoehn D, Spoormaker VI, Peters H, Tully C, et al. Development of the brain's default mode network from wakefulness to slow wave sleep. Cerebral cortex. 2011; 21(9): 2082-93.
168. Benchenane K, Tiesinga PH, Battaglia FP. Oscillations in the prefrontal cortex: a gateway to memory and attention. Current opinion in neurobiology. 2011; 21(3): 475-85.
169. Bruno MA, Vanhaudenhuyse A, Thibaut A, Moonen G, Laureys S. From unresponsive wakefulness to minimally conscious PLUS and functional locked-in syndromes: recent advances in our understanding of disorders of consciousness. Journal of neurology. 2011; 258(7): 1373-84.
170. Giacino JT, Ashwal S, Childs N, Cranford R, Jennett B, Katz DI, et al. The minimally conscious state: definition and diagnostic criteria. Neurology. 2002; 58(3): 349-53.
171. Schnakers C, Perrin F, Schabus M, Hustinx R, Majerus S, Moonen G, et al. Detecting consciousness in a total locked-in syndrome: an active event-related paradigm. Neurocase. 2009; 15(4): 271-7.
172. Raichle ME, Snyder AZ. A default mode of brain function: a brief history of an evolving idea. NeuroImage. 2007; 37(4): 1083-90; discussion 97-9.
173. Heine L, Soddu A, Gomez F, Vanhaudenhuyse A, Tshibanda L, Thonnard M, et al. Resting state networks and consciousness: alterations of multiple resting state network connectivity in physiological, pharmacological, and pathological consciousness States. Frontiers in psychology. 2012; 3: 295.
174. Meindl T, Teipel S, Elmouden R, Mueller S, Koch W, Dietrich O, et al. Test-retest reproducibility of the default-mode network in healthy individuals. Human brain mapping. 2010; 31(2): 237-46.
175. Crone JS, Soddu A, Holler Y, Vanhaudenhuyse A, Schurz M, Bergmann J, et al. Altered network properties of the fronto-parietal network and the thalamus in impaired consciousness. NeuroImage Clinical. 2013; 4: 240-8.
176. Huang Z, Dai R, Wu X, Yang Z, Liu D, Hu J, et al. The self and its resting state in consciousness: an investigation of the vegetative state. Hum Brain Mapp. 2014; 35(5): 1997-2008.
177. Soddu A, Vanhaudenhuyse A, Demertzi A, Bruno MA, Tshibanda L, Di H, et al. Resting state activity in patients with disorders of consciousness. Funct Neurol. 2011; 26(1): 37-43.
178. Gili T, Saxena N, Diukova A, Murphy K, Hall JE, Wise RG. The thalamus and brainstem act as key hubs in alterations of human brain network connectivity induced by mild propofol sedation. J Neurosci. 2013; 33(9): 4024-31.
179. Power JD, Barnes KA, Snyder AZ, Schlaggar BL, Petersen SE. Spurious but systematic correlations in functional connectivity MRI networks arise from subject motion. NeuroImage. 2012; 59(3): 2142-54.
180. Baquero K, Gómez F, Cifuentes C, Guldenmund P, Demertzi A. A multiscale method for a robust detection of the default mode network. Proc SPIE. 2013; 8922.
181. Stender J, Gosseries O, Bruno MA, Charland-Verville V, Vanhaudenhuyse A, Demertzi A, et al. Diagnostic precision of PET imaging and functional MRI in disorders of consciousness: a clinical validation study. Lancet. 2014.
182. Galanaud D, Naccache L, Puybasset L. Exploring impaired consciousness: the MRI approach. Current opinion in neurology. 2007; 20(6): 627-31.
183. Young C, Knudsen N, Hilton A, Reves JG. Sedation in the intensive care unit. Critical care medicine. 2000; 28(3): 854-66.

184. Giacino JT, Kalmar K, Whyte J. The JFK Coma Recovery Scale-Revised: measurement characteristics and diagnostic utility. Archives of physical medicine and rehabilitation. 2004; 85(12): 2020-9.
185. Seel RT, Sherer M, Whyte J, Katz DI, Giacino JT, Rosenbaum AM, et al. Assessment scales for disorders of consciousness: evidence-based recommendations for clinical practice and research. Archives of physical medicine and rehabilitation. 2010; 91(12): 1795-813.
186. Marsh B, White M, Morton N, Kenny GN. Pharmacokinetic model driven infusion of propofol in children. Br J Anaesth. 1991; 67(1): 41-8.
187. Ashburner J. A fast diffeomorphic image registration algorithm. NeuroImage. 2007; 38(1): 95-113.
188. Takahashi R, Ishii K, Miyamoto N, Yoshikawa T, Shimada K, Ohkawa S, et al. Measurement of gray and white matter atrophy in dementia with Lewy bodies using diffeomorphic anatomic registration through exponentiated lie algebra: A comparison with conventional voxel-based morphometry. AJNR American journal of neuroradiology. 2010; 31(10): 1873-8.
189. Peelle JE, Cusack R, Henson RN. Adjusting for global effects in voxel-based morphometry: gray matter decline in normal aging. NeuroImage. 2012; 60(2): 1503-16.
190. Mazaika P, Hoeft F, Glover GH, Reiss AL. Methods and Software for fMRI Analysis for Clinical Subjects. Human brain mapping. 2009.
191. McKeown MJ, Hansen LK, Sejnowsk TJ. Independent component analysis of functional MRI: what is signal and what is noise? Current opinion in neurobiology. 2003; 13(5): 620-9.
192. Khalsa S, Mayhew SD, Chechlacz M, Bagary M, Bagshaw AP. The structural and functional connectivity of the posterior cingulate cortex: Comparison between deterministic and probabilistic tractography for the investigation of structure-function relationships. Neuroimage. 2013.
193. Hudetz AG. General anesthesia and human brain connectivity. Brain Connect. 2012; 2(6): 291-302.
194. Leech R, Kamourieh S, Beckmann CF, Sharp DJ. Fractionating the default mode network: distinct contributions of the ventral and dorsal posterior cingulate cortex to cognitive control. J Neurosci. 2011; 31(9): 3217-24.
195. Leech R, Braga R, Sharp DJ. Echoes of the brain within the posterior cingulate cortex. J Neurosci. 2012; 32(1): 215-22.
196. Mhuircheartaigh RN, Rosenorn-Lanng D, Wise R, Jbabdi S, Rogers R, Tracey I. Cortical and subcortical connectivity changes during decreasing levels of consciousness in humans: a functional magnetic resonance imaging study using propofol. J Neurosci. 2010; 30(27): 9095-102.
197. Hudetz AG, Liu X, Pillay S. Dynamic Repertoire of Intrinsic Brain States Is Reduced in Propofol-Induced Unconsciousness. Brain Connect. 2014.
198. Haber SN, Calzavara R. The cortico-basal ganglia integrative network: the role of the thalamus. Brain Res Bull. 2009; 78(2-3): 69-74.
199. Smith Y, Galvan A, Ellender TJ, Doig N, Villalba RM, Huerta-Ocampo I, et al. The thalamostriatal system in normal and diseased states. Front Syst Neurosci. 2014; 8: 5.
200. Hoffstaedter F, Grefkes C, Caspers S, Roski C, Palomero-Gallagher N, Laird AR, et al. The role of anterior midcingulate cortex in cognitive motor control: evidence from functional connectivity analyses. Hum Brain Mapp. 2014; 35(6): 2741-53.
201. Deng J, Lei C, Chen Y, Fang Z, Yang Q, Zhang H, et al. Neuroprotective gases--fantasy or reality for clinical use? Prog Neurobiol. 2014; 115: 210-45.
202. Yu Q, Wang H, Chen J, Gao Y, Liang W. Neuroprotections and mechanisms of inhalational anesthetics against brain ischemia. Front Biosci (Elite Ed). 2010; 2: 1275-98.
203. Zuo Z. Are volatile anesthetics neuroprotective or neurotoxic? Medical gas research. 2012; 2(1): 10.
204. Hudson AE, Hemmings HC, Jr. Are anaesthetics toxic to the brain? Br J Anaesth. 2011; 107(1): 30-7.

205. Loepke AW, Soriano SG. An assessment of the effects of general anesthetics on developing brain structure and neurocognitive function. Anesth Analg. 2008; 106(6): 1681-707.
206. Strom C, Rasmussen LS, Sieber FE. Should general anaesthesia be avoided in the elderly? Anaesthesia. 2014; 69 Suppl 1: 35-44.
207. Fodale V, Quattrone D, Trecroci C, Caminiti V, Santamaria LB. Alzheimer's disease and anaesthesia: implications for the central cholinergic system. Br J Anaesth. 2006; 97(4): 445-52.
208. Phillips CL, Bruno MA, Maquet P, Boly M, Noirhomme Q, Schnakers C, et al. "Relevance vector machine" consciousness classifier applied to cerebral metabolism of vegetative and locked-in patients. NeuroImage. 2011; 56(2): 797-808.
209. Sharp DJ, Beckmann CF, Greenwood R, Kinnunen KM, Bonnelle V, De Boissezon X, et al. Default mode network functional and structural connectivity after traumatic brain injury. Brain : a journal of neurology. 2011; 134(Pt 8): 2233-47.
210. Lull N, Noe E, Lull JJ, Garcia-Panach J, Chirivella J, Ferri J, et al. Voxel-based statistical analysis of thalamic glucose metabolism in traumatic brain injury: relationship with consciousness and cognition. Brain Inj. 2010; 24(9): 1098-107.
211. Lull N, Noe E, Lull JJ, Garcia-Panach J, Garcia-Marti G, Chirivella J, et al. [Thalamic metabolism and neurological outcome after traumatic brain injury. A voxel-based morphometric FDG-PET study]. Neurologia. 2010; 25(3): 174-80.
212. Toyama Y, Kobayashi T, Nishiyama Y, Satoh K, Ohkawa M, Seki K. CT for acute stage of closed head injury. Radiation medicine. 2005; 23(5): 309-16.
213. Rovegno M, Soto PA, Saez JC, von Bernhardi R. [Biological mechanisms involved in the spread of traumatic brain damage]. Medicina intensiva / Sociedad Espanola de Medicina Intensiva y Unidades Coronarias. 2012; 36(1): 37-44.
214. Rousseau MC, Confort-Gouny S, Catala A, Graperon J, Blaya J, Soulier E, et al. A MRS-MRI-fMRI exploration of the brain. Impact of long-lasting persistent vegetative state. Brain Inj. 2008; 22(2): 123-34.
215. Rudolf J, Ghaemi M, Haupt WF, Szelies B, Heiss WD. Cerebral glucose metabolism in acute and persistent vegetative state. Journal of neurosurgical anesthesiology. 1999; 11(1): 17-24.
216. Ashburner J, Friston KJ. Voxel-based morphometry--the methods. NeuroImage. 2000; 11(6 Pt 1): 805-21.
217. Good CD, Johnsrude IS, Ashburner J, Henson RN, Friston KJ, Frackowiak RS. A voxel-based morphometric study of ageing in 465 normal adult human brains. NeuroImage. 2001; 14(1 Pt 1): 21-36.
218. Graham DI, Maxwell WL, Adams JH, Jennett B. Novel aspects of the neuropathology of the vegetative state after blunt head injury. Prog Brain Res. 2005; 150: 445-55.
219. Sato H, Tanaka T, Kasai K, Tanaka N. An autopsy case of acute carbon monoxide poisoning after a long-term vegetative state. The American journal of forensic medicine and pathology. 2012; 33(4): 341-3.
220. Chu NS. Early and late CT manifestations in the persistent vegetative state due to cerebral anoxia-ischemia. Journal of the Formosan Medical Association = Taiwan yi zhi. 1993; 92(8): 697-701.
221. Trivedi MA, Ward MA, Hess TM, Gale SD, Dempsey RJ, Rowley HA, et al. Longitudinal changes in global brain volume between 79 and 409 days after traumatic brain injury: relationship with duration of coma. Journal of neurotrauma. 2007; 24(5): 766-71.
222. Hertz L. Bioenergetics of cerebral ischemia: a cellular perspective. Neuropharmacology. 2008; 55(3): 289-309.
223. Kozlowski Moreau O, Yollin E, Merlen E, Daveluy W, Rousseaux M. Lasting pituitary hormone deficiency after traumatic brain injury. Journal of neurotrauma. 2012; 29(1): 81-9.
224. Willie JT, Lim MM, Bennett RE, Azarion AA, Schwetye KE, Brody DL. Controlled cortical impact traumatic brain injury acutely disrupts wakefulness and extracellular orexin dynamics as

determined by intracerebral microdialysis in mice. Journal of neurotrauma. 2012; 29(10): 1908-21.
225. McAllister TW. Neuropsychiatric sequelae of head injuries. The Psychiatric clinics of North America. 1992; 15(2): 395-413.
226. Gitelman DR, Ashburner J, Friston KJ, Tyler LK, Price CJ. Voxel-based morphometry of herpes simplex encephalitis. NeuroImage. 2001; 13(4): 623-31.
227. Salmond CH, Ashburner J, Vargha-Khadem F, Connelly A, Gadian DG, Friston KJ. Distributional assumptions in voxel-based morphometry. NeuroImage. 2002; 17(2): 1027-30.
228. Giacino J KK, Whyte J. The JFK Coma Recovery Scale-Revised: Measurement characteristics and diagnostic utility. Archives of Physical Medicine and Rehabilitation. 2004; 85(12): 2020-9.
229. Manjon JV, Coupe P, Marti-Bonmati L, Collins DL, Robles M. Adaptive non-local means denoising of MR images with spatially varying noise levels. Journal of magnetic resonance imaging : JMRI. 2010; 31(1): 192-203.
230. Rajapakse JC, Giedd JN, Rapoport JL. Statistical approach to segmentation of single-channel cerebral MR images. IEEE transactions on medical imaging. 1997; 16(2): 176-86.
231. Mikl M, Marecek R, Hlustik P, Pavlicova M, Drastich A, Chlebus P, et al. Effects of spatial smoothing on fMRI group inferences. Magnetic resonance imaging. 2008; 26(4): 490-503.
232. Henley SM, Ridgway GR, Scahill RI, Kloppel S, Tabrizi SJ, Fox NC, et al. Pitfalls in the use of voxel-based morphometry as a biomarker: examples from huntington disease. AJNR American journal of neuroradiology. 2010; 31(4): 711-9.
233. Weibull A, Gustavsson H, Mattsson S, Svensson J. Investigation of spatial resolution, partial volume effects and smoothing in functional MRI using artificial 3D time series. NeuroImage. 2008; 41(2): 346-53.
234. Ho AK, Nestor PJ, Williams GB, Bradshaw JL, Sahakian BJ, Robbins TW, et al. Pseudo-neglect in Huntington's disease correlates with decreased angular gyrus density. Neuroreport. 2004; 15(6): 1061-4.
235. Hellewell SC, Yan EB, Agyapomaa DA, Bye N, Morganti-Kossmann MC. Post-traumatic hypoxia exacerbates brain tissue damage: analysis of axonal injury and glial responses. Journal of neurotrauma. 2010; 27(11): 1997-2010.
236. Ekmark-Lewen S, Flygt J, Kiwanuka O, Meyerson BJ, Lewen A, Hillered L, et al. Traumatic axonal injury in the mouse is accompanied by a dynamic inflammatory response, astroglial reactivity and complex behavioral changes. Journal of neuroinflammation. 2013; 10(1): 44.
237. Aldskogius H, Kozlova EN. Central neuron-glial and glial-glial interactions following axon injury. Prog Neurobiol. 1998; 55(1): 1-26.
238. Ripolles P, Marco-Pallares J, de Diego-Balaguer R, Miro J, Falip M, Juncadella M, et al. Analysis of automated methods for spatial normalization of lesioned brains. NeuroImage. 2012; 60(2): 1296-306.
239. Karas GB, Scheltens P, Rombouts SA, Visser PJ, van Schijndel RA, Fox NC, et al. Global and local gray matter loss in mild cognitive impairment and Alzheimer's disease. NeuroImage. 2004; 23(2): 708-16.
240. Genovese CR, Lazar NA, Nichols T. Thresholding of statistical maps in functional neuroimaging using the false discovery rate. NeuroImage. 2002; 15(4): 870-8.
241. Nugent AC, Milham MP, Bain EE, Mah L, Cannon DM, Marrett S, et al. Cortical abnormalities in bipolar disorder investigated with MRI and voxel-based morphometry. NeuroImage. 2006; 30(2): 485-97.
242. Deniz Can D, Richards T, Kuhl PK. Early gray-matter and white-matter concentration in infancy predict later language skills: a whole brain voxel-based morphometry study. Brain and language. 2013; 124(1): 34-44.
243. Braga B, Yasuda CL, Cendes F. White Matter Atrophy in Patients with Mesial Temporal Lobe Epilepsy: Voxel-Based Morphometry Analysis of T1- and T2-Weighted MR Images. Radiology research and practice. 2012; 2012: 481378.

244. Goldfine AM, Schiff ND. Consciousness: its neurobiology and the major classes of impairment. Neurologic clinics. 2011; 29(4): 723-37.
245. Saleh A, Schroeter M, Jonkmanns C, Hartung HP, Modder U, Jander S. In vivo MRI of brain inflammation in human ischaemic stroke. Brain : a journal of neurology. 2004; 127(Pt 7): 1670-7.
246. Helmy A, Carpenter KL, Menon DK, Pickard JD, Hutchinson PJ. The cytokine response to human traumatic brain injury: temporal profiles and evidence for cerebral parenchymal production. Journal of cerebral blood flow and metabolism : official journal of the International Society of Cerebral Blood Flow and Metabolism. 2011; 31(2): 658-70.
247. Mura E, Pistoia F, Sara M, Sacco S, Carolei A, Govoni S. Pharmacological modulation of the state of awareness in patients with Disorders of Consciousness: an Overview. Current pharmaceutical design. 2013.
248. Gosseries O, Charland-Verville V, Thonnard M, Bodart O, Laureys S, Demertzi A. Amantadine, Apomorphine and Zolpidem in the Treatment of Disorders of Consciousness. Current pharmaceutical design. 2013.
249. Weiss N, Galanaud D, Carpentier A, Tezenas de Montcel S, Naccache L, Coriat P, et al. A combined clinical and MRI approach for outcome assessment of traumatic head injured comatose patients. Journal of neurology. 2008; 255(2): 217-23.
250. Scott SK. The neurobiology of speech perception and production--can functional imaging tell us anything we did not already know? Journal of communication disorders. 2012; 45(6): 419-25.
251. Hattingen E, Blasel S, Nichtweiss M, Zanella FE, Weidauer S. MR imaging of midbrain pathologies. Clinical neuroradiology. 2010; 20(2): 81-97.
252. Edlow BL, Haynes RL, Takahashi E, Klein JP, Cummings P, Benner T, et al. Disconnection of the Ascending Arousal System in Traumatic Coma. Journal of neuropathology and experimental neurology. 2013; 72(6): 505-23.
253. Lingor P, Koch JC, Tonges L, Bahr M. Axonal degeneration as a therapeutic target in the CNS. Cell and tissue research. 2012; 349(1): 289-311.
254. Monti MM. Cognition in the vegetative state. Annual review of clinical psychology. 2012; 8: 431-54.
255. Giraud AL, Kell C, Thierfelder C, Sterzer P, Russ MO, Preibisch C, et al. Contributions of sensory input, auditory search and verbal comprehension to cortical activity during speech processing. Cerebral cortex. 2004; 14(3): 247-55.
256. Soderfeldt B, Ingvar M, Ronnberg J, Eriksson L, Serrander M, Stone-Elander S. Signed and spoken language perception studied by positron emission tomography. Neurology. 1997; 49(1): 82-7.
257. Vorobyev VA, Alho K, Medvedev SV, Pakhomov SV, Roudas MS, Rutkovskaya JM, et al. Linguistic processing in visual and modality-nonspecific brain areas: PET recordings during selective attention. Brain research Cognitive brain research. 2004; 20(2): 309-22.
258. Laureys S, Faymonville ME, De Tiege X, Peigneux P, Berre J, Moonen G, et al. Brain function in the vegetative state. Adv Exp Med Biol. 2004; 550: 229-38.
259. Goulden N, Khusnulina A, Davis NJ, Bracewell RM, Bokde AL, McNulty JP, et al. The salience network is responsible for switching between the default mode network and the central executive network: Replication from DCM. Neuroimage. 2014.
260. Boly M, Balteau E, Schnakers C, Degueldre C, Moonen G, Luxen A, et al. Baseline brain activity fluctuations predict somatosensory perception in humans. Proc Natl Acad Sci U S A. 2007; 104(29): 12187-92.
261. Langsjo JW, Alkire MT, Kaskinoro K, Hayama H, Maksimow A, Kaisti KK, et al. Returning from oblivion: imaging the neural core of consciousness. J Neurosci. 2012; 32(14): 4935-43.
262. Nelson LE, Lu J, Guo T, Saper CB, Franks NP, Maze M. The alpha2-adrenoceptor agonist dexmedetomidine converges on an endogenous sleep-promoting pathway to exert its sedative effects. Anesthesiology. 2003; 98(2): 428-36.

263. Schiff ND. Central thalamic deep brain stimulation for support of forebrain arousal regulation in the minimally conscious state. Handb Clin Neurol. 2013; 116: 295-306.
264. van den Heuvel MP, Mandl RC, Kahn RS, Hulshoff Pol HE. Functionally linked resting-state networks reflect the underlying structural connectivity architecture of the human brain. Human brain mapping. 2009; 30(10): 3127-41.
265. Mo Y, Zimmermann AE. Role of dexmedetomidine for the prevention and treatment of delirium in intensive care unit patients. Ann Pharmacother. 2013; 47(6): 869-76.
266. Rozet I. Anesthesia for functional neurosurgery: the role of dexmedetomidine. Curr Opin Anaesthesiol. 2008; 21(5): 537-43.
267. Xia ZQ, Chen SQ, Yao X, Xie CB, Wen SH, Liu KX. Clinical benefits of dexmedetomidine versus propofol in adult intensive care unit patients: a meta-analysis of randomized clinical trials. J Surg Res. 2013; 185(2): 833-43.
268. Bradley C. Dexmedetomidine--a novel sedative for postoperative sedation. Intensive Crit Care Nurs. 2000; 16(5): 328-9.
269. Mizobe T, Maghsoudi K, Sitwala K, Tianzhi G, Ou J, Maze M. Antisense technology reveals the alpha2A adrenoceptor to be the subtype mediating the hypnotic response to the highly selective agonist, dexmedetomidine, in the locus coeruleus of the rat. J Clin Invest. 1996; 98(5): 1076-80.
270. Coursin DB, Maccioli GA. Dexmedetomidine. Curr Opin Crit Care. 2001; 7(4): 221-6.
271. Rainville P. Brain mechanisms of pain affect and pain modulation. Curr Opin Neurobiol. 2002; 12(2): 195-204.
272. Boly M, Perlbarg V, Marrelec G, Schabus M, Laureys S, Doyon J, et al. Hierarchical clustering of brain activity during human nonrapid eye movement sleep. Proc Natl Acad Sci U S A. 2012; 109(15): 5856-61.

ACKNOWLEDGEMENTS

This thesis has been made possible thanks to the expert supervision of Professor Steven Laureys and Professor Andrea Soddu. I am also in great debt to my colleagues at the Coma Science Group, the Cyclotron Research Center, and the CHU University Hospital, who have been involved in patient care, data acquisition and analysis, without which the examinations of the unconscious described in this thesis would have been impossible. A special mention should be made of the families and friends of the patients that have been hospitalized at the CHU University Hospital in Liège. They have surprised me time and time again by their courage, positive attitude, and friendliness in a position that nobody should be in: divided from their loved one. My loved ones include my family, who supported me in every step of life in so many ways. My friends, who have had the incredible kindness to be who they are in my presence. And last but not least, my Katherine, for being lovely and wonderful, thus adding so much more happiness to my existence.

LIST OF PUBLICATIONS

As first author:

A default mode of brain function in altered states of consciousness. Guldenmund P., Vanhaudenhuyse A., Boly M., Laureys S., Soddu A. Arch Ital Biol. 2012 Jun;150(2-3):107-21.

Mindsight: diagnostics in disorders of consciousness. Guldenmund P., Stender J., Heine L., Laureys S. Crit Care Res Pract. 2012 Nov 14.

Thalamus, brainstem and salience network connectivity changes in propofol-induced mild sedation and unconsciousness. Guldenmund P., Demertzi A., Boveroux P., Boly M., Vanhaudenhuyse A., Bruno M.A., Gosseries O., Noirhomme Q., Brichant J.F., Bonhomme V., Laureys S., Soddu A. Brain Connect. 2013;3(3):273-85.

Brain damage in patients with disorders of consciousness. Guldenmund P., Soddu A., Baquero K., Vanhaudenhuyse A., Bruno M.A., Gosseries O., Laureys S.#, Gómez F.# (submitted)

Propofol-induced frontal cortex disconnection: a study of resting state networks, BOLD oscillatory frequencies and their generalized-Ising model interpretation. Das T.*, Gantner S.*, Guldenmund P.*, Baquero K., Khajehabdollahi S., Sosnowski A., Ge B., Demertzi A., Boveroux P., Bonhomme V., Vanhaudenhuyse A., Bruno M.-A., Gosseries O., Noirhomme Q., Kirsch M., Boly M., Owen A.M., Laureys S., Gómez F., Soddu A. (submitted)

Sedation of patients with disorders of consciousness during neuroimaging: effects on resting state functional brain connectivity. Kirsch M.*, Guldenmund P.*, Bahri M., Bonhomme V., Boveroux P., Baquero K., Brichant J.-F., Di Perri C., Ziegler E., Amico E., Vanhaudenhuyse A., Bruno M.-A., Gosseries O., Gómez F., Soddu A., Laureys S. (submitted)

Unconsciousness induced by dexmedetomidine, propofol, and during slow wave sleep: a resting state connectivity comparison. Vanhaudenhuyse A.*, Guldenmund P.*, Bonhomme V., Sleigh J., Sanders R., Laureys S. (in preparation)

As co-author:

A multiscale method for resting state fMRI in disorders of consciousness. Baquero K., Gómez F., Guldenmund P., Demertzi A., Vanhaudenhuyse A, Tshibanda L., Noirhomme Q., Laureys S., Soddu A., Romero E. (submitted)

Functional imaging and impaired consciousness. Di Perri C., Demertzi A., Heine L., Thibaut A., Amico E., Guldenmund P., Soddu A., Antonopoulos Y., Preziosi M., Tschibanda L., Laureys S. (accepted)

* = co-first authors # = co-last authors